

REPORT DOCUMENTATION PAGE

Form Approved OMB No. 0704-0188

Public reporting burden for this collection of information is estimated to average 1 hour per response, including the time for reviewing instructions, searching existing data sources, gathering and maintaining the data needed, and completing and reviewing the collection of information. Send comments regarding this burden estimate or any other aspect of this collection of information, including suggestions for reducing the burden, to Department of Defense, Washington Headquarters Services, Directorate for Information Operations and Reports (0704-0188), 1215 Jefferson Davis Highway, Suite 1204, Arlington, VA 22202-4302. Respondents should be aware that notwithstanding any other provision of law, no person shall be subject to any penalty for failing to comply with a collection of information if it does not display a currently valid OMB control number.
PLEASE DO NOT RETURN YOUR FORM TO THE ABOVE ADDRESS.

1. REPORT DATE (DD-MM-YYYY) 20-04-2006	2. REPORT TYPE Final Report	3. DATES COVERED (From – To) 01-Mar-03 - 01-Mar-06
--	---------------------------------------	--

4. TITLE AND SUBTITLE Advanced Nozzle Concepts for the Chemical Oxygen-Iodine Laser (COIL)	5a. CONTRACT NUMBER ISTC Registration No: 2230p
	5b. GRANT NUMBER
	5c. PROGRAM ELEMENT NUMBER

6. AUTHOR(S) Dr. Valery Dmitrievich Nikolaev	5d. PROJECT NUMBER
	5d. TASK NUMBER
	5e. WORK UNIT NUMBER

7. PERFORMING ORGANIZATION NAME(S) AND ADDRESS(ES) P. N. Lebedev Physical Institute Nova-Sadovaya Str. 221 Samara 443011 Russia	8. PERFORMING ORGANIZATION REPORT NUMBER N/A
--	--

9. SPONSORING/MONITORING AGENCY NAME(S) AND ADDRESS(ES) EOARD PSC 821 BOX 14 FPO 09421-0014	10. SPONSOR/MONITOR'S ACRONYM(S)
	11. SPONSOR/MONITOR'S REPORT NUMBER(S) ISTC 01-7041

12. DISTRIBUTION/AVAILABILITY STATEMENT
Approved for public release; distribution is unlimited.

13. SUPPLEMENTARY NOTES

14. ABSTRACT

This report results from a contract tasking P. N. Lebedev Physical Institute as follows: Iodine lasers offer the possibility of producing high average powers at a wavelength compatible with conventional fiber optic delivery systems, making them attractive for industrial applications. The planned experimental and theoretical investigations are aimed to a great extent for further understanding of physical processes taking place during mixing of gaseous components and laser active medium preparation. The knowledge obtained during this project will be largely of a general physics nature.

15. SUBJECT TERMS
EOARD, Physics, Fluid Mechanics

16. SECURITY CLASSIFICATION OF:			17. LIMITATION OF ABSTRACT UL	18, NUMBER OF PAGES 83	19a. NAME OF RESPONSIBLE PERSON DONALD J SMITH
a. REPORT UNCLAS	b. ABSTRACT UNCLAS	c. THIS PAGE UNCLAS			19b. TELEPHONE NUMBER (Include area code) +44 (0)20 7514 4953

ISTC 2230P - 00

**Final
Project Technical Report
of ISTC 22130P-00**

**Advanced Nozzle Concepts for the Chemical
OXYGEN-IODINE LASER (COIL)**

(From 1 March 2003 to 28 February 2006 for 36 months)

Director

LPI SB



A.L. Petrov

“10” March 2006

Project Manager



V.D. Nikolaev

“10” March 2006

March 2006

This work was supported financially by United States Air Force / The European Office of Aerospace Research and Development and performed under the contract to the International Science and Technology Center (ISTC), Moscow.

ISTC 2230P- 00

Advanced Nozzle Concepts for the Chemical
OXYGEN-IODINE LASER (COIL)

(From 1 March 2003 to 28 February 2006 for 36 months)

Valeri Dmitrievich Nikolaev
(Project Manager)
Lebedev Physical Institute RAS, Samara Branch *)

The objective of this project is to develop the optimal ejector nozzle bank (with additional nozzles for injection iodine vapor at low stagnation pressure) for chemical oxygen iodine laser, to test the gasdynamic characteristics of the laser gain medium applying the usual standard gasdynamic methods, laser induced fluorescence (LIF), monitoring luminescence of the excited iodine atoms along gas flow and to diagnose the small signal gain (SSG) by employing of the Rigrod dependencies of the laser power. An application of an ejector-like nozzle bank to produce a gain medium in the COIL device provides an opportunity to simplify a pressure recovery system or to reduce requirements to it. Mixing rate of the flows, iodine dissociation, singlet oxygen losses and chemical efficiency, however, are sensitive to details of the nozzle bank design. It is well known that the mixing of sonic/supersonic jets is very slow and it is necessary to use some kind of mixing enhancement schemes. Such mixing enhancement in the ejector nozzle bank may be realized due to the mixing of free jets with large differences in stagnation pressures. Under these conditions the under-expanded nitrogen jets with high stagnation pressure generate transverse momentum components which do not vanish when the static pressures of nitrogen and oxygen jets become equal. As result the driver nitrogen jets continue to expand compressing oxygen stream downstream the nozzle exit plane forming an aerodynamic throat. On the other hand the formation of the aerodynamic throat leads to an increase of singlet oxygen generator (SOG) pressure and a decrease in $O_2(^1\Delta)$ yield and the COIL chemical efficiency.

Several ejector nozzle bank (ENB) designs have been developed, manufactured and tested. The mixing efficiencies of the gas flows (LIF and Pitot pressure distributions) have been comprised for these nozzle banks. Only one ENB provided comparatively good mixing efficiency at the distances ~ 100 mm downstream and the lowest pressure in the reaction zone of the singlet oxygen generator. Design of this ENB contains set of the small scale conical supersonic nozzles for driver nitrogen with Mach number $M \approx 5$ and with 4 turbulizing tabs. It was found the considerable drop of the excited iodine atoms luminescence and SSG along gas flow which can't be explained by any quenching processes. Indeed the known quenching reactions in the oxygen-iodine medium can't cause substantial losses of $O_2(^1\Delta)$ during the dwell time of the flow through the cavity chamber, approximately equal to 10^{-4} seconds.

The partial pressures of water and iodine vapor in the cavity are several orders of magnitude higher than the saturated pressures for the estimated temperature of the gain medium. The formation iodine, water or water-iodine clusters is possible at these conditions. Several collisions are required prior to the formation of the clusters with the critical size. It is known that the rate constants for the iodine atom recombination reactions dramatically increase with decreasing the temperature. Recombination with formation of the simplest complex ($I-H_2O$) or I_3 can also take place. Therefore lasing experiments were executed at optical axis location ~ 50 mm downstream ENB.

The typical chemical efficiencies of all COIL with the tested nozzle banks were reached in the lasing experiments equal to (22÷25)%. The average Pitot pressures were measured at the different distances Z downstream ENB at cold gasdynamic tests presented in the Table

G_{Iair} mmole/s	$G_{Driver N2}$ mmole/s	$G_{Sec N2}$ mmole/s	Z, mm	Average P_{Pitot} , torr
75	500	60	45	97
75	500	60	83	92
75	500	60	113	85

It was found also the fast decrease of the excited iodine atom concentration and small signal gain along gas flow due to the low gas temperature and formation different clusters and iodine atom attachment to its. Dilution chlorine with He up to 1:4 did not result in noticeable weakening of the SSG degradation.

Keywords: chemical oxygen iodine laser, singlet oxygen, ejector, recovery pressure, mixing sonic-supersonic gas jets, laser induced fluorescence.

*) 443011, Samara, Novosadovaya str., 221,
Phone: (846)3356-654; fax: (846)3355-600
E-mail: laser@fian.smr.ru

ISTC 2230P-00

**The work has been performed by
the following institutes and collaborators.**

1. Participated institutes: The project was performed by one Institution.
Lebedev Physical Institute RAS, Samara Branch (LPI SB)
221, Novosadovaya st., Samara, Russia, 443011
Telephone: (846) 334 -14-81
Fax: (846) 335-56-00;
E-mail: laser@fian.smr.ru
2. Foreign Collaborators: This is a partner project

CONTENT

Introduction	
1. One-dimensional aerodynamic model of an ejector nozzle bank.	8
1.1 The main approximations of the model.	8
1.2 Designations.	9
1.3 Equations	12
1.4 Results of calculations and tests	14
1.4.1 Nozzle bank with cylindrical nozzles for driver nitrogen	14
1.4.2 Nozzle bank with the conical supersonic nozzles for driver nitrogen	16
1.4.3 Nozzle bank with shaped supersonic micro nozzles	17
2. Development of the scaleable nozzle bank design for (60÷80) mmole/s chlorine flow rate	19
2.1. Appendix. Estimation of the static pressure drop and pressure losses inside supplying driver N ₂ tubes	25
3. Pitot pressure distributions in cross sections of the mixing chamber	26
4. The upgrade of JSOG design with purpose to improve operation stability and to decrease the BHP aerosol content in the output oxygen stream at flow rate of ~80mmole/s	34
4.1 Description of the filament guided jet generator	35
4.2 Measurements of Cl ₂ utilization, gas temperature, water vapor pressure and O ₂ (¹ Δ) yield	36
4.3 Results of the FGJSOG-1 tests	37
4.3.1. Cl ₂ utilization and O ₂ (¹ Δ) yield dependencies as a functions of Cl ₂ molar flow rate and working pressure	37
4.3.2. Influence of BHP temperature on chlorine utilization, water vapor fraction and O ₂ (¹ Δ) yield	39
4.3.3. Influence of the BHP volumetric flow rate on FGJSOG-1 performance	40
4.3.4. Influence of the KOH molarity on FGJSOG-1 performance	41
4.3.5. FGJSOG -1 operation stability	42
4.4 Results of FGJSOG –2 tests	42
5. Investigation of the mixing efficiency of iodine at chlorine flow rates of (60÷80)mmole/s and nitrogen flow rates of (250÷500)mmole/s using the LIF method	42
5.1. LIF visualization of the flows produced by ENB-1	43
5.2. LIF visualization of the flows produced by ENB-2 and ENB-3	49
6. Measurement small signal gain with aid of the Rigrod curves	50
6.1. SSG of the lasing medium produced by ENB-1	51
6.2. SSG of the lasing medium produced by ENB-2	53
6.3. SSG of the lasing medium produced by ENB-3	55
6.4 Distribution of the excited iodine atoms I* along the gas flow	56
7. COIL performance with ENB-1 and ENB-2 and dilution free of primary gas with He	58
7.1. COIL performance with ENB-1	58
7.1.1. COIL performance at using FGJSOG-1 with as a source of O ₂ (¹ Δ)	58
7.1.2. COIL performance at using FGJSOG-2 with as a source of O ₂ (¹ Δ)	59
7.1.3. COIL performance at using He as secondary buffer gas	60
7.1.4. COIL performance at lower driver nitrogen flow rate G _{DN} ~250 mmole/s	61
7.2. COIL performance with ENB-2	62
7.2.1. COIL performance at the driver N ₂ molar flow rate G _{DN} =500mmole/s	62
7.2.2. COIL performance at lower driver N ₂ molar flow rate G _{DN} =250 mmole/s	63
8. COIL performance at chlorine dilution with helium with ratio Cl ₂ :He≈1:1	65
8.1. COIL performance with ENB-1	65
8.1.1. COIL performance at G _{DN} = 260 mmole/s, G ₁ =57 mmole/s and FGJSOG-1	65
8.1.2. COIL performance at G _{ND} = 260 mmole/s, G ₁ =57 mmole/s and FGJSOG-2	66
8.1.3. COIL performance at G _{DN} = 500 mmole/s, G ₁ =57 mmole/s and FGJSOG-1	67
8.1.4. COIL performance at G _{DN} = 500 mmole/s, G ₁ =72 mmole/s and FGJSOG-2	67

8.2.	COIL performance with ENB-2 at $G_{DN}= 500$ mmole/s, $G_1=72$ mmole/s	68
8.3.	COIL performance with ENB-3 at $G_{ND}=380$ mmole/s, $G_1=72$ mmole/s	68
9.	COIL performance with ENB-1 at higher chlorine dilution with helium $Cl_2:He\approx 1:2\div 4$	70
9.1.	Results of LIF and “cold” gasdynamic tests	70
9.2.	Development of the centrifugal bubble singlet oxygen generator (CBSOG).	75
9.3.	Distribution of the excited iodine atoms I^* emission along the gas flow in the experiments with the blocked ENB-1 at higher dilution primary gas with helium	76
9.4.	Results of the lasing experiments with the blocked ENB-1 at higher dilution primary gas with helium	77
10.	Discussion and conclusion	78
11.	References	81
12.	List of the published papers and reports with abstracts	82
13.	List of presentations at conferences and meetings with abstracts	83

Introduction

The main objective of this project is to develop according Technical Task the optimal ejector nozzle bank with the additional nozzles for injection iodine at the low stagnation pressure for chemical oxygen iodine laser and to diagnose the gasdynamic and gain characteristics of the laser active medium employing the usual standard methods.

It is necessary to develop one-dimensional mathematical model of the ejector nozzle bank with the mixing chamber of the interacting high full pressure underexpanded supersonic nitrogen jets with oxygen flow which will allow to estimate the “choke” effect” and influence of the driver gas flow rate on the pressure in SOG. To develop the optimal ejector nozzle bank for COIL, to test the gasdynamic characteristics of the laser active medium by applying the usual standard gasdynamic methods, monitoring luminescence of the excited iodine atoms along gas flow and to diagnose the small signal gain (SSG) using of the Rigrod dependencies of the laser power.

Scope of Work and Technical Approach

The fulfillment of the project was in conjunction with the following items:

- 1) to develop one-dimensional mathematical model of the ejector nozzle bank with the mixing chamber of the interacting high full pressure underexpanded nitrogen jets with oxygen which will allow to estimate the “choke” effect” and influence of the ejecting gas flow rate on the pressure in JSOG;
- 2) to develop the scaleable nozzle bank design for (60÷80)mmole/s chlorine flow rate and to manufacture it;
- 3) to upgrade JSOG design with purpose of to improve operation stability and to decrease the BHP aerosol content in the output oxygen stream at flow rate of 80mmole/s ;
- 4) to perform “cold” gasdynamic tests of the new nozzle bank at (60÷80)mmole/s chlorine flow rates and nitrogen flow rates of (250÷500)mmole/s;
- 5) to investigate the mixing efficiency at chlorine flow rates of (60÷80)mmole/s and nitrogen flow rates of (250÷500)mmole/s by LIF method;
- 6) to measure small signal gain distribution within the resonator cavity cross section employing tunable single mode semiconductor laser, temporarily provided by the Partner or with the Rigrod curves aid;
- 7) to perform lasing experiments at chlorine flow rates of (60÷80)mmole/s and nitrogen flow rates of (250÷500)mmole/s;
- 8) to perform lasing experiments with chlorine pre-diluted with helium in the ratio of $Cl_2:He=1:1$ to increase conductivity of the oxygen nozzles, singlet oxygen yield, small signal gain and output power;

- 9) to perform “cold” gasdynamic tests of some ejector nozzle banks at chlorine flow rate of 60mmole/s, the driver nitrogen flow rate of 500mmole/s and pre-dilution of chlorine with helium in the ratio of Cl₂:He=1:1; 1:2; 1:3; 1:4. To choose the nozzle bank which provide the plenum pressure ~60torr at Cl₂:He=1:4. To employ Pitot tube scanning across duct and LIF method for determination of a mixing efficiency of the interacting gas flows and potential recovery pressure at given conditions;
- 10) to perform optimization lasing experiments at chlorine pre-diluted with helium in the ratio of Cl₂:He=1:2; 1:3; 1:4, chlorine flow rate of 60mmole/s and the driver nitrogen flow rate of 500mmole/s. Registration of the I* luminescence along gas flow.

The small signal gain g and the potentially extractable power E of a chemical oxygen-iodine laser, (COIL), are given by:

$$g = N_1 \sigma \times \frac{(K_e + 0.5)Y - 0.5}{(K_e - 1)Y + 1} \quad (1)$$

$$E = 91 \times 10^3 \times G_o \times \left(Y - \frac{1}{2K_e + 1} \right) \quad (2).$$

Here N_1 is the concentration of atomic iodine, T is the temperature in °K, G_o is the oxygen molar flow rate, $K_e = 0.75 \exp(401/T)$ is the equilibrium constant for energy exchange between oxygen and atomic iodine $O_2(^1\Delta) + I(^2P_{3/2}) \leftrightarrow O_2(^3\Sigma) + I(^2P_{1/2})$, Y is the $O_2(^1\Delta)$ yield, defined as the ratio of $O_2(^1\Delta)$ concentration to the total oxygen concentration of $O_2(^1\Delta) + O_2(^3\Sigma)$. For the low pressure gain medium the Doppler-broadened stimulated emission cross section is given by $\sigma = 1.3 \times 10^{-16} \times T^{-0.5}$. As evident from (1) and (2) the extractable power and the gain increase with decreasing temperature. Moreover with a decrease in temperature the small signal gain depends only weakly on Y and higher optical extraction is possible for a given gain/threshold ratio. Therefore production of a supersonic COIL gain medium at low temperature and with high SSG is preferable for high power operation. Simultaneously it is necessary to ensure high chemical efficiency and high potential pressure recovery of the exhaust gas. The most promising method to achieve these goals is to use an ejector nozzle bank, (ENB), for the formation of the gain medium [1]. At the exit of the ENB the singlet oxygen flow with Mach number $M \leq 1$ is mixed with the supersonic driver buffer gas flow. The molecular iodine can be premixed with this driver buffer gas flow or injected in a separate manifold with small buffer gas flow. The ENB with the driver gas premixed with molecular iodine was used in a small scale COIL [1] and substantially improved in [2]. The ENB with additional injector for a small flow of the buffer gas containing molecular iodine permits control of the generated gain medium over a wider range. Cylindrical nozzles for the injection of the driver buffer gas flow with initial Mach number $M \approx 1$ were employed in the first version of the ENB [3]. It was found that efficient mixing was accomplished within a distance of several centimeters from the nozzle exit plane. With this system the following parameters were attained: small signal gain $\sim 0.5 \text{ cm}^{-1}$, Mach number ~ 2 , temperature $\sim 200 \text{ K}$ and a potential recovered pressure $\sim 100 \text{ torr}$ [4]. The maximum chemical efficiency for this configuration was 25% [5]. However, the expansion of the high pressure sonic driver nitrogen jets resulted in the formation of an aerodynamic throat downstream of the nozzle exit plane and partial choking of the primary oxygen flow. The transport of the oxygen-iodine mixture at high pressure from the nozzle exit plane to the aerodynamic throat resulted in losses of extractable energy. The generation of the oblique shock waves downstream

from the aerodynamic throat resulted in total pressure loss and the reduction of the cavity Mach number.

The use of high Mach number supersonic nozzles for the driver nitrogen instead of constant area sonic cylindrical nozzles provides for the possibility of minimizing the choking effect of the primary oxygen flow. Elimination of the choking effect permits to provide higher singlet oxygen flux through the ENB at a moderate pressure. It was also expected that the active medium flow in the cavity with higher Mach number, lower temperature, and a higher small signal gain can be produced. In the present report characteristics of the gain medium and laser performance at using ENB with supersonic nozzles for the driver nitrogen are investigated.

The planned experimental and theoretical investigations were aimed to a great extent for further understanding of physical processes taking place during mixing of the gaseous components and the laser active medium formation. The information was obtained about the typical spatial mixing scales of iodine vapor with other flow components, about the typical distances downstream of nozzle bank where molecular iodine dissociation starts and finishes, about small signal gain (SSG) value and its evolution along the flow, which is important for the optimal placement of the resonator optical axis. Also, the information was obtained about the influence of the nozzle bank design and the gas jets initial parameters on the full pressure after the straight shock wave, which is close to the recovery pressure at the diffuser outlet. The mathematical model of the ejector nozzle bank with the mixing chamber have to predict the "choke effect" of the primary flow and influence of the ENB design and the driver nitrogen flow rate on the pressure in JSOG. Several designs of the ENB were developed, manufactured and tested. Employing of the various ejector nozzle banks results in difference of the static pressures, gas velocities in the SOG reaction zone and causes changes in the chlorine utilization and $O_2(^1\Delta)$ yield. The SOG operation stability depends on ENB type also. Indeed, "choking effect" weakening at fixed chlorine flow rate M_c leads to SOG pressure decreasing but at the same time the velocity head $\sim \rho V^2 = (\rho V F)^2 / \rho F^2 = (M_c)^2 / \rho F^2 \sim 1/\rho$ increases promoting disintegration of the BHP jets and the aerosol carry-over from generator. Then water of the BHP droplets is evaporated and hard sediment is formed. The dry salt aerosol deposited on the back surface of the driver N_2 and I_2 manifolds clogs the free cross section of the ejector nozzle bank for oxygen flow from SOG. This leads to the raise of the working pressure, gas transport time and the decrease of $O_2(^1\Delta)$ yield. Generally optimization ENB and SOG should be made simultaneously as the single device. Two new SOG types - the filament guided jet singlet oxygen generator and the centrifugal bubble SOG were developed to minimize aerosol carry-over from generator and to provide high COIL stability operation with all ENBs. Observed the small signal gain drop along the gas flow was conditioned with the very low static temperature of the supersonic driver nitrogen flow. All known quenching reactions in the oxygen-iodine medium can't cause substantial losses of $O_2(^1\Delta)$ during the dwell time of the flow in the mixing chamber equal to approximately 10^{-4} seconds. The partial pressures of water and iodine vapor at the estimated temperature of the gain medium in the cavity are several orders of magnitude higher than the saturated pressures for these conditions. Therefore formation iodine, water or water-iodine clusters is possible. Several collisions are required prior to the formation of the clusters with the critical size. It is known also that the rate constant for the iodine atom recombination reactions dramatically increase with decreasing the temperature. Recombination with formation of the simplest complex (I-H₂O) or I₃ can also take place. With as increase in the driver nitrogen molar rate the cavity pressure becomes higher and the temperature lower. The formation of the clusters therefore should be faster as it was observed in the experiments. The heterogeneous condensation of iodine on the surfaces of submicron size aerosol particles contained in the output from the SOG is also possible. Therefore the formation of clusters and heterogeneous condensation of the iodine atoms can be the reason of the observed excited iodine atoms emission and SSG decays. It was supposed that premixing helium with the primary flow may increase the static gas temperature of the completely mixed flow and weaken this SSG degradation along gas flow. It were planned lasing experiments with dilution up to Cl₂:He=1:4.

1. One-dimensional aerodynamic model of an ejector nozzle bank.

The employing of an ejector nozzle to produce the gain medium in the COIL device results in the possibility of simplifying or reducing requirements for the pressure recovery system. Mixing, iodine dissociation, singlet oxygen losses and chemical efficiency, however, are sensitive to details of the nozzle bank design. It is well known that the mixing of sonic and supersonic jets is very slow and it is necessary to employ some kinds of mixing enhancement schemes. Such mixing enhancement in the first ejector nozzle bank was realized due to the mixing of free jets with large differences in stagnation pressures. Under these conditions the under-expanded driver nitrogen jets with high stagnation pressure generate the transverse momentum components which do not vanish when the static pressures of nitrogen and oxygen jets become equal. As result the driver nitrogen continues to expand compressing oxygen stream down stream from the nozzle exit plane forming an aerodynamic throat. The driver nitrogen static pressure on the jet's axis becomes considerably lower than the oxygen static pressure in the region of the aerodynamic throat. Then oxygen flow expands downstream of the throat compressing the driver nitrogen while accelerating to supersonic velocities. This process may consist of several sequential stages of compression and expansion generating vortex structures which enhance mixing. On the other hand the formation of an aerodynamic throat downstream from the nozzle exit plane leads to an increase of the singlet oxygen generator (SOG) pressure and a decrease in $O_2(^1\Delta)$ yield and the COIL chemical efficiency. One-dimensional mathematical model for description of the interaction of the high full pressure of the under-expanded nitrogen jets with the oxygen stream was developed. This model allows to determine JSOG pressure as a function on the driver gas flow rate and the geometrical parameters of the nozzle bank and to find the dependence of flow characteristics at the outlet of the mixing chamber.

1.1 The main approximations of the model.

a) Secondary nitrogen with iodine flow rate is small usually comparison with the oxygen flow rate because as the first step interaction of the nitrogen jets with oxygen stream will be considered only. General scheme of the interacting streams is presented on the fig.1. For simplicity consider the mixing chamber with the parallel walls for two equivalent streams (driver nitrogen and oxygen) separated by plate with the base cross section area dA which equal to total cross section area of the driver nitrogen nozzles and the supplying ducts.

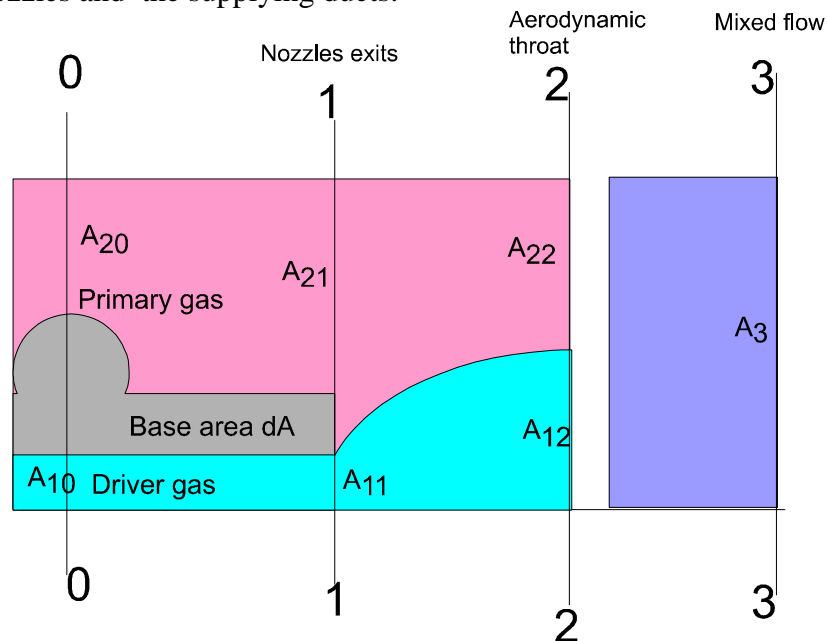


Fig.1. The schematic diagram of the ejector nozzle bank

- b) There is not entropy increasing of the primary flow (or stagnation pressure of the primary flow is constant).
- c) The velocity field of the free expanding jet becomes practically parallel at the plane where maximal jet's size is reached (plane 2 – 2, maximal size of the first “barrel”) and one dimensional gasdynamic conservation laws may be used for parameters at plane 1 – 1 and 2 – 2.
- d) The fields of the static pressure, gas velocity and other parameters of the free expanding jet are inhomogeneous strongly (for example, static pressure may decrease in 10-20 times from the edge to axis). But when it's necessary to know some general parameters of the jet only such as total momentum, total pressure losses, cross section area and knowledge of the inner structure of the jet is not requested then the use one dimensional theory for calculation of the average gasdynamic values gives correct results. Total energy, molar flow rate, momentum calculated at the same cross section size with the usage the average gas parameters (\bar{P}_0 , \bar{T}_0 , $\bar{\lambda}$) coincide with real values of the stream [6, 7]. One important proper of the flow namely parity of the pressure at the jet's border and surround pressure is lost in this case. It is necessary to count conditionally that a constant pressure exists at the each cross section and differs of surround pressure in the general case.
- e) Neglect by mixing of the expanding driver nitrogen supersonic jet with sub- and trans-sonic oxygen flow between planes 1-1 and 2-2 what corresponds to real situation with good approximation [6, 7].
- f) Experiments with the employing LIF for visualization mixing secondary N_2+I_2 with oxygen flow demonstrate its' very fast mixing in the space between 1-1 and 2-2 plane because influence secondary N_2+I_2 on cross section area of the aerodynamic throat may be corrected as the first approximation by increasing G_2 on value of N_2+I_2 mass flow rate and corresponding increased effective stagnation pressure P_{eff}^* of this mixture. Indeed, experiments demonstrate that local ejection effect (with N_2+I_2 as driver stream at $P_{N_2+I_2}^* \gg P_{O_2}^*$) compensate the increase flow rate through the aerodynamic throat and SOG pressure is independent practically on the secondary nitrogen flow rate.
- g) Influence of the heat release between 1-1 and 2-2 planes may be taken in to account by the correspondent increase of the initial stagnation temperature T_{12}^* .
- f) The base pressure is equal to the static oxygen pressure.

1.2 . Designations.

0-0 is the plane where the cross section area of the primary stream is minimal. There can be located the manifolds for iodine+ N_2 and for the driver N_2 flows.

1-1 is the exit plane of the driver gas nozzles

2-2 is the plane of the primary gas aerodynamic throat

3-3 is the plane where the mixing of all gases is completed

a) General designations

$R=8.31\text{J/mole/K}^\circ$ is the universal gas constant

$\lambda=U/a_{\text{crit}}$ is the reduced gas velocity;

k is the adiabatic exponent

Gas-dynamic functions for a gas flow:

$$q(\lambda) = \left(\frac{k+1}{2} \right)^{\frac{1}{k-1}} \lambda \left(1 - \frac{k-1}{k+1} \lambda^2 \right)^{\frac{1}{k-1}}$$

$$y(\lambda) = \left(\frac{k+1}{2} \right)^{\frac{1}{k-1}} \lambda \left(1 - \frac{k-1}{k+1} \lambda^2 \right)^{-1}$$

$$Z(\lambda) = \lambda + \frac{1}{\lambda}; \quad \pi(\lambda) = \left(1 - \frac{k-1}{k+1} \lambda^2 \right)^{\frac{k}{k-1}};$$

$$\tau(\lambda) = 1 - \frac{k-1}{k+1} \lambda^2,$$

dA is the base area.

b) Designations of the driver gas flow

	Parameter	Plane 1-1	Plane 2-2
1	Molar flow rate	G_1	G_1
2	Molar weight	μ_1	μ_1
3	Adiabatic exponent	k_1	k_1
4	Stagnation temperature	T_{11}^*	T_{12}^*
5	Static temperature	T_{11}	T_{12}
6	Stagnation pressure	P_{11}^*	P_{12}^*
7	Static pressure	P_{11}	P_{12}
8	Cross section area	A_{11}	A_{12}
9	Absolute gas velocity	U_{11}	U_{12}
10	Gas velocity in the critical point (critical velocity)	$a_{11} = \sqrt{\frac{2k_1RT_{11}^*}{(1+k_1)\mu_1}}$	$a_{12} = \sqrt{\frac{2k_1RT_{12}^*}{(1+k_1)\mu_1}}$
11	Reduced velocity	$\lambda_{11} = U_{11} / a_{11}$	$\lambda_{12} = U_{12} / a_{12}$
12	Mach number	M_{11}	M_{12}

$\sigma = P_{12}^* / P_{11}^*$ is the pressure losses coefficient for the colliding driver gas jets. $\sigma \approx 1$ in the case of the free non-interacting expanding jets, but $\sigma < 1$ in the case when driver gas is injected through set of closely located nozzles due to colliding of the expanding jets and generation intense shock waves. It's very difficult to determine this parameter and it may be estimated from experimental results. It's possible to find the upper limit for σ only. Indeed, available driver gas pressure drop $P_{11}^* / P_{12} \approx P_{11}^* / 10\text{torr}$ gives estimation for the reduced gas velocity λ_{12} from relation $P_{12} / P_{11}^* = \pi(\lambda_{12})$. Maximal pressure losses take place at the transition through the straight shock wave and gives minimal value for pressure losses coefficient equal to $\sigma_{\min} = q(\lambda_{12}) / q(1/\lambda_{12})$. For example, at $P_{11}^* / P_{12} \approx 200 \div 500$ or $\pi(\lambda_{12}) = (2 \div 5) \cdot 10^{-3}$ reduced velocity $\lambda_{12} \approx 2,16 \div 2,23$ and $\sigma_{\min} = q(\lambda_{12}) / q(1/\lambda_{12}) \approx 0,066 \div 0,12$.

The driver gas molar flow rate G_1 is

$$G_1 = \sqrt{\frac{1}{\mu_1 R} k_1 \left(\frac{2}{k_1 + 1} \right)^{\frac{k_1 + 1}{k_1 - 1}} \frac{P_{11}^* A_{11} q(\lambda_{11})}{\sqrt{T_{11}^*}}} = \sqrt{\frac{1}{\mu_1 R} k_1 \left(\frac{2}{k_1 + 1} \right)^{\frac{k_1 + 1}{k_1 - 1}} \frac{P_{12}^* A_{12} q(\lambda_{12})}{\sqrt{T_{12}^*}}} \quad (3)$$

The generalized momentum of the driver gas in the 1-1 plane is

$$I_{11} = \frac{k_1 + 1}{2k_1} \mu_1 G_1 a_{11} z(\lambda_{11}) \quad (4)$$

The generalized momentum of the driver gas in the 2-2 plane is

$$I_{12} = \frac{k_1 + 1}{2k_1} \mu_1 G_1 a_{12} z(\lambda_{12}) \quad (5)$$

c). Designations of the primary gas flow

	Parameter	Plane 0-0	Plane 1-1	Plane 2-2
1	Molar flow rate	G_2	G_2	G_2
2	Molar weight	μ_2	μ_2	μ_2
3	Adiabatic exponent	k_2	k_2	k_2

4	Stagnation temperature	T_{20}^*	T_{21}^*	T_{22}^*
5	Temperature	T_{20}	T_{21}	T_{22}
6	Stagnation pressure	P_{20}^*	P_{21}^*	P_{22}^*
7	Static pressure	P_{20}	P_{21}	P_{22}
8	Cross section area	A_{20}	A_{21}	A_{22}
9	Absolute velocity	U_{20}	U_{21}	U_{22}
10	Gas velocity in critical point (critical velocity)	$a_{20} = \sqrt{\frac{(1+k_2)RT_{20}^*}{2k_2\mu_2}}$	$a_{21} = \sqrt{\frac{(1+k_2)RT_{21}^*}{2k_2\mu_2}}$	$a_{22} = \sqrt{\frac{2k_2RT_{22}^*}{(1+k_2)\mu_2}}$
11	Specific velocity	$\lambda_{20}=U_{20}/a_{20}$	$\lambda_{21}=U_{21}/a_{21}$	$\lambda_{22}=U_{22}/a_{22}$
12	Mach number	M_{20}	M_{21}	M_{22}

The stagnation pressure P_{20}^* is equal to the singlet oxygen generator pressure in COIL experiments.

Molar flow rate of the primary gas flow is

$$G_2 = \sqrt{\frac{1}{\mu_2 R} k_2 \left(\frac{2}{k_2 + 1} \right)^{\frac{k_2+1}{k_2-1}} \frac{P_{21}^* A_{21} q(\lambda_{21})}{\sqrt{T_{21}^*}}} = \sqrt{\frac{1}{\mu_2 R} k_2 \left(\frac{2}{k_2 + 1} \right)^{\frac{k_2+1}{k_2-1}} \frac{P_{22}^* A_{22} q(\lambda_{22})}{\sqrt{T_{22}^*}}} \quad (6)$$

Initial generalized momentum of the primary flow in 1-1 plane is

$$I_{21} = \frac{k_2 + 1}{2k_2} \mu_2 G_2 a_{21} z(\lambda_{21}) \quad (7)$$

Generalized momentum of the primary flow in 2-2 plane is

$$I_{22} = \frac{k_2 + 1}{2k_2} \mu_2 G_2 a_{22} z(\lambda_{22}) \quad (8)$$

d). Designations of mixed flow in chamber (cross section 3-3)

	Parameter	Designation
1	Molar flow rate	G_3
2	Molar weight	$\mu_3 = (\mu_1 G_1 + \mu_2 G_2) / (G_1 + G_2)$
3	Adiabatic exponent	k_3
4	Stagnation temperature	T_3^*
5	Temperature	T_3
6	Stagnation pressure	P_3^*
7	Static pressure	P_3
8	Cross section area	A_3
9	Gas velocity in critical point (critical velocity)	$a_3 = \sqrt{\frac{2k_3RT_3^*}{(1+k_3)\mu_3}}$
10	Absolute velocity	U_3
11	Specific velocity	$\lambda_3 = U_3/a_3$
12	Mach number	M_3
13	Recovered pressure (Pitot pressure)	$P_p = P_3^* q(\lambda_3) / q(1/\lambda_3)$

$$\mathbf{G}_3 = \sqrt{\frac{1}{\mu_3 \mathbf{R}} k_3 \left(\frac{2}{k_2 + 1} \right)^{\frac{k_3 + 1}{k_3 - 1}} \frac{\mathbf{P}_3^* \mathbf{A}_3 \mathbf{q}(\lambda_3)}{\sqrt{\mathbf{T}_3^*}}} \quad (9)$$

Initial generalized momentum of the mixed flow in 3-3 plane is

$$\mathbf{I}_3 = \frac{k_3 + 1}{2k_3} \mu_3 \mathbf{G}_3 \mathbf{a}_3 \mathbf{z}(\lambda_3) \quad (10)$$

e). The modified expressions in the case of axial conical nozzle for driver gas flow have to be used for a molar flow rate and a generalized momentum [6, 7].

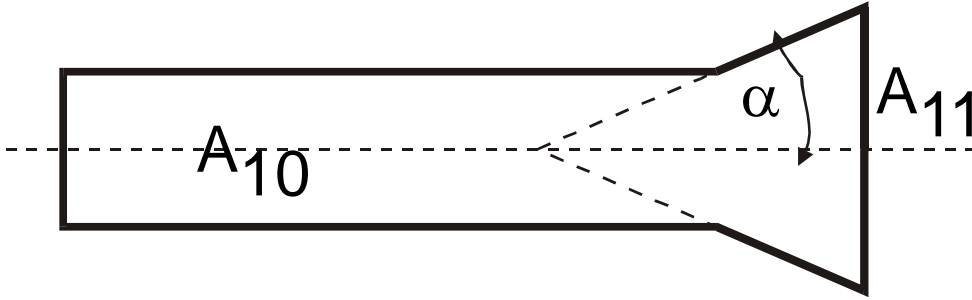


Fig.2

Molar flow rate is

$$\mathbf{G}_1 = \sqrt{\frac{1}{\mu_1 \mathbf{R}} k_1 \left(\frac{2}{k_1 + 1} \right)^{\frac{k_1 + 1}{k_1 - 1}} \frac{\mathbf{P}_{11}^* \mathbf{A}_{11} \mathbf{q}(\lambda_{11})}{\sqrt{\mathbf{T}_{11}^*}} \frac{2 \cos(\alpha)}{1 + \cos(\alpha)}} \quad (11)$$

The generalized momentum of the driver gas flow in the 1-1 plane is

$$\mathbf{I}_{11} = \frac{k_1 + 1}{2k_1} \mu_1 \mathbf{G}_1 \mathbf{a}_{11} \left[\lambda_{11} \left(\frac{4 \cos(\alpha) k_1}{(k_1 + 1)(1 + \cos(\alpha))} - \frac{2(k_1 - 1)(1 + \cos(\alpha) + \cos^2(\alpha))}{3(k_1 + 1) \cos(\alpha)(1 + \cos(\alpha))} \right) + \frac{1}{\lambda_{11}} \right] \quad (12)$$

Here λ_{11} is the reduced gas velocity at the nozzle exit, α is the angle between axis and the nozzle wall.

1.3 Equations.

a) Four conservation laws for the mass flow rates, energy, entropy and momentum at the cross sections 1–1 and 2–2 of the mixing chamber are used. Constancy of the cross section area of the mixing chamber is also assumed.

$$\mathbf{T}_{21}^* = \mathbf{T}_{22}^* ; \quad \mathbf{T}_{11}^* = \mathbf{T}_{12}^* \quad (13)$$

$$\frac{\mathbf{P}_{21}^* \mathbf{A}_{21} \mathbf{q}(\lambda_{21})}{\sqrt{\mathbf{T}_{21}^*}} = \frac{\mathbf{P}_{22}^* \mathbf{A}_{22} \mathbf{q}(\lambda_{22})}{\sqrt{\mathbf{T}_{22}^*}} \quad (14)$$

$$\frac{\mathbf{P}_{11}^* \mathbf{A}_{11} \mathbf{q}(\lambda_{11})}{\sqrt{\mathbf{T}_{11}^*}} = \frac{\mathbf{P}_{12}^* \mathbf{A}_{12} \mathbf{q}(\lambda_{12})}{\sqrt{\mathbf{T}_{12}^*}} \quad (15)$$

$$\mathbf{P}_{21}^* = \mathbf{P}_{22}^* \quad (16)$$

$$\mathbf{P}_{11}^* = \mathbf{P}_{12}^* / \sigma \quad (17)$$

$$I_{11} + I_{21} + P_{21} dA = I_{12} + I_{22} \quad (18)$$

$$A_{11} + A_{21} + dA = A_{12} + A_{22} = A_3 \quad (19)$$

$$P_{21} = \pi(\lambda_{21}) \mathbf{P}_{21}^* \quad (20)$$

List of the known parameters

Stagnation temperatures	$\mathbf{T}_{21}^*, \mathbf{T}_{11}^*$
Flow rates	G_1, G_2
Cross section areas	A_{11}, A_{21}, dA, A_3
Initial reduced velocity of the driver gas. This value is determined by expansion ratio of nozzles for driver gas	λ_{11}
Reduced velocity of the oxygen flow at the aerodynamic throat	$\lambda_{22}=1$
Total pressure losses	σ

List of the known parameters

Reduced velocities	$\lambda_{21}, \lambda_{12}$
Stagnation pressures	$\mathbf{P}_{21}^*, \mathbf{P}_{11}^*$
Cross section areas	A_{12}, A_{22}
Pressure	P_{21}

One has 7 equations (14)-(20) and 7 unknown quantity $\lambda_{21}, \lambda_{12}, \mathbf{P}_{21}^*, \mathbf{P}_{11}^*, A_{12}, A_{22}, P_{21}$.

Simple computer code allows to solve these equations and to find values

$\lambda_{21}, \lambda_{12}, \mathbf{P}_{21}^*, \mathbf{P}_{11}^*, A_{12}, A_{22}, P_{21}$.

Assuming that primary gas between 0-0 and 1-1 planes is isentropic ($\mathbf{T}_{20}^* = \mathbf{T}_{21}^*, \mathbf{P}_{20}^* = \mathbf{P}_{21}^*$) the reduced velocity of the primary gas at the plane 0-0 can be found from the correlation

$$\mathbf{q}(\lambda_{20}) = A_{21} \mathbf{q}(\lambda_{21}) / A_{20}$$

If $A_{20} \leq A_{22}$ then it means the geometrical throat occurs at the plane 0-0 rather than at the plane 2-2 and $\lambda_{20}=1$. In this case the assumption $\mathbf{P}_{20}^* = \mathbf{P}_{21}^*$ is not valid, $\mathbf{P}_{20}^* \geq \mathbf{P}_{21}^*$ and SOG pressure is determined by geometrical throat A_{20} .

b) After that one can find parameters of mixed stream ($\lambda_3, \mathbf{P}_3^*, P_3, T_3, P_p$) at the section 3-3 from equations

$$A_{11} + A_{21} + dA = A_3$$

$$I_{11} + I_{21} + P_{21} dA = I_3$$

$$G_1 + G_2 = G_3$$

The stagnation temperature of mixed stream

$$\mathbf{T}_3^* = \frac{Q + G_1 \mathbf{T}_{11}^* C_{p1} + G_2 \mathbf{T}_{21}^* C_{p2}}{G_1 C_{p1} + G_2 C_{p2}}, \text{ where } Q \text{-is the heat power released in the mixed stream,}$$

C_{pi} is the specific molar heat capacity.

1.4 Results of calculations and tests.

The main purpose of this simplified model was prediction of the primary gas stagnation pressure \mathbf{P}_{20}^* and determination influence of the geometrical and gas flow conditions on parameters of the completely mixed flow. In fact \mathbf{P}_{20}^* is the pressure inside SOG reaction zone.

About aerodynamic tests briefly. The aerodynamic tests of these nozzle banks have been performed with air as the primary gas and nitrogen as the driver gas. The next pressures have been measured: stagnation pressure of the primary gas (\mathbf{P}_{20}^*), static pressure of the mixed flow P_3 , distribution of the Pitot pressure across the mixing chamber. Some results of calculations and theirs comparison with experimental aerodynamic tests of the developed nozzle banks are presented.

1.4.1 Nozzle bank with cylindrical nozzles for driver nitrogen.

The sketch of this nozzle bank is presented in Fig.3.

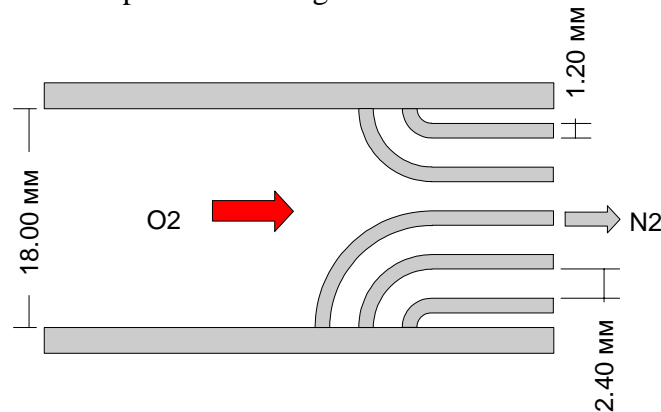


Fig.3

The nozzle bank consists of 70 cylindrical nozzles with i.d. 0.95 mm, o.d.1.2 mm. The outlet cross section area of the nozzle bank (1-1 plane) is rectangular 18×53 mm². The geometrical and other parameters are in Table.

A_{20}	4.6cm ²
A_{11}	0.495cm ²
A_{21}	8.75 cm ²
dA	0.295cm ²
A_3	9.54cm ²
λ_{11}	=1 for cylindrical nozzles

Dependencies of the primary gas stagnation pressure P^*_{20} and static pressure in the mixing chamber P_3 on the driver N₂ molar flow rate are presented in fig 4 and 5

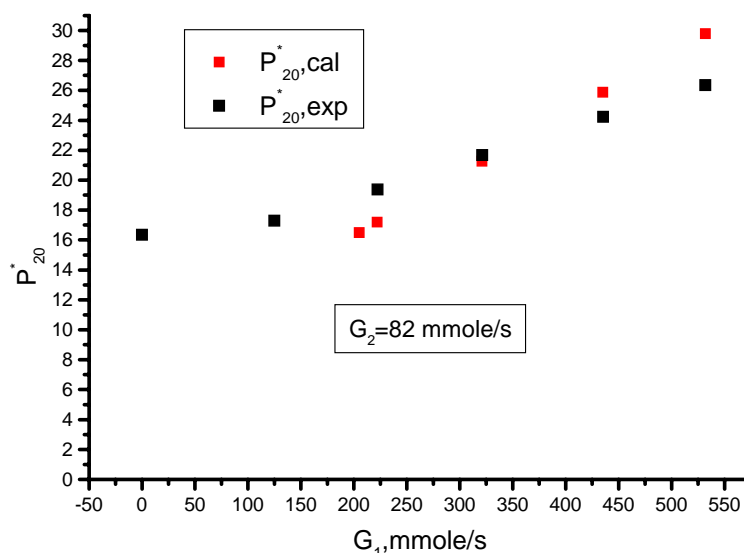


Fig.4. Dependence of the primary gas stagnation pressure P^*_{20} on the driver nitrogen molar flow rate G_1 . Assumed that the pressure losses of the driver nitrogen are absent ($\sigma=1$).

Calculation shows that $\lambda_{20}=1$ or $M_{20}=1$ at $G_1 \approx 200$ mmole/s. It means at these conditions the throat for primary flow located in plane 0-0. The calculated values P_{20}^* and P_3 are in a good agreement with measured one.

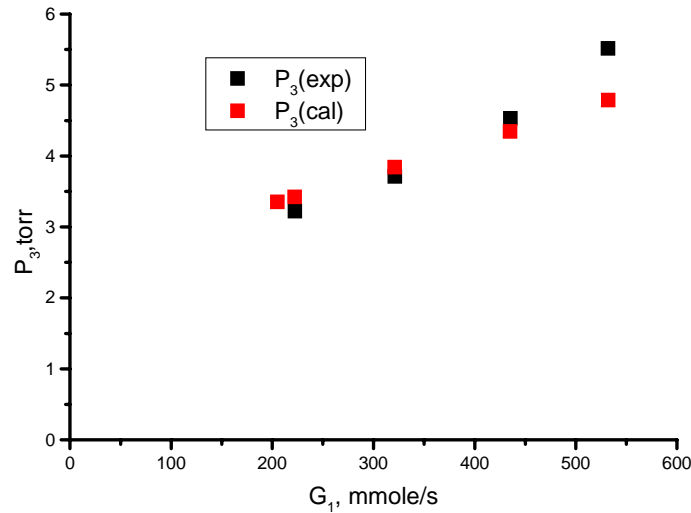


Fig.5. Dependence of the static pressure P_3 of the mixed flow on the driver gas molar flow rate G_1 .

Dependence of the primary gas stagnation pressure P_{20}^* on the primary gas molar flow rate. Calculation has been performed for $G_1=532$ mmole/s and different σ values.

G_2 , mmole/s	P_{20}^* (experiment)	$\sigma=1$ P_{20}^*	$\sigma=0.5$ P_{20}^*	$\sigma=0.25$ P_{20}^*
39	18.4	25.3	23	19.4
60	22.	27.5	25	21.2
82	26.3	29.7	27.1	23
100	30.	31.6	28.8	24.5

The supersonic jets of the driver nitrogen expand more strongly with the decrease of the primary gas flow rate G_2 . In this case the expected pressure losses of the driver gas are higher (σ is less). So calculations are in agreement with experimental results at less primary gas molar flow rate when σ is small and at $\sigma \approx 1$ for higher G_2 .

1.4.2 Nozzle bank with the conical supersonic nozzles for driver nitrogen.

The elementary periodically repeated cell of this nozzle bank with height of 16.5mm and width of 8mm ($A_3=1.32\text{cm}^2$) has 8 conical supersonic nozzles with expansion ratio 3 (calculated $\lambda_{11}=1.86$), angle $\alpha=20^\circ$ and cross section area of $A_3=16.5 \times 8 \text{ mm}^2$. Diameter of the nozzle throat is equal to 0.9mm (or $A_{10}=0.00636 \times 8=0.0508\text{cm}^2$). Other parameters are indicated in the Table.

A_{20}	0.666cm^2
A_{10}	0.0508cm^2
A_{11}	0.153cm^2
A_{21}	0.66cm^2
dA	0.507 cm^2
σ	1

Dependencies of the primary gas stagnation pressure P_{20}^* on molar flow rates of the driver nitrogen G_1 and on the primary G_2 flow rates are presented in fig. 6 and 7.

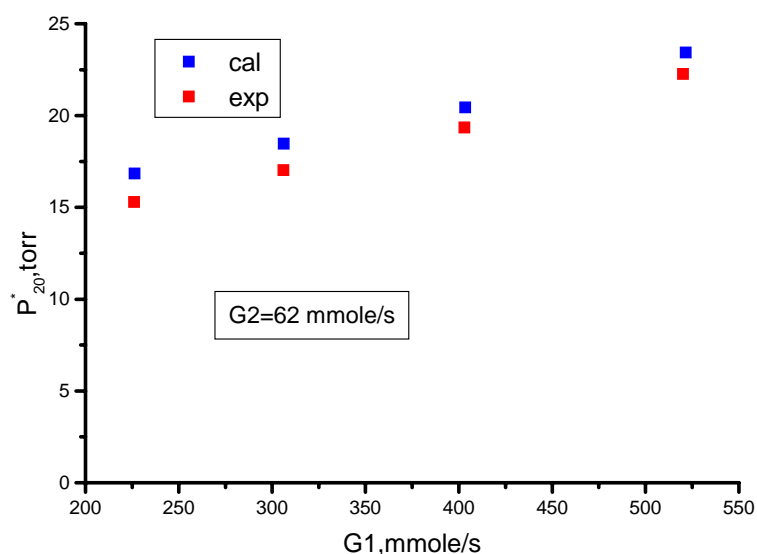


Fig.6. Dependence of the primary gas stagnation pressure P_{20}^* on the driver nitrogen molar flow rate G_1

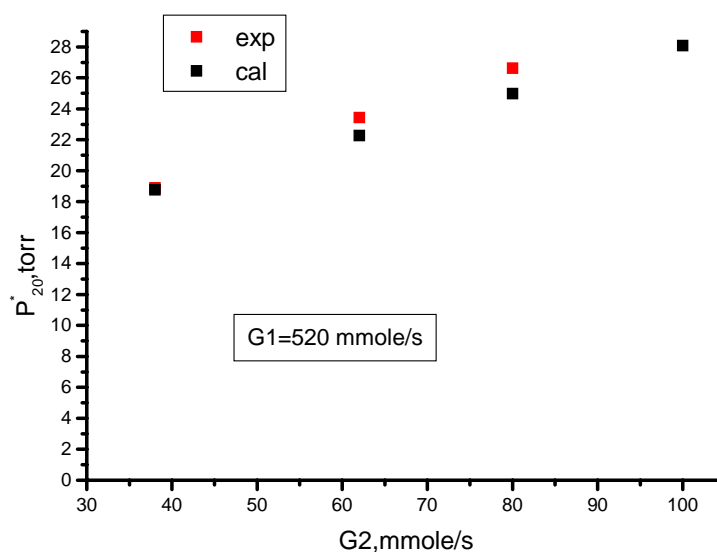


Fig.7. Primary gas stagnation pressure P_{20}^* as a function of the molar flow rate G_2 .

Parameter $P\tau = V_{\text{sog}}(P_{20}^*)^2 / G_2 / 18260$ (where $P = P_{20}^*$ and τ is the primary gas residence time inside the singlet oxygen generator with volume of $V_{\text{sog}} = 300 \text{ cm}^3$, G_2 is measured in mmole/s) calculated for the singlet oxygen generator at $G_1 = 520 \text{ mmole/s}$ is presented in fig 8. This parameter $P\tau$ defines $\text{O}_2(^1\Delta)$ yield from SOG. For each G_1 there is optimal G_2 to achieve minimal $P\tau$.

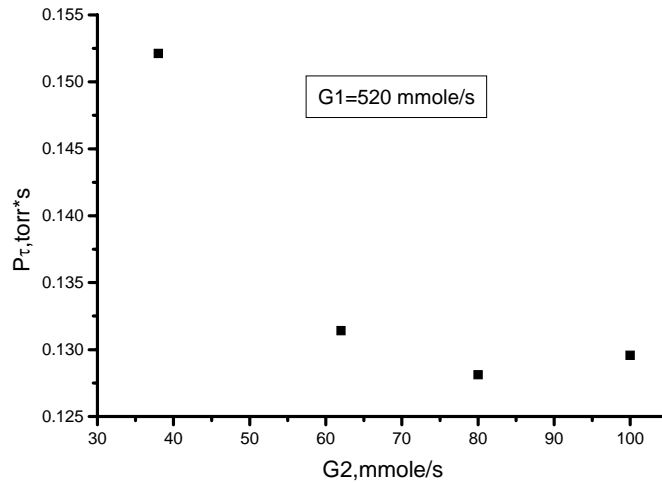


Fig.8. Dependence of $P\tau$ on the primary gas molar flow rate G_2 .

1.4.3 Nozzle bank with shaped supersonic micro nozzles.

Let us place the shaped supersonic micro nozzles on the tubes the nozzle bank (fig 3) and consider effect of the driver nitrogen reduced velocity λ_{11} (or initial Mach number) on SOG pressure and some important parameters of the mixed flow. The nozzle bank has 70 nozzles. Total critical cross section area $A_{10}=0.495\text{cm}^2$, other parameters are presented in the table. Results of the calculations are presented on fig 9÷11.

G_1	0.55 mole/s
G_2	0.08 mole/s
σ	1
A_{20}	4.6cm^2
A_{10}	0.495cm^2
A_{11}	$A_{10}/q(\lambda_{11})$
dA	0.295cm^2
A_3	9.54cm^2
A_{21}	A_3-dA-A_{11}
λ_{11}	Variable parameter
α	0°

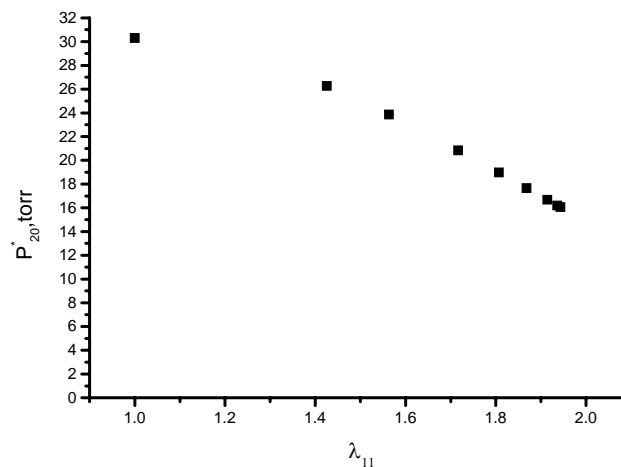


Fig.9. Dependence of the primary gas total pressure P_{20}^* on the reduced driver gas velocity λ_{11} at fixed molar flow rate G_1

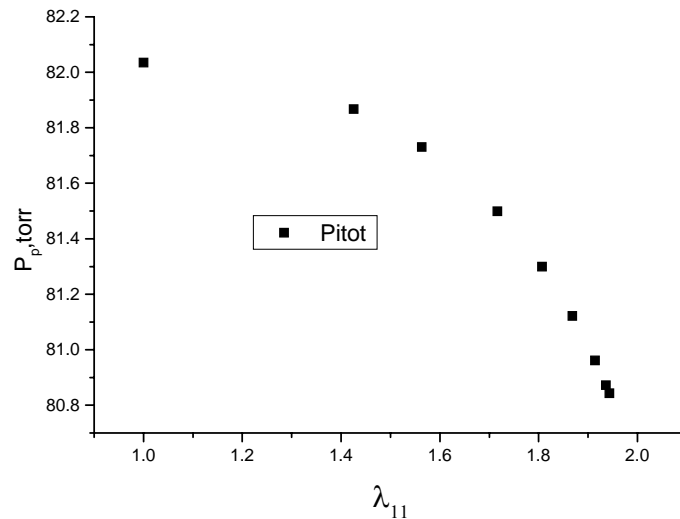


Fig.10. Dependence of the Pitot pressure on the reduced driver gas velocity λ_{11} at fixed molar flow rate G_1

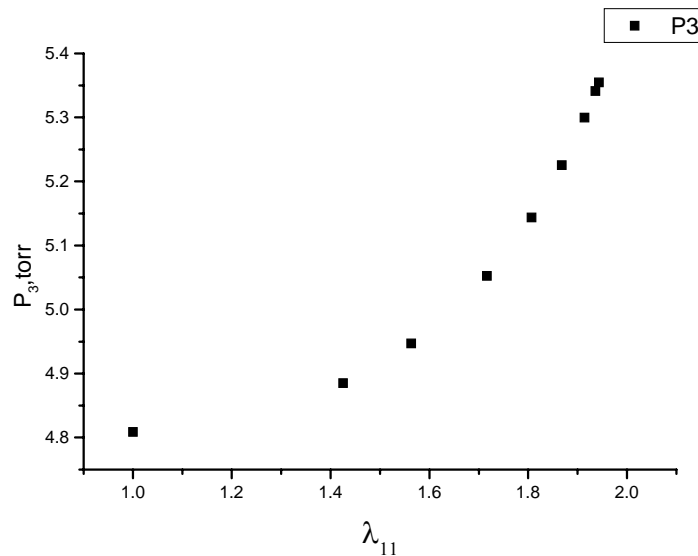


Fig.11. Dependence of the static pressure P_3 on the reduced driver gas velocity λ_{11} at fixed molar flow rate G_1 .

Increasing of the initial reduced velocity λ_{11} (Mach number M_{11}) of the driver nitrogen results in the decrease of choking effect for primary gas, reduction SOG pressure and singlet oxygen losses due to decreasing of the over-expansion N_2 jets. On the other hand the increase of the driver nitrogen Mach number has very small effect on the Pitot pressure, but leads to increase of the static pressure P_3 . Maximal initial reduced velocity λ_{11} of the driver nitrogen is restricted by N_2 condensation inside output stream and depends on initial stagnation temperature T_{11}^* .

The results of calculations are in a good agreement with measured values. This model allows qualitatively (and often quantitatively even) to predict dependencies of different parameters on the nozzle bank geometry and the initial gas flows conditions. The choking effect for the primary gas is necessary to take into account at designing of singlet oxygen generator for an ejector nozzle bank.

Minimal blockage of the oxygen flow and minimal $O_2(^1\Delta)$ losses take place at the employing the shaped micro nozzles with large Mach number for driver gas. Obviously, it's necessary to use additional methods enhancement of the mixing sonic/supersonic streams in this case.

2. Development of the scaleable nozzle bank design for (60÷80) mmole/s chlorine flow rate.

Advanced nozzle bank of the ejector COIL with additional nozzles for injection iodine vapor provides high local iodine concentrations at contact with the high-pressure oxygen and the fast iodine dissociation such as in the classical COIL. It's to be noted that processes in the oxygen-iodine mixture at expansion in the supersonic nozzle of the classical COIL are the same as at mixing with the driver nitrogen in ejector laser: a) decreasing along flow the partial oxygen pressure, iodine and water vapor concentrations; b) accelerating gas flow to supersonic velocities and decreasing static temperature of the active medium.

So expansion rate of the active medium in the supersonic nozzle of the classical laser plays the same role as the mixing rate the oxygen-iodine mixture with cold high Mach number driver nitrogen in ejector COIL. For successful ejector COIL operation the mixing length should be the same as specific length of the density drop in the supersonic nozzle of the classical laser. It's possible if the transverse spatial period of the ejector nozzle bank is small enough.

The free expanding driver nitrogen jet is over expanded always at the aerodynamic throat plane and has cross section area more than at expansion in the calculated shaped supersonic nozzle. So the use of the calculated shaped supersonic micro nozzles for the driver nitrogen gives possibility to increase the duct minimal cross section area for oxygen stream and to decrease SOG pressure (see Fig.9). It's necessary to employ special mixing enhancement methods in this case (for example nozzle tabs similar as in Boeing ejector-like nozzle which produce streamwise vorticity for mixing enhancement with small pressure losses[8]).

SOG pressure and $O_2(^1\Delta)$ losses in the generator are due to blockage of the oxygen flow by design parts of the nozzle bank (the manifolds of the driver and secondary nitrogen nozzles) also. If these manifolds and nozzle outlets are located at different planes (to prevent summing the blockage of the oxygen flow) then it's possible to realize the minimal cross section area of the oxygen flow at the outlet plane of the driver nitrogen micro nozzles. So let the shaped supersonic micro nozzles are used for acceleration of the driver nitrogen and mixing of the flows take place downstream the nozzle bank outlet at the equal pressures P_{mix} for all flows.

Consider effect of the driver nitrogen stagnation pressure on the blockage oxygen flow at the fixed static pressure P_{mix} at the inlet of the mixing chamber. Let $G = \rho(\lambda)uF(\lambda) \equiv \rho(\lambda)a_{crit}F(\lambda)u/a_{crit} = \rho(\lambda)\lambda F(\lambda)a(\lambda)$ is mass flow rate of the driver nitrogen and $F(\lambda)$ is the total nozzle outlet cross section area which is sustained constant and determines the blockage of the oxygen stream

$$F_{outlet} \equiv F(\lambda) = G / (a_{crit} \lambda \rho(\lambda)) \quad (21)$$

Where a_{crit} is the sonic velocity at the throat, $\lambda = u/a_{crit}$ is the reduced gas velocity, $\rho(\lambda)$ is gas density.

Simplify expression (21) using well-known correlations $P = R\rho T = R\rho T_0(T/T_0)$; $R = R_0/m$; $\rho = P(T_0/T)/(RT_0) = P(P_0/P)^{(k-1)/k}/(RT_0)$;

$$\lambda = \lambda_{\infty} \left[1 - \left(\frac{P_{mix}}{P_0} \right)^{\frac{k-1}{k}} \right]^{0.5} \quad (22)$$

where $k=1.4$ is N_2 adiabatic exponent, P_0 and T_0 are stagnation pressure and temperature, R_0 is the universal gas constant, m is molar weight, $P \equiv P_{mix}$.

$$\begin{aligned}
F(\lambda) \equiv F(P_0/P_{\text{mix}}) &= [GRT_0 / (a_{\text{crit}} \lambda_{\infty} P_{\text{mix}})] \cdot \frac{1}{\left(\frac{P_0}{P_{\text{mix}}} \right)^{\frac{k-1}{2k}} \left[\left(\frac{P_0}{P_{\text{mix}}} \right)^{\frac{k-1}{k}} - 1 \right]^{0.5}} = \\
&= \frac{C}{\left(\frac{P_0}{P_{\text{mix}}} \right)^{\frac{k-1}{2k}} \left[\left(\frac{P_0}{P_{\text{mix}}} \right)^{\frac{k-1}{k}} - 1 \right]^{0.5}} \approx C \left(\frac{P_{\text{mix}}}{P_0} \right)^{\frac{k-1}{k}} = C \left(\frac{P_{\text{mix}}}{P_0} \right)^{\frac{2}{7}} \quad (23)
\end{aligned}$$

where $C = GRT_0 / (a_{\text{crit}} \lambda_{\infty} P_{\text{mix}})$ is constant.

Formula (23) gives dependence of the total outlet cross section area of the driver nitrogen nozzle on the stagnation pressure P_0 at the given fixed P_{mix} .

Let $P_{\text{mix}} = 10 \text{ torr}$. In this case the plot $y(x=P_0) = F(P_0)/F(P_0=1 \text{ atm})$ (fig.12) demonstrates twice decreasing outlet cross section area with the raise of the driver nitrogen stagnation pressure from 1 atm up to 13.6 atm.

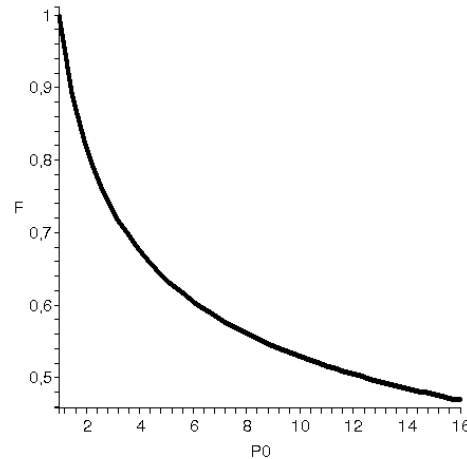


Fig. 12. Dependence $y = F(P_0)/F(P_0=1 \text{ atm})$ on the driver N_2 stagnation pressure. P_0 (in atm)

It's easily to explain such dependence. The raise of the stagnation pressure at the fixed P_{mix} results in increasing of Mach number M . The absolute and reduced gas velocities change slightly at large Mach numbers but the gas density increases due to decreasing of the static temperature. At the fixed driver N_2 molar flow rate and P_{mix} the required outlet cross section area F_{outlet} decreases $\sim 1/\rho \sim (P_{\text{mix}}/P_0)^{2/7}$ at the first approximation. The maximal possible $(P_0/P_{\text{mix}})_{\text{max}}$ value is restricted by driver N_2 condensation near nozzle's outlet [9]. The N_2 saturated vapor pressure as a function of the static temperature is presented in the Table.

T, °K	40	41	42	43	44	45	46	47	48	49
P, torr	0.07	0.12	0.19	0.3	0.46	0.69	1.02	1.47	2.09	2.91
T, °K	50	51	52	53	54	55	56	57	58	59
P, torr	4	5.43	7.27	9.61	12.56	16.23	20.76	26.3	33.02	41.09
T, °K	60	61	62	63	64	65	66	67	68	69
P, torr	50.73	62.14	75.56	91.25	109.5	130.5	154.7	182.3	213.7	249.2
T, °K	70	71	72	73	74	75	76	77	78	79
P, torr	289.3	334.2	384.3	440.2	502.2	570.5	646.1	729	820	918.9

Easily to see that saturated N_2 pressure $P \approx 10$ torr is reached at the static temperature $T \approx 53^\circ\text{K}$. Although condensation starts at overcooling of the supersonic jet $\Delta T \approx 35^\circ\text{K}$ and relaxation time τ is about $20\mu\text{s}$ ($u\tau \approx 1\text{cm}$) [9] one will count the feasible minimal static temperature $T \approx 53^\circ\text{K}$. If the driver N_2 stagnation temperature is T_0 then available static temperature drop inside nozzle is $(T_0/53^\circ)$ and available pressure drop equal to $(P_0/P_{\text{mix}}) = (T_0/53^\circ)^{k/(k-1)} = (T_0/53^\circ)^{7/2}$. For example, $P_0 = 3832\text{torr}$ or $\approx 5\text{atm}$ at $T_0 = 290^\circ\text{K}$ and $P_{\text{mix}} = 10\text{torr}$.

Such static pressure drop is reached in the nozzle with area ratio $(F_{\text{outlet}}/F_{\text{th}}) \approx 20$ or diameter ratio $(D_{\text{outlet}}/D_{\text{th}}) \approx 4.5$ (at neglecting by the boundary layer thickness). This nozzle provides acceleration N_2 flow to supersonic velocity with $\lambda \approx 2.215$ or $M \approx 4.75$.

If rows of the driver N_2 micro nozzles forms structure with square elementary cells, then it's possible to find area of this elementary cell F_{cell} at the given oxygen stagnation pressure P_{0,O_2} , throat cross section area F_{th} and ratio molar flow rates of the driver N_2 and oxygen $g = m_{O_2}G_{N_2}/m_{N_2}G_{O_2}$. Neglecting by the difference of the stagnation temperature and the critical sonic velocities one finds correlation

$$g = m_{O_2}G_{N_2}/m_{N_2}G_{O_2} \approx P_{0,N_2}F_{\text{th}}/P_{0,O_2}(F_{\text{cell}} - F_{\text{outlet}})$$

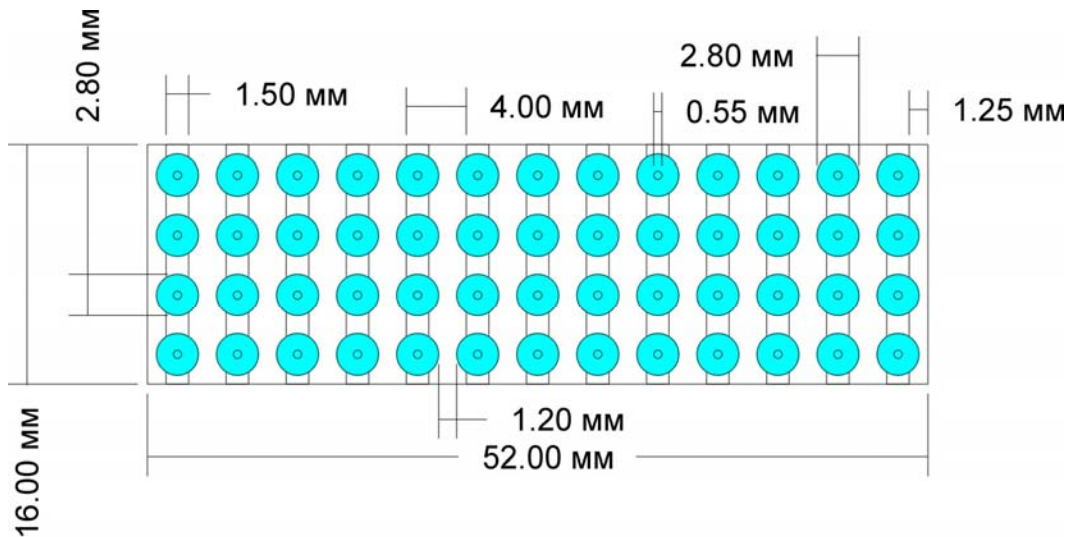
or

$$F_{\text{cell}} \approx F_{\text{outlet}} + P_{0,N_2}F_{\text{th}}/g P_{0,O_2} = F_{\text{th}}(1/q(\lambda) + P_{0,N_2}/g P_{0,O_2}) \quad (24)$$

where $q(\lambda) = F_{\text{th}}/F_{\text{outlet}}$ is well-known gasdynamic function.

Our experience of operation with different designs of the ejector-like nozzle banks shows that injection of the secondary $N_2 + I_2$ may lead to the raise SOG pressure not more on $1 \div 3$ torr only. Explanation of such behavior connected with local ejector effect due to $N_2 + I_2$ stagnation pressure several times higher than P_{0,O_2} and premixing additional $N_2 + I_2$ flow is accompanied by the raise the effective $(N_2 + I_2 + O_2)$ stagnation pressure. As result the influence of the secondary N_2 injection on SOG pressure is very weak and formula (24) is valid.

The throat cross-section areas F_{th} and F_{cell} in (24) are determined from compromise requirements. Indeed, from one hand these values should be as small as possible from the view point of the fast mixing but from the other hand decreasing throat diameter is accompanied by the raise relative effect of the boundary layer thickness in the nozzles, increasing the driver N_2 pressure losses in supplying manifolds and general design complication. We employed for driver N_2 supplying manifold medical needles of 0.8mm o.d. and of 0.55mm i.d. The conical micro nozzles with angle between axis and wall equal to 20° were installed on the end of these needles. The outlet diameter was equal to 2.8mm (the wall thickness at the outlet was equal to 0.1mm). The estimation of the elementary cell area determined from (24) at $g = 5$ gives $F_{\text{cell}} \approx 14.3\text{mm}^2$. We developed nozzle bank with $4 \times 4\text{mm}^2$ elementary cell (Fig. 13). Four of 0.8mm supplying tubes were connected to vertical manifold (medical needles of 1.5mm o.d. and 1.2mm i.d.) which is supplied from two sides. Cross section area of this manifold exceeds area of two supplying tubes more than 2 times to prevent pressure gradient inside vertical manifold. Tests of these manifolds demonstrate enough its' strength at pressure more 10 atm.



$$F(N_1)=0.062\text{cm}^2; 52F(N_1)=3.22\text{cm}^2; F(O_2)=(8.32-3.22)\text{cm}^2=5.1\text{cm}^2$$

Fig.13. General scheme of the driver N_2 nozzle array with $4 \times 4 \text{mm}^2$ elementary cell. The edge wall thickness of the nozzle is of 0.1mm.

Special turbulizing tabs at the bronze micro nozzle outlet with thickness of 0.1mm, length of $L=1\text{mm}$ and width of $\pi D_{\text{outlet}}/8$ were installed (Fig.14.). These tabs were oriented parallel to channel walls where the distances between nozzles are minimal and equal to 1.2mm.

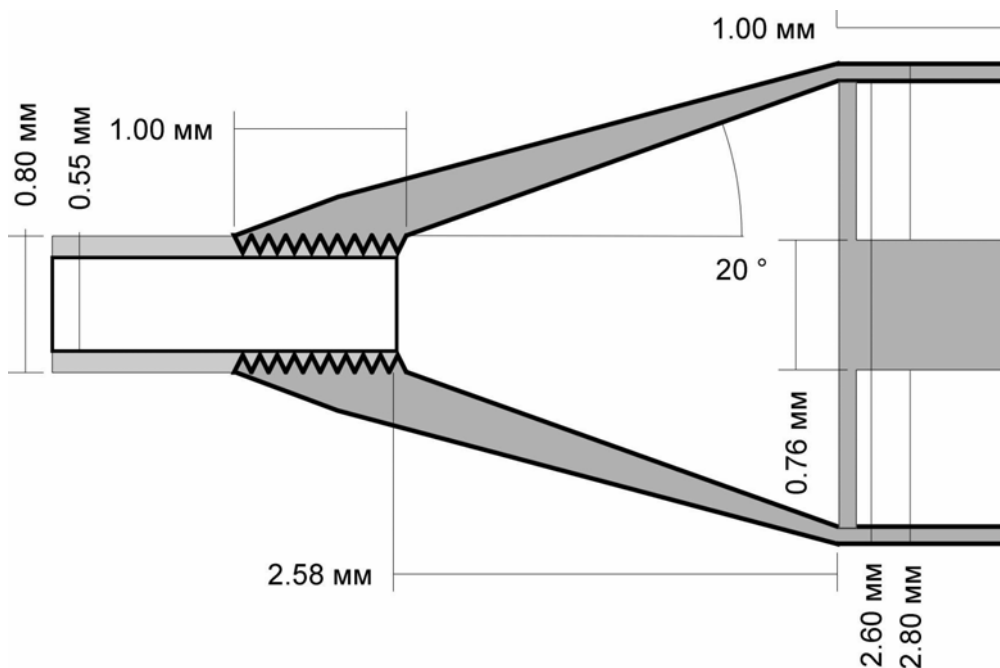


Fig.14. The driver N_2 supplying line with micro nozzle.

Secondary N_2 with iodine vapor was injected through planar manifolds $1 \times 5 \text{mm}^2$ with 8 orifices of 0.8mm. The wall thickness of the copper I_2 manifold was equal to 0.05mm. Side view of the horizontal section of the nozzle bank is presented in Fig.15. Iodine planar manifolds are located upstream micro nozzles to prevent summing of the oxygen flow blockage.

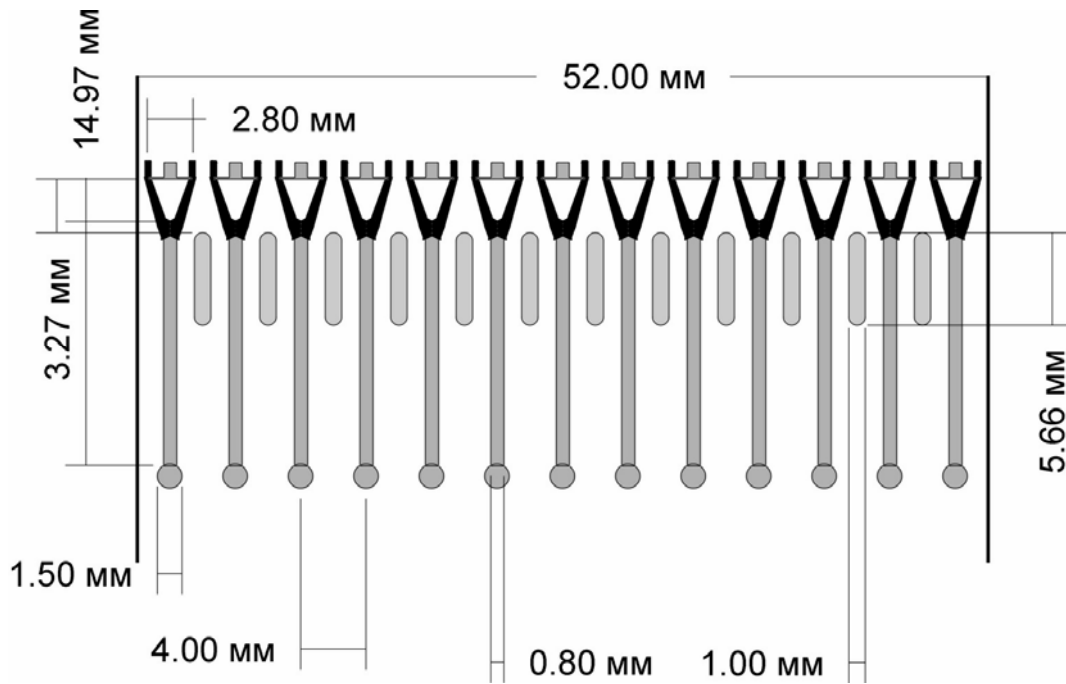


Fig. 15. Side view of the ENB horizontal section.

The iodine manifolds and 52 driver N₂ supplying tubes block of 2.18cm² of 8.32cm² nozzle bank area or 26% of the total cross section only. Of course, the real blockage effect higher due to presence of the boundary layers. Given ejector nozzle bank has been manufactured in LPI SB. The photograph of the front side of one is presented in Fig. 16.

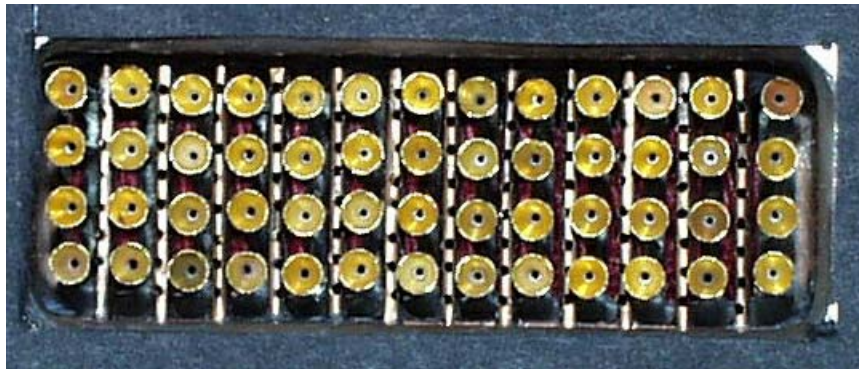


Fig.16. Photograph of the ENB front side.

Cold tests with the usage of air instead of O₂(¹Δ) demonstrated that the driver and secondary N₂ flow rates had weak influences on P_{SOG}:

- 1) G_{air}=80mmole/s; G_{driverN2}=G_{sec.N2}=0; P_{SOG}=19.3torr. This SOG pressure is minimal possible for given nozzle bank and determined by the ENB design only.
- 2) G_{air}=80mmole/s; G_{sec.N2}=60mmole/s; G_{driverN2}=0; P_{SOG}=22.6torr;
- 3) G_{air}=80mmole/s; G_{sec.N2}=60mmole/s; G_{driverN2}=530 mmole/s; P_{SOG}=23.3torr;
P_{cavity}=7torr; P_{Pitot}=82torr (the inlet of the Pitot tube was located on the distance of 85mm downstream nozzle bank in the central point of the duct where it's height was equal to 25.5mm; P_{Pitot}~1/h_{duct}).The static pressure was measured near wall on 25mm upstream this plane (under optical axis).

Obviously, static pressure near Pitot tube should be less measured value P_{cavity}=7torr due to the duct expansion because estimation of the Mach number at using the measured static pressure P_{cavity} gives less value M=2.95. Real M>2.95.

The main concept of the nozzle bank presented in Fig.16 may be adapted to larger nozzle bank. The tested nozzle bank may be considered as periodically repeating element of the grid nozzle

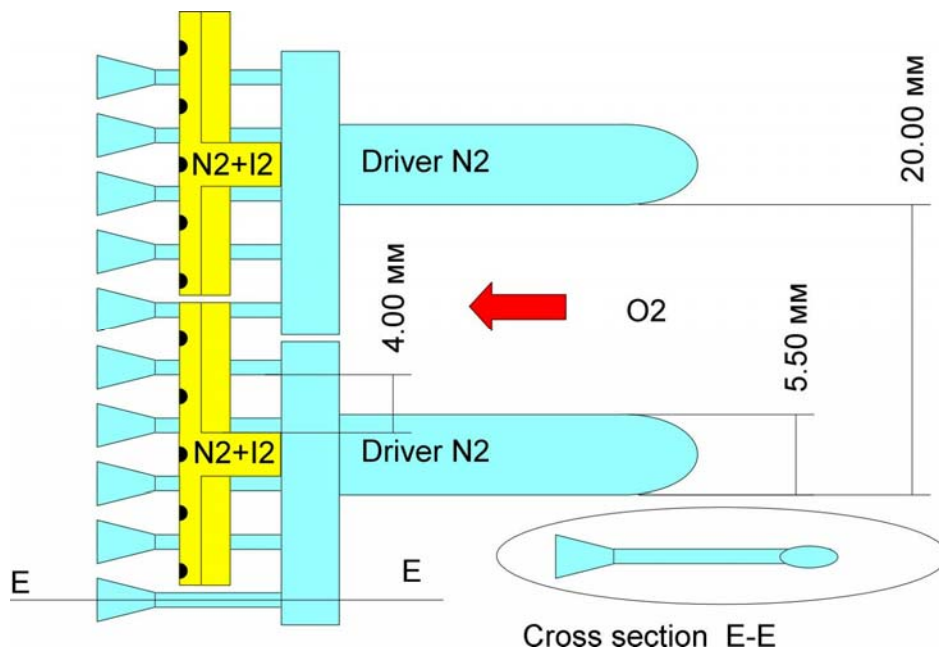


Fig. 17. Two blades of the scalable ejector nozzle bank with $4 \times 4 \text{ mm}^2$ elementary cell (top view). Tabs on the micro nozzles are not shown.

It's well-known that volumetric heat release in the supersonic flow with constant cross section may cause the thermal crisis. Turning duct walls can't eliminate this negative influence of the heat release. But according equation for gas velocity u of the flow with heat release dQ [7]

$$(M^2 - 1) \frac{du}{u} = \frac{dF}{F} - \frac{k-1}{a^2} dQ$$

thermal crisis may be suppressed. Indeed, if all stream lines diverge at the nozzle bank outlet, the cross section area of all elementary flow tubes increases then at $dF/F \approx (k-1)dQ/a^2 > 0$ compensation of the volumetric heat release influence takes place. By other words, the axes of the micro nozzles in the each vertical row must be turned relatively each other on some small angle $d\theta$ which depends on value dQ . All axes must intersect in one point and micro nozzle outlets are located on some cylindrical surface. For example, let $d\theta/dy = 0.1^\circ \text{ mm}^{-1}$ (radius of cylindrical surface equal to 57.3cm) then axes of the neighboring micro nozzles should be tuned on the angle $d\theta = 0.4^\circ$ but wall cavity must be turned on angle $\pm 0.05^\circ H$ for considered hardware. Where H is the nozzle bank height in mm. General scheme of one vertical row of the driver N_2 nozzles is presented in Fig. 18

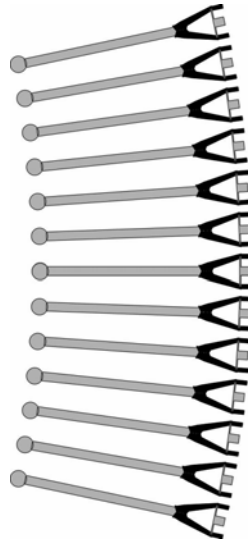


Fig.18. General view of the driver N₂ nozzle array (at suppression of the thermal crisis in the supersonic flow downstream nozzle bank).

2.1. Appendix

Estimation of the static pressure drop and the stagnation pressure losses inside supplying driver N₂ tubes.

Let us find pressures P₁ and P₀₁ in the initial cross section of the small supplying tubes for driver N₂ counting d=d_{tube}=0.055cm, L=1.5cm, m=28g/mole, P_{0,outlet}= P₀₂=5atm = 3800torr, G_{N2}=10.mmole/s, G≡m G_{N2}=0.28g/s, k=1.4.

Coefficient of the turbulent gas flow resistance ζ in the smooth tubes may be estimated with using the Blazius formula for the turbulent flow in the smooth-wall tube [7]

$$\zeta = \frac{0.316}{\text{Re}^{0.25}} \approx 0.0228$$

where $\text{Re} = \frac{\rho \mathbf{u}_{av} \mathbf{d}}{\mu} = \frac{1.273 \mathbf{G}}{\mu \mathbf{d}} \approx 3.7 \cdot 10^4$ is Reynolds number,

$\mu \approx 1.75 \cdot 10^{-4}$ g/cm*s is gas viscosity, $G = \rho \mathbf{u}_{av} \cdot \pi d^2 / 4 = 0.28$ g/s is mass flow rate through tube with d=0.055cm.

The reduced gas velocity at the tube inlet λ₁ may be determined from well-known correlation for flow in the tube with friction [7] (at outlet reduced gas velocity λ₂=1):

$$\frac{1}{\lambda_1^2} - 1 - \ln \frac{1}{\lambda_1^2} = \frac{2k}{k+1} \cdot \zeta \cdot \frac{L}{d} \equiv \chi$$

λ₁≈0.61 at L=1.5cm, d=0.055cm, k=1.4, χ=0.725

Writing mass flow rate at the both tube ends one finds correlation of the static pressure at the initial cross section of the supplying tube p₁ with the stagnation pressure P₀₂ at the tube outlet (nozzle throat)

$$P_{02} q(\lambda_2) = p_1 y(\lambda_1)$$

where $q(\lambda) = \left(\frac{k+1}{2} \right)^{\frac{1}{k-1}} \lambda [1 - (k-1)\lambda^2 / (k+1)]^{1/(k-1)}$; $y(\lambda) = \left(\frac{k+1}{2} \right)^{\frac{1}{k-1}} \cdot \frac{\lambda}{1 - \frac{k-1}{k+1} \cdot \lambda^2}$ are well-known gas

dynamic functions.

Let $P_{02}=5\text{atm}$; $\lambda_1=0.61$; $\lambda_2=1$; $k=1.4$; $\pi(\lambda_1)=\left[1-\frac{k-1}{k+1}\cdot\lambda_1^2\right]^{\frac{k}{k-1}}=0.7992$; $\pi(\lambda_2)=0.5283$ then $q(\lambda_2)=1$;
 $y(\lambda_1)=1.0258$; $p_1=P_{02}/y(\lambda_1)=5\text{atm}/1.0258=4.875\text{atm}$; $P_{01}=p_1/\pi(\lambda_1)=p_1/0.7992\approx 6.1\text{atm}$; pressure drop
 $p_1-p_2=p_1-\pi(\lambda_2)P_{02}=3.46\text{atm}$; stagnation pressure losses $P_{01}-P_{02}\approx 1.1\text{atm}$.

3. Pitot pressure distributions in cross sections of the mixing chamber.

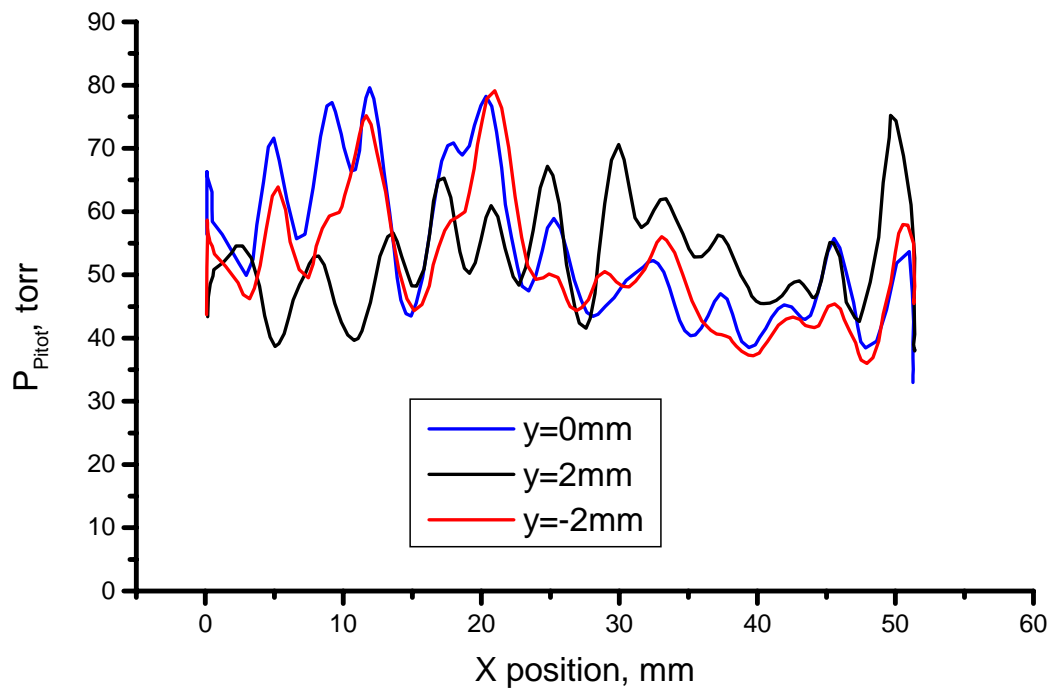
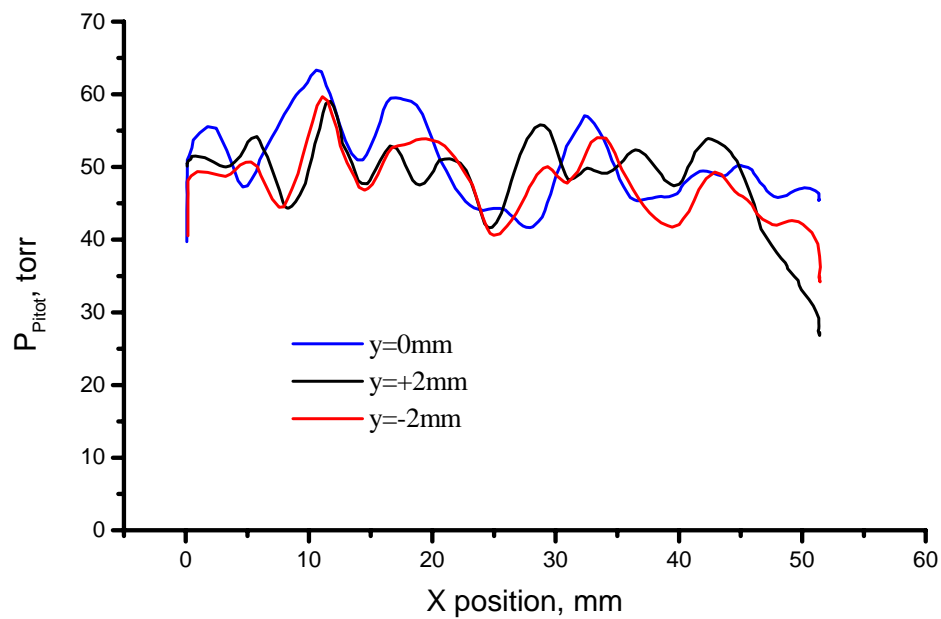
The mixing rate of the oxygen-iodine mixture with cold high-pressure driver nitrogen is a very important parameter of ejector laser and performs the same role as expansion and acceleration of the active medium in the classical supersonic nozzle. Measurements of the Pitot pressure distributions in the cross sections at the different distances from nozzle bank give information about mixing rate primary and driver flows and about potential possibility of the pressure recovery in a supersonic diffuser.

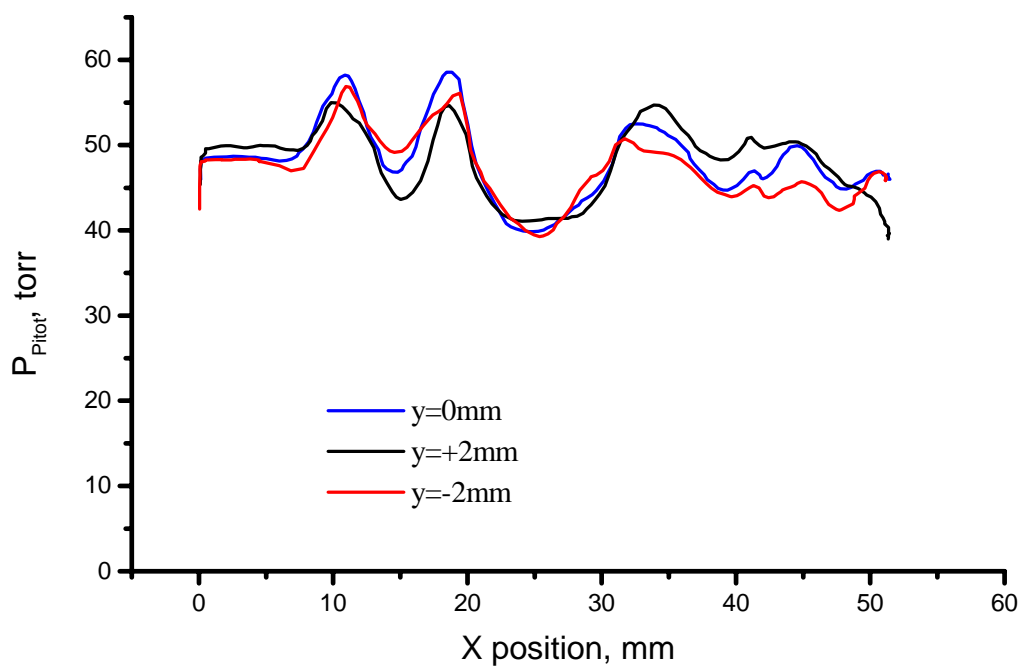
The special device which allowed to replace the Pitot tube with outer diameter 1.5mm on all duct wideness ($\Delta x\sim 50\text{mm}$) during $\sim(5\div 7)\text{sec}$ test with the position coordinate monitoring has been developed. This device had possibility also to change the scanning line location of the Pitot pressure gauge in vertical direction (along Y axis).

Pitot pressure distribution $P_{\text{Pitot}}(x)$ was measured in the special mixing chamber with parallel side walls. Low and upper walls were turned on the angle $\pm 1^\circ$ relatively the duct axis to compensate influence of the boundary layers. Nozzle banks were connected to mixing chamber with aid of the rubber O-ring seal and it was possible the appearance of small non-coincidence axes of the nozzle bank and duct. This might result in small shift of the periodical flow structure. The nozzle bank (fig. 16) has periodical structure with the spatial periods $\Delta x_b = \Delta y_b = 4\text{mm}$ and Pitot tube scanning was carried out with step $\Delta y = \pm 2\text{mm}$ relatively the central duct plane to guarantee determination of the Pitot pressure within the limits of one period. Since the side walls of the mixing chamber were parallel the growth of the boundary layers generates of the weak oblique shock waves which might produce flow inhomogeneity with the spatial scale considerably more than 4mm. Therefore it's necessary to make estimations of the mixing efficiency on the base of the damping of pressure pulsations with specific small scale $\sim \Delta x_b$.

In the case nozzle bank with 20° conical tabs free nozzles described in item 1.4.2 having specific spatial period $\Delta x = 8\text{mm}$ the Pitot pressure distributions $P_{\text{Pitot}}(x)$ were considerably inhomogeneous up to distances $\Delta z \sim 113\text{mm}$ from the mixing chamber inlet. This indicates on bad flow mixing.

Distributions $P_{\text{Pitot}}(x)$ for the scalable nozzle bank (fig. 16) at scanning along the central line of the duct ($y=0$) and at $\Delta y=\pm 2\text{mm}$ shifted scanning lines are presented in fig.19÷21. Tests were made at the next molar flow rates: primary gas (air) $G_{1a} = 75\text{mmole/s}$, secondary nitrogen $G_{2N} = 60\text{mmole/s}$ and driver nitrogen $G_{DN} = 250$ and 500mmole/s .

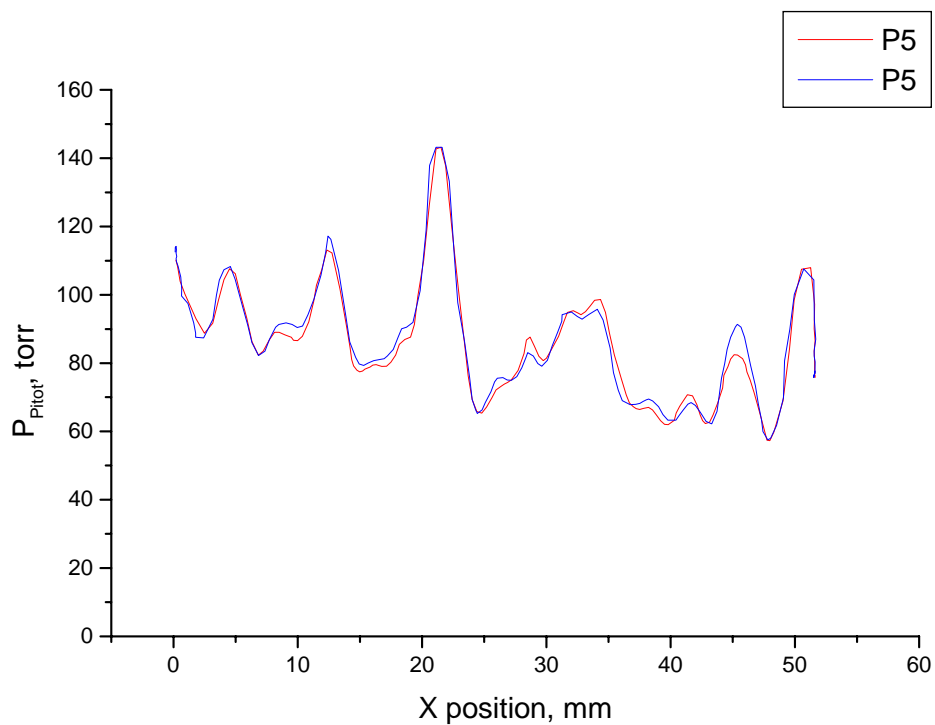
a) $\Delta z = 45\text{mm}$ b) $\Delta z = 83\text{mm}$



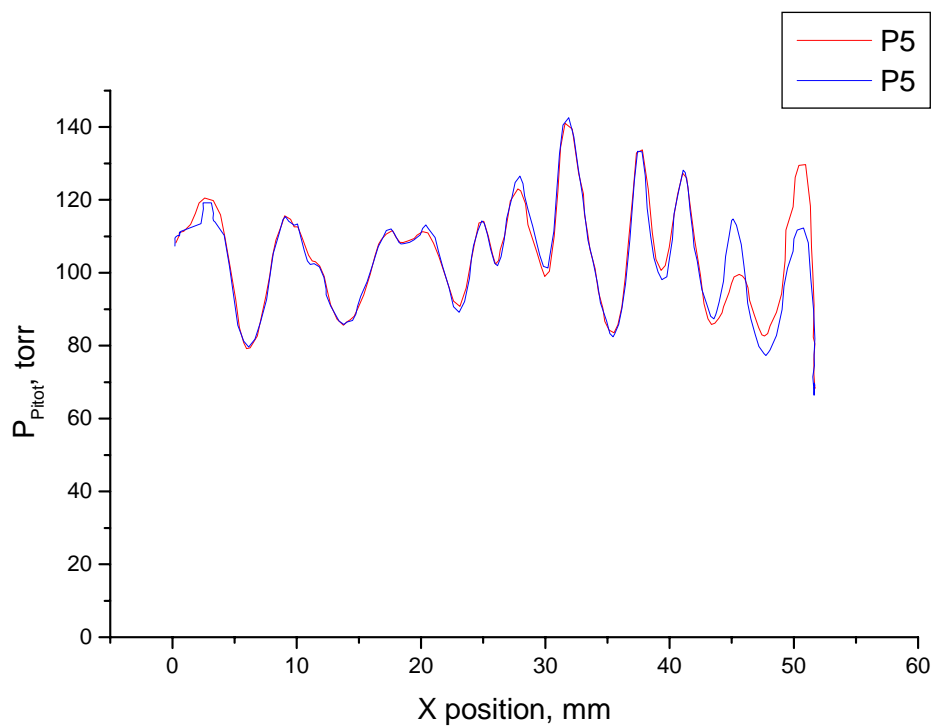
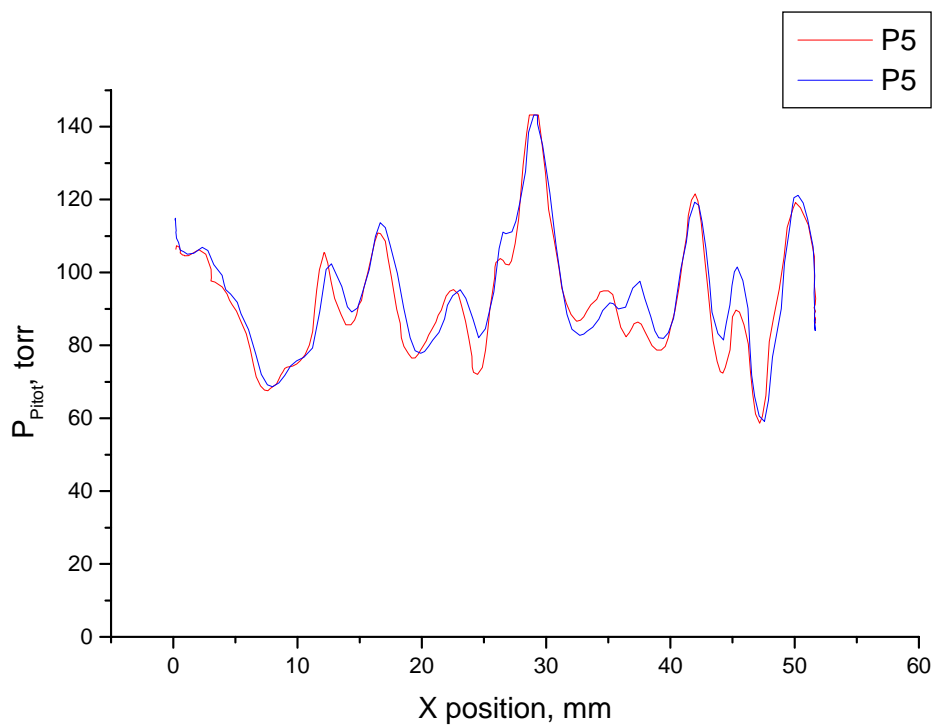
$\Delta z = 113\text{mm}$

c)

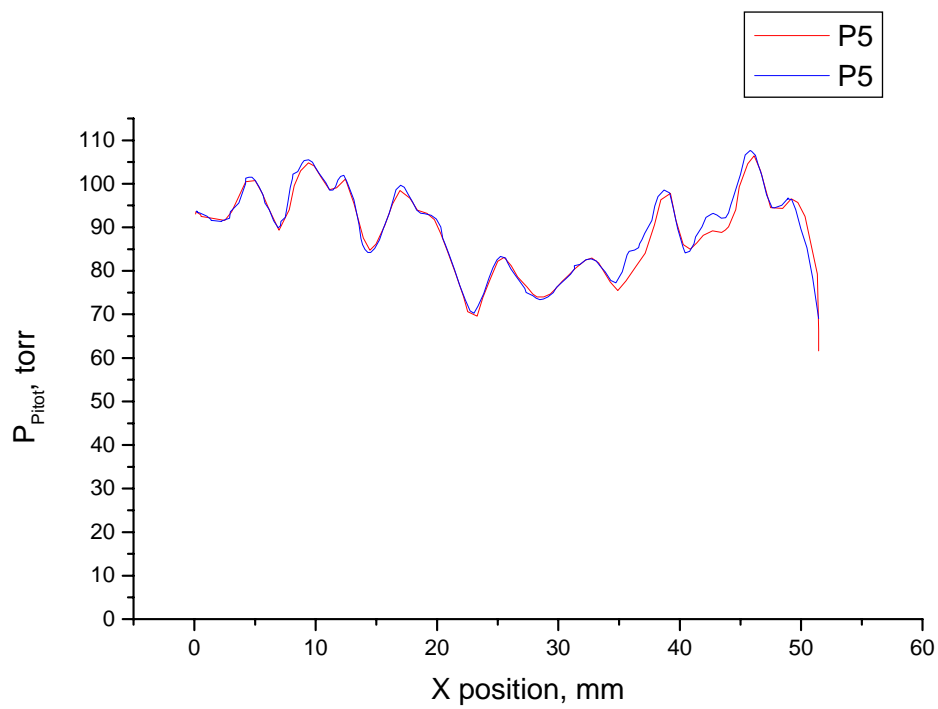
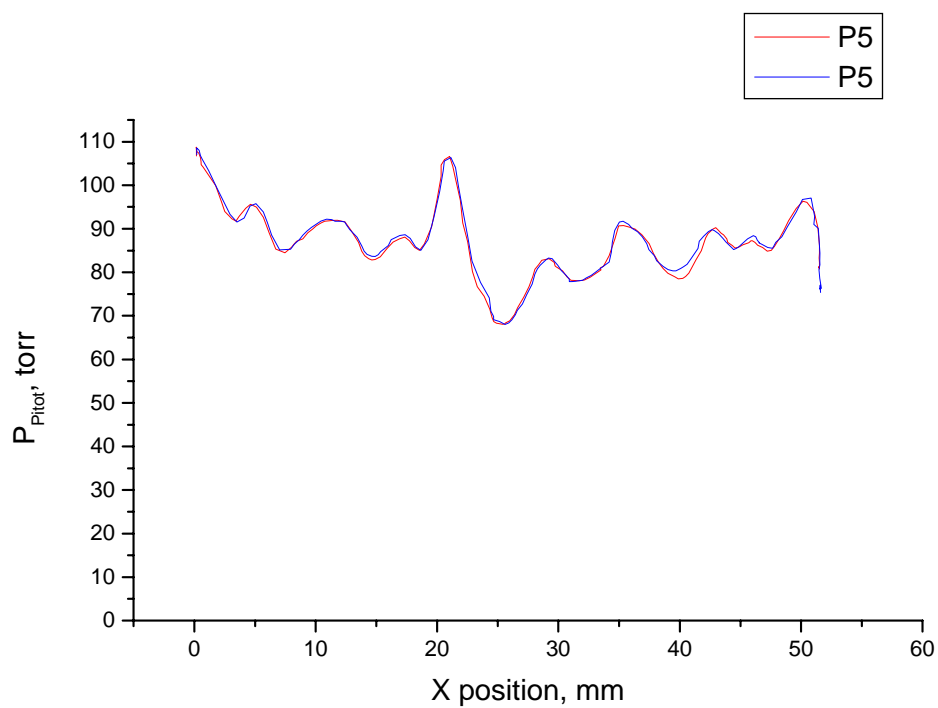
Fig.19. Pitot pressure distribution $P_{\text{Pitot}}(x)$ at driver nitrogen flow rate of 250mmole/s.

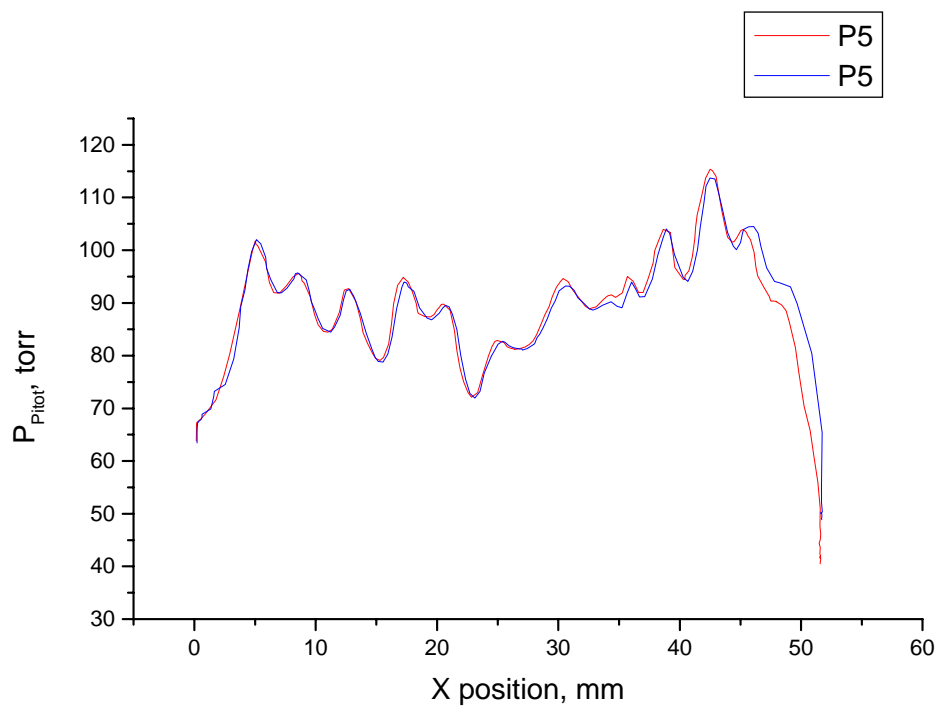


a) $\Delta z = 45\text{mm}$, $y = 0$

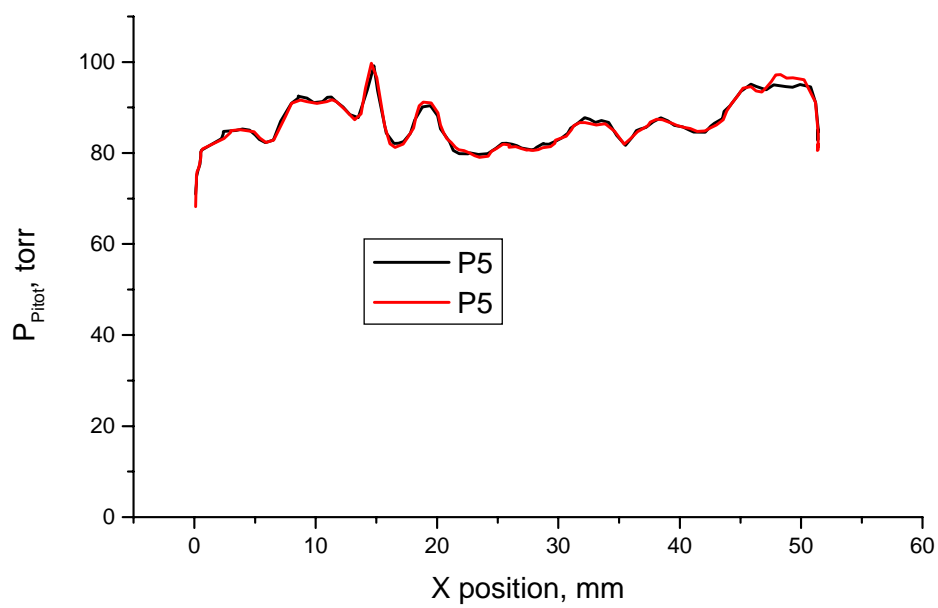


b) $\Delta z = 45\text{mm}$, $y = +2\text{mm}$

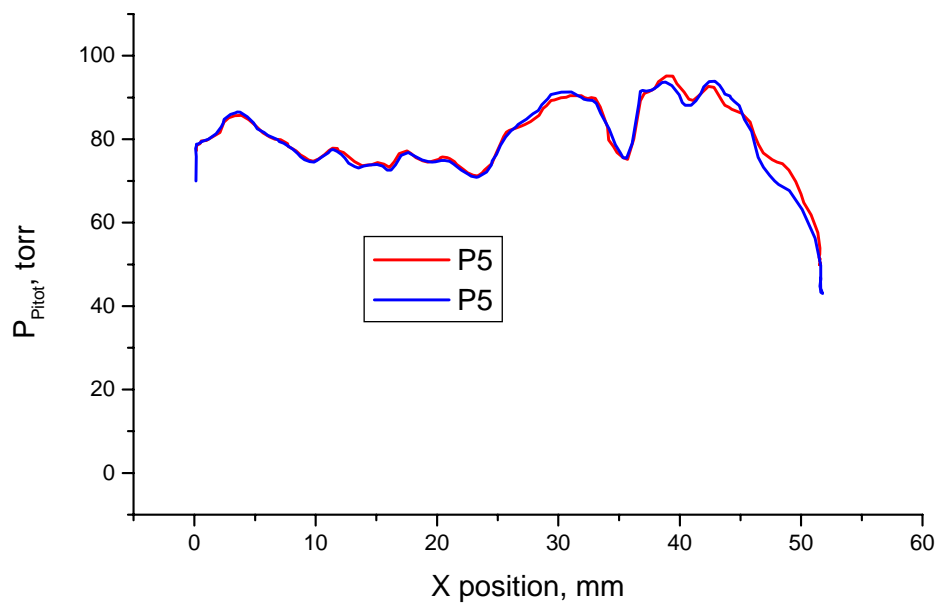
c) $\Delta z = 83\text{mm}$, $y = 0$ d) $\Delta z = 83\text{ mm}$, $y = -2\text{mm}$



e) $\Delta z = 83\text{mm}$, $y = +2\text{mm}$

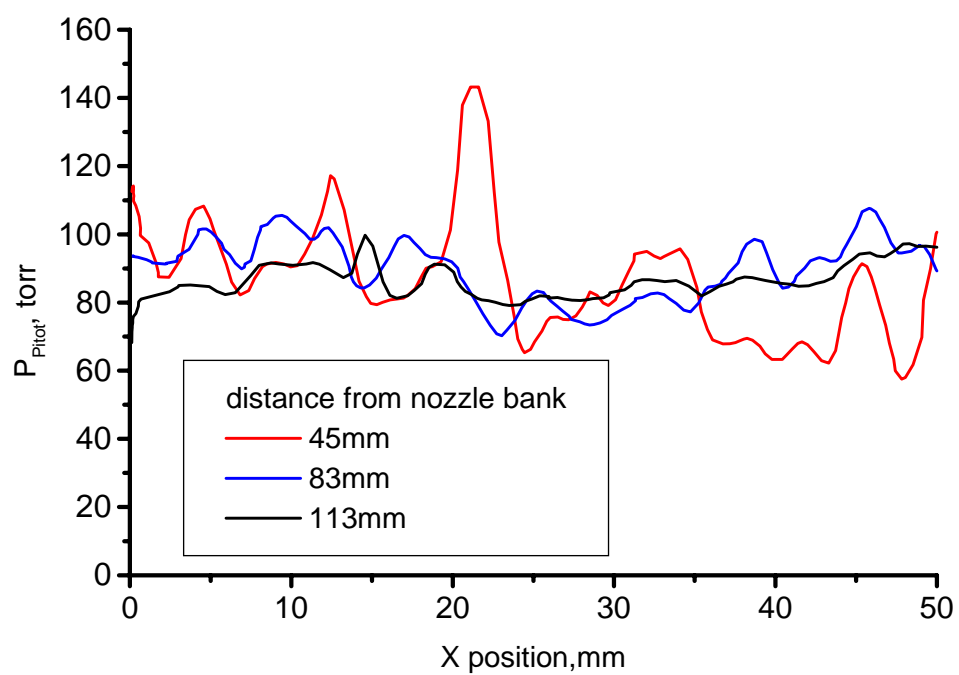


f) $\Delta z = 113\text{ mm}$, $y=0$

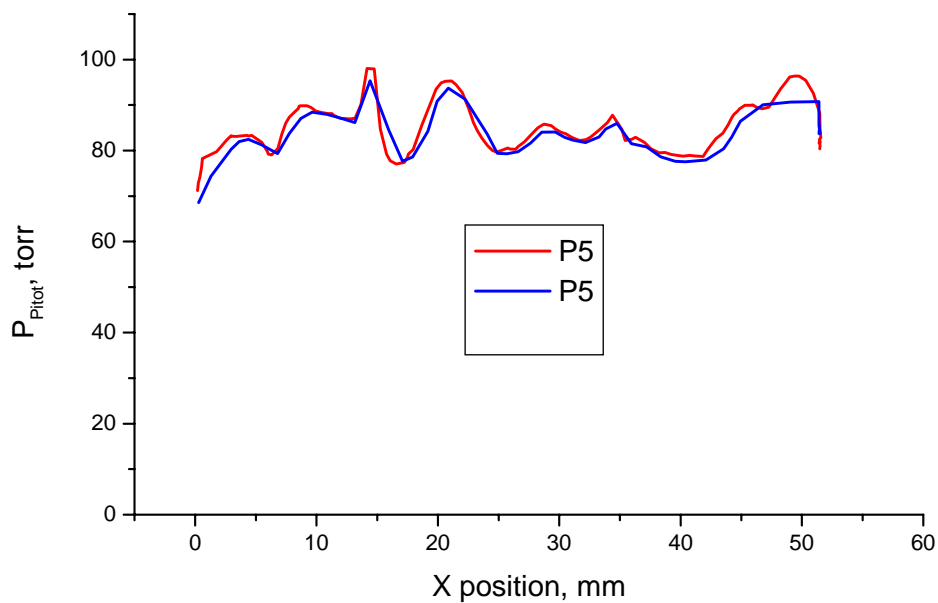


g) $\Delta z = 113\text{mm}$, $y = +2\text{mm}$

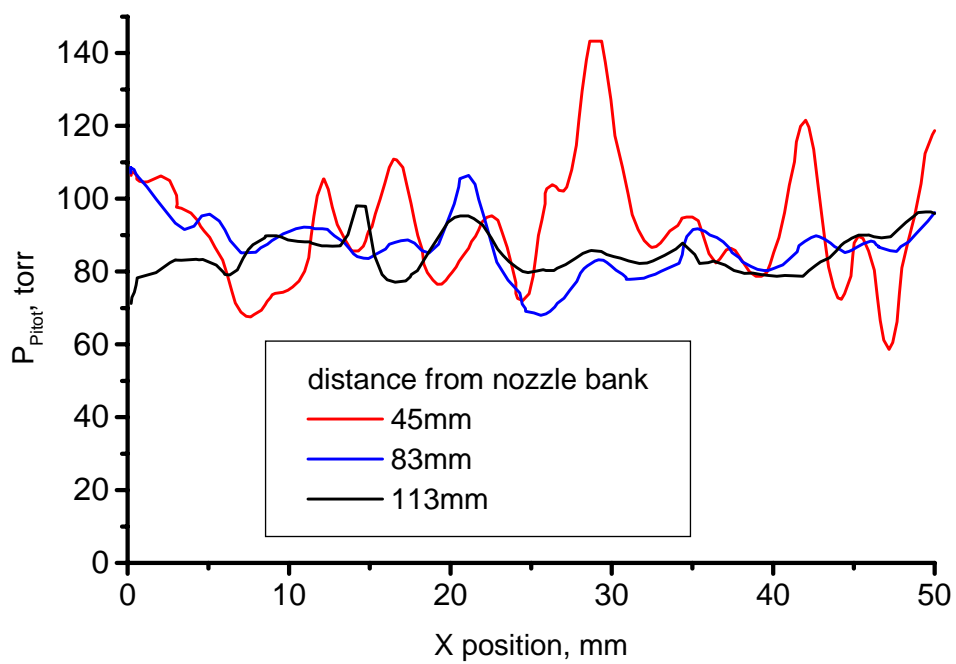
Fig. 20 Pitot pressure distribution $P_{\text{Pitot}}(x)$ at driver nitrogen flow rate of 500mmole/s. Curves correspond to straight and back replacement of the Pitot tube during one test.



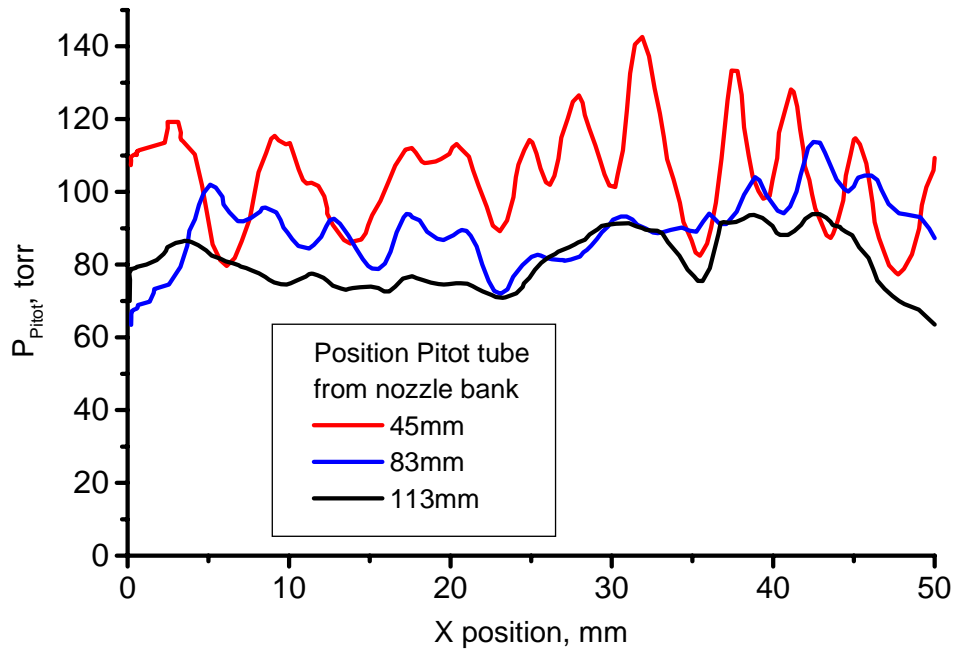
a) $y=0$



h) $\Delta z = 113$ mm, $y = -2$ mm



b) $y = -2$ mm



c) $y=+2\text{mm}$

Fig. 21. Pitot pressure distribution $P_{\text{Pitot}}(x)$ at driver nitrogen flow rate of 500mmole/s.

It's easily to see from given dependencies that substantial mixing of the flows takes place already at distances $\sim 50\text{mm}$, but at distances $\sim 110\text{mm}$ the small-scale pressure pulsation are absent practically (fig. 19g÷19i и 21). Although large-scale inhomogeneity of $P_{\text{Pitot}}(x)$ distribution is kept but its appearance connected with production of oblique shock waves due to the growth of the boundary layers on the parallel side walls. Indeed, as it's easily to see from fig. 19 c) large-scale inhomogeneity of $P_{\text{Pitot}}(x)$ at all duct heights ($y=0; \pm 2\text{mm}$) are similar. Average parameters of distributions $P_{\text{Pitot}}(x)$ measured at the central plane of the mixing chamber on the different distances are presented in the Table.

G_{1a} mmole/s	G_{DN} mmole/s	G_{2N} mmole/s	Z, mm	Average P_{Pitot} , torr
75	500	60	45	97
75	500	60	83	92
75	500	60	113	85
75	250	60	45	54
75	250	60	83	50
75	250	60	113	49

Average value of the Pitot pressure $P_{\text{Pitot}}(x)$ at driver nitrogen molar flow rate $G_{DN}=500\text{mmole/s}$ is nearly to 100 torr at the inlet of the mixing chamber and then decreases. This may be connected with increasing of the duct height $H(x)$ along gas flow ($P_{\text{Pitot}}(x) \sim 1/H(x)$) and pressure losses in the boundary layers.

Additional information about mixing rate of the flows may be obtained from experiments at employing LIF molecular iodine.

4. The upgrade of JSOG design with purpose to improve operation stability and to decrease the BHP aerosol content in the output oxygen stream at flow rate of $\sim 80 \text{ mmole/s}$

Disintegration of the free jets in the traditional counter-flow JSOG results in the droplets production. Carry-over of these BHP droplets was observed in JSOG at operation with a high specific chlorine molar flow rate in the reaction zone. Employing of this generator with ejector nozzle bank leads to precipitation of these droplets on the back surface of the driver N_2 and I_2 manifolds. Then water evaporated and the dry sediment clogs the free cross section of the ejector nozzle bank for oxygen flow. This leads to the raise of the working pressure, transport time and to the decrease of $\text{O}_2(^1\Delta)$ yield. Clogging effect is much less in the case of the slit nozzle bank having large free cross section area for the oxygen flow. But this effect is extremely undesirable at COIL operation with the ejector nozzle bank.

The liquid jet guided by filament much more stable than the free jet. The filaments inside the liquid jets prevent its distraction. So it was expected that jets guided by filaments would be more stable at the cross gas flow with high velocity head. Thus the droplets carry-over from the filament guided jet SOG (FGJSOG) expected much less than in the case of the free jet SOG. The concept of the cross flow FGJSOG was proposed by J. Vetrovec [10]. Lebedev Physical Institute Samara Branch has undertaken independent development and study FGJSOG for the ejector COIL. The main goal of this investigation was to develop reliable laboratory source of oxygen with high $\text{O}_2(^1\Delta)$ yield and with minimal droplets carry-over.

4.1 Description of the filament guided jet generator.

The sketch and photo of the first version of the filament guided jet singlet oxygen generator (FGJSOG-1) are presented in Fig. 22 and 23.

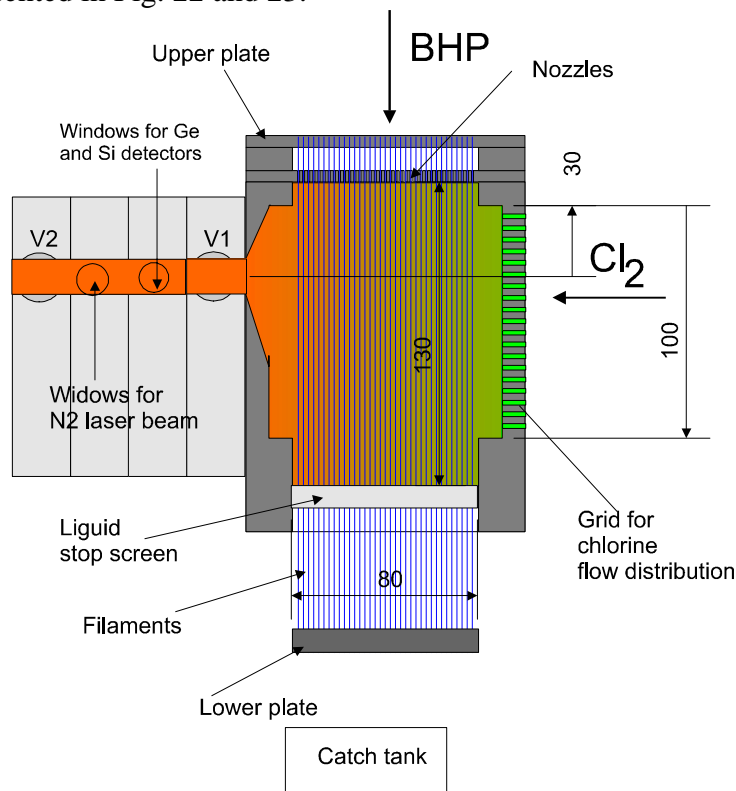


Fig.22

The FGJSOG-1 working volume is equal to 520cm^3 (80 mm along gas flow, 50 mm across the gas flow and of 130 mm in height). The nozzle for BHP input was of 1mm in diameter. The diameter of the nylon filament was of 0.2 mm. One end of the filaments was fixed in the upper plate in which a number of slits were made for BHP input. The total number nozzles and filaments were equal to 560. The second ends of the filaments are fixed in the lower plate. The tension of the filaments was provided by bolts (not shown in figure) between the upper and lower plates. The distances between centers of BHP nozzles were of 2.2 mm in the gas flow direction and of 2.9 mm across the gas flow. The expected gravity stabilized diameter of BHP jets was of 2 mm. The gravity stabilized diameter was preliminary found from experiments with single water-glycerin jet (viscosity of $0.1\text{ cm}^2/\text{s}$ and volume flow rate of $2.3\text{cm}^3/\text{s}$). The liquid stop screen consisted of the Plexiglas stripes installed between filaments of 15 mm in height and of 2 mm in thickness. This liquid stop screen provided approximately 1 cm of BHP layer upper of liquid stop screen when dump tank was pumped out. This BHP layer prevented chlorine penetration into catch tank and fixed the gas residence time in the SOG working volume. Pure chlorine (no diluted with any buffer gas) flowed in working volume through perforated plate and stainless steel mesh. It was provided uniform intake chlorine in the working volume. The oxygen flow leaves FGJSOG through slit valve V1. The pressures in the FGJSOG, the diagnostic “photocell” and the “Cl₂ cell” were controlled by slit valve V2. Working FGJSOG is presented in Fig.24.

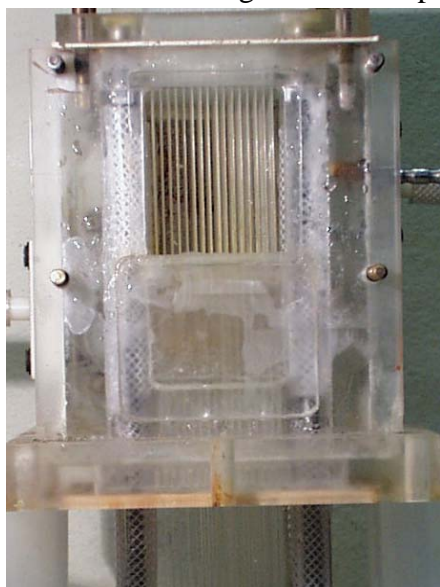


Fig.23.

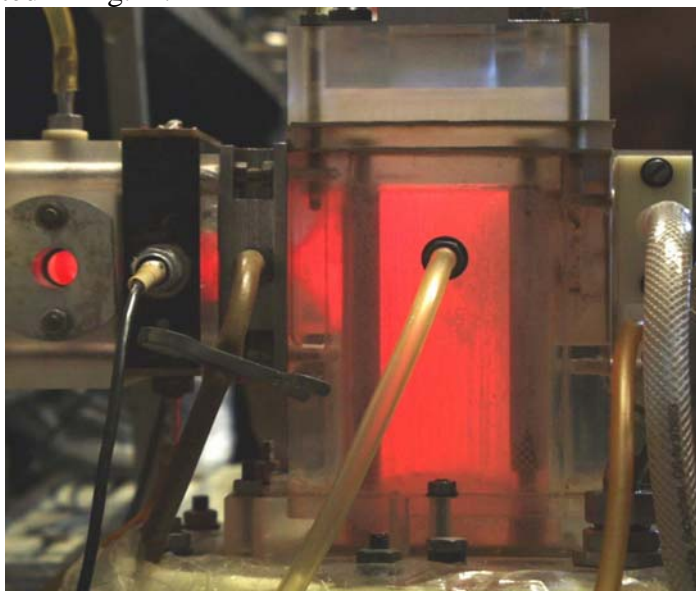


Fig.24.

The FGJSOG-2 was analogous to FGJSOG-1 but with enlarged working volume. The working volume had of 90 mm along gas flow, 125 mm in height and 60 mm in width. The nozzles for BHP inlet were of 1.2 mm in diameter. The nylon filament diameters were of 0.2 mm. One end of the filaments is fixed in upper plate. A number of slits were made for BHP inlet in the upper plate. Total number of the nozzles with filaments was 720. The distances between centers of BHP nozzles were of 2.4 mm in the gas flow direction and of 3 mm across the gas flow.

4.2 Measurements of Cl₂ utilization, gas temperature, water vapor pressure and O₂(¹Δ) yield.

Two special cells were installed downstream FGJSOG to measure O₂(¹Δ) yield, chlorine utilization and water vapor concentration. The methodology of measurements is similar to used in previous investigations described in the final technical report of contract SPC-97-4059. Emission of $1.27\text{ }\mu\text{m}$ from O₂(¹Δ) was recorded by Ge-photo detector, of $0.762\text{ }\mu\text{m}$ from O₂(¹Σ) by Si-photo detector. The photo signals and gas temperature were measured in the first “photocell” installed

immediately downstream slit valve V1. The gas temperature T_g was measured by glass covered thermocouple. The water vapor concentration was determined from ratio

$$N_w = C \frac{I_{1.27}^2}{I_{0.762}}$$

where $I_{1.27}$ and $I_{0.762}$ are signals from 1.27 μm and 0.762 μm detectors respectively, C is the coefficient earlier found from calibration procedure similar to that described in the final technical report SPC-97-4059. The fraction of water vapor in the gas flow was calculated as $\eta_w = N_w / (P_2 / RT)$, where P_2 is the pressure in the measuring cell. The residual Cl_2 concentration N_c was measured by absorption emission with $\lambda = 337 \text{ nm}$ from N_2 -laser in the second “ Cl_2 cell” installed downstream “photocell”. Sensitivity of chlorine detection was \sim of 0.1 torr. The chlorine utilization was calculated as

$$U = 1 - \frac{N_c}{(P_3 / RT - N_w)}$$

The $\text{O}_2(^1\Delta)$ yield was calculated as

$$Y = \frac{AI_{1.27}}{(P_2 / RT - N_w)U}$$

where A is the calibration factor. The error of Y detection was estimated $\pm 15\%$. So the Y is rather a relative value of $\text{O}_2(^1\Delta)$ fraction to within Y_{nascent} but is not real $\text{O}_2(^1\Delta)$ yield. Real $\text{O}_2(^1\Delta)$ yield is $Y_{\Delta} = Y \cdot Y_{\text{nascent}}$. Where Y_{nascent} is the nascent yield.

4.3 Results of the FGJSOG-1 tests.

Designations

P_1	pressure in the reaction zone of the FGJSOG, torr
P_2	pressure in the “photocell”, torr
P_3	pressure in the “ Cl_2 cell”, torr
G_c	chlorine molar flow rate, mmole/s
P_c	$N_c * RT$, chlorine partial pressure, torr
U	Chlorine utilization
Y	“ $\text{O}_2(^1\Delta)$ yield”
η_w	water vapor fraction
$P\tau$	“Ptau” parameter equals to product of gas residence time in working volume by partial oxygen pressure in the reaction zone $P_1(1-\eta_w)$, torr*s

4.3.1. Cl_2 utilization and $\text{O}_2(^1\Delta)$ yield dependencies as functions of Cl_2 molar flow rate and working pressure.

In this runs gas temperature was not measured (the thermocouple was broken) and was assumed equal to $T = 300^\circ\text{K}$.

Input parameters:

BHP composition	6.5M of KOH and 7.5 M H_2O_2
BHP temperature, t(BHP)	-16°C
BHP volumetric flow rate, V(BHP)	$1200 \text{ cm}^3/\text{s}$

Summary of results are presented in the Table and in fig. 25 and 26

N	G_c	P_1	P_2	P_3	P_c	U	Y	η_w	$P\tau$
1	20	7	4.7	5	0	1.00	1.02	0.24	0.030
2	20	7.6	5.7	5.8	0.3	0.95	1.02	0.19	0.036
3	20	11.3	10.4	10.4	0.25	0.98	0.77	0.09	0.087
4	39	18.9	16.6	16.3	1.5	0.91	0.75	0.05	0.132
5	39	16	13.2	13	1	0.92	0.75	0.06	0.092
6	39	13.7	9.9	9.9	0.8	0.92	0.88	0.09	0.066
7	57	25.8	23	--	2.7	0.88	0.66	0.03	0.168
8	57	33.8	31.4	--	2.9	0.91	0.51	0.02	0.295
9	57	19.5	14.9	14.5	1.8	0.88	0.76	0.07	0.094
10	75	41.6	37.3	--	5.8	0.84	0.53	0.03	0.339
11	75	41.8	37.4	--	4.8	0.87	0.51	0.02	0.342
12	75	33	27.6	--	4.3	0.84	0.60	0.03	0.210
13	75	32.4	27.5	--	4.3	0.84	0.57	0.03	0.202
14	75	26.7	19.6	18.8	3.9	0.80	0.70	0.05	0.136
15	75	27.2	19.7	18.9	4.54	0.77	0.73	0.05	0.141

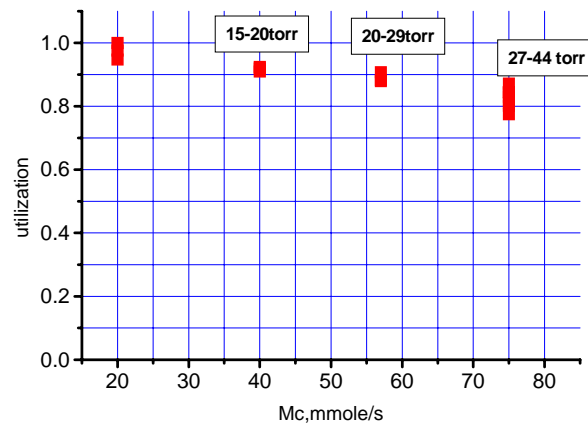


Fig. 25. Chlorine utilization as a function of chlorine molar flow rate

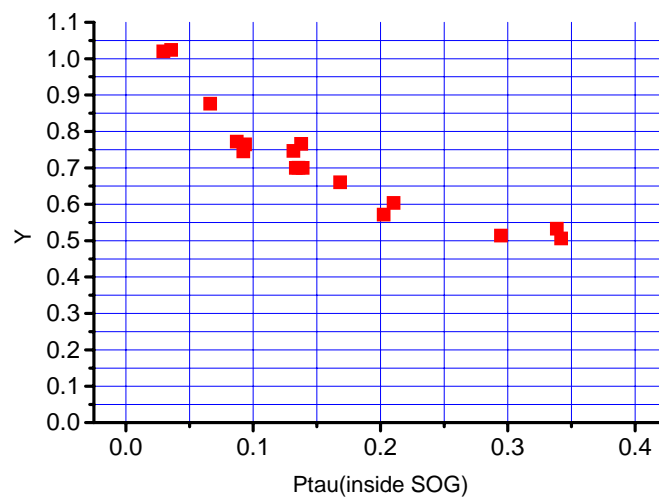


Fig. 26. Y as a function of the parameter $P\tau$

Then tests were repeated with measurements gas temperature. Results are presented in the Table

	G_c	P_1	P_2	P_3	T	P_c	η_w	U	Y	$P\tau$
1	20	8.0	6.5	6.7	291	0.4	0.137	0.93	0.92	0.05
2	40	16.7	14.0	14.6	331	1.6	0.061	0.87	0.80	0.11
3	40	12.8	8.6	9.1	300	1.4	0.086	0.84	0.83	0.07
4	57	20.0	15.6	16.5	338	1.8	0.052	0.87	0.80	0.12
5	57	24.1	21.3	21.7	371	2.8	0.041	0.83	0.72	0.17

Obviously the increase of $P\tau$ results in the raise of the gas temperature. At lower SOG pressure P_1 the water vapor fraction became higher. The expected SOG working pressure equals to $P_1 = 20 \div 25$ torr when generator operates with ejector nozzle bank at chlorine molar flow rate $57 \div 75$ mmole/s and the driver nitrogen molar flow rates $250 \div 500$ mmole/s. The Cl_2 utilization $U < 80\%$ at $G_c = 75$ mmole/s and $P_1 < 27$ torr. Low chlorine utilization is result of the bad renew BHP jet surface.

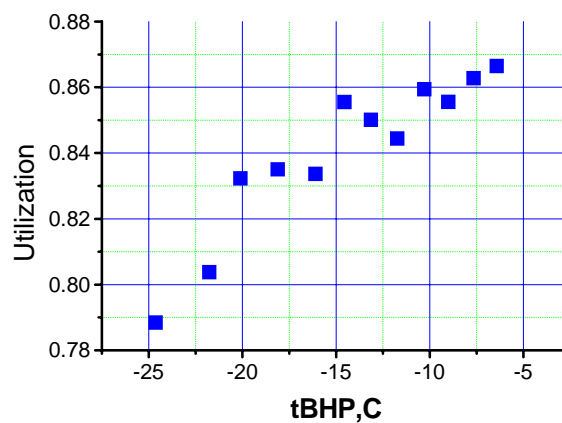
4.3.2. Influence of BHP temperature on chlorine utilization, water vapor fraction and $O_2(^1\Delta)$ yield.

The decrease of BHP temperature results in the raise of BHP viscosity, changing of the diffusion coefficients, Henry constant for chlorine solubility and the reaction rate constant.

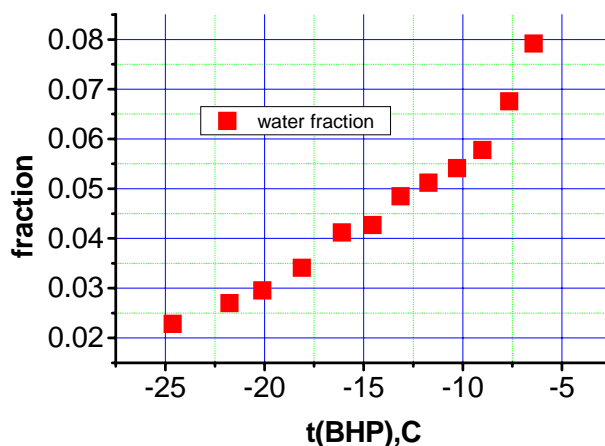
Experimental results at $M_c = 57$ mmole/s are presented in the Table and fig. 27

BHP composition	6.5M of KOH and 7.5 M H_2O_2
BHP temperature, t(BHP)	varied
BHP volume flow rate, V(BHP)	1200 cm^3/s

#	G_c	P_1	P_2	P_3	t(BHP)	T	P_c	η_w	U	Y	$P\tau$
1	57	23.9	21.5	21.1	-24.6	353	3.8	0.023	0.79	0.84	0.16
2	57	23.9	21.6	21.2	-21.8	358	3.4	0.027	0.80	0.85	0.17
3	57	23.9	21.5	21.1	-20.1	359	2.9	0.030	0.83	0.83	0.17
4	57	24.0	21.6	21.2	-18.1	369	2.8	0.034	0.84	0.86	0.17
5	57	24.1	21.7	21.3	-16.1	371	2.8	0.041	0.83	0.87	0.17
6	57	24.1	21.7	21.3	-14.6	363	2.5	0.043	0.86	0.83	0.17
7	57	24.3	21.8	21.4	-13.1	371	2.5	0.048	0.85	0.86	0.17
8	57	24.4	22.0	21.6	-11.7	371	2.6	0.051	0.84	0.85	0.17
9	57	24.5	22.0	21.6	-10.3	366	2.4	0.054	0.86	0.82	0.17
10	57	24.8	22.3	21.9	-9.0	364	2.5	0.058	0.86	0.81	0.18
11	57	24.9	22.3	21.9	-7.7	370	2.3	0.068	0.86	0.83	0.18
12	57	25.2	22.3	21.9	-6.4	370	2.2	0.079	0.87	0.86	0.18



a)



b)

Fig. 27. Dependencies of chlorine utilization (a) and water vapor fraction (b) on BHP temperature.

The raise of BHP temperature results in the increase of chlorine utilization and water vapor fraction. But $O_2(^1\Delta)$ yield doesn't depend on BHP temperature. The gas temperature increases with the raise of BHP temperature.

4.3.3. Influence of the BHP volumetric flow rate on FGJSOG-1 performance.

BHP composition	6.5M of KOH and 7.5 M H_2O_2
BHP temperature t(BHP)	~-16C
BHP volume flow rate , V(BHP)	varied
G_c , mmole/s	57

	V(BHP), L/s	P_1	P_2	P_3	t(BHP)	T	P_c	$P\tau$	η_w	U	Y
1	1.26	20.8	16	17	-16.2	345	1.8	0.11	0.06	0.87	0.85
2	1.15	20.9	16	17	-16.5	341	1.9	0.11	0.07	0.86	0.93
3	0.915	21.2	17	17	-17.0	335	2.6	0.11	0.06	0.81	0.93
4	0.67	22.1	18	18	-16.7	342	3.1	0.12	0.07	0.78	0.94
5	1.7	21.4	18	18	-17.1	348	1.6	0.12	0.05	0.89	0.87

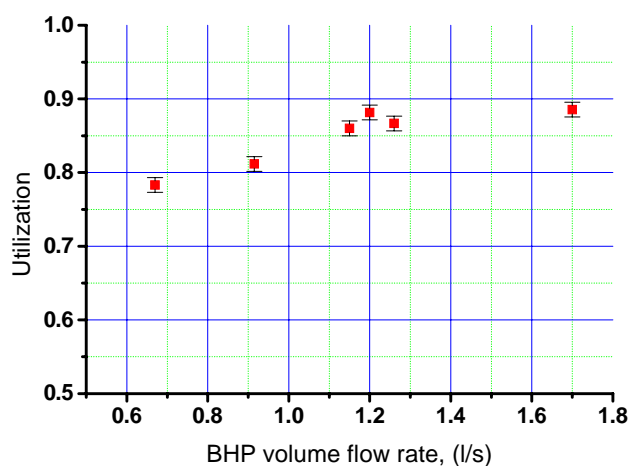


Fig.28. Chlorine utilization as a function of the volumetric BHP flow rate.

Chlorine utilization is independent practically on volumetric BHP flow rate at $V(\text{BHP}) \geq 1.2 \text{ L/s}$.

4.3.4. Influence of the KOH molarity on FGJSOG-1 performance.

The BHP was prepared from 13M H_2O_2 and some amount of 15M KOH. The KOH molarity was varied and measured by acid-base titration.

BHP composition	7.5 M H_2O_2 and M KOH was varied
BHP temperature t(BHP)	~-16C
BHP volume flow rate , V(BHP)	1.2 L/s
G_c	57mmole/s

	KOH molarity mole/L	P_1	P_2	P_3	T	P_c	η_w	U	Y	P_τ
1	3.2	22.6	19	19	359	2.8	0.09	0.80	1.13	0.12
2	3.2	19.7	14	14	330	2.4	0.08	0.79	0.93	0.09
3	3.2	21.3	17	17	334	2.9	0.06	0.79	0.91	0.11
4	3.7	21.0	16	17	344	2.2	0.08	0.83	0.96	0.11
5	3.7	21.2	16	17	341	2.2	0.07	0.83	0.94	0.11
6	4.5	21.0	16	17	343	1.8	0.07	0.86	0.93	0.11
7	4.5	21.1	16	17	341	2.0	0.07	0.85	0.94	0.11
9	5.6	21.3	17	17	338	1.4	0.07	0.90	0.91	0.11
10	6.5	21.3	17	17	346	1.6	0.07	0.88	0.95	0.11

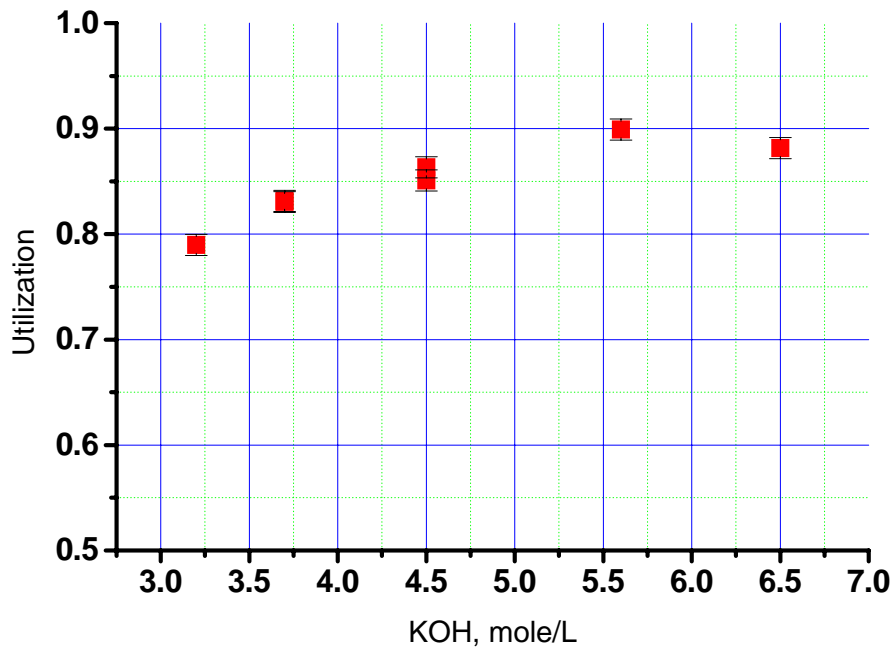


Fig.29. Dependence of the chlorine utilization as a function of the KOH molarity.

Chlorine utilization is independent practically on the KOH molarity at $M_{\text{KOH}} > 5$

4.3.5. FGJSOG -1 operation stability.

BHP was preliminary pumped out at all runs to eliminate dissolved oxygen produced as a result of BHP spontaneous decomposition. At these conditions the FGJSOG operated very stable at

57 mmole/s and $P_1 > 19$ torr and droplets were absent at the FGJSOG exit. 14 runs of 7s duration have been performed during one experimental day with ejector nozzle bank at chlorine molar flow rate 57 mmole/s and working pressure $P_1 = 20$ torr. The pressure P_1 didn't change from the first to last run. After COIL set-up disassembling no droplets was observed on the back side of the ENB supplying manifolds.

We observed sometimes the coalescence of jets in the case of 75 mmole/s chlorine molar flow rate and working pressure $P_1 < 27$ torr. This caused an unstable FGJSOG operation.

4.4. Results of FGJSOG –2 tests.

The FGJSOG-2 was developed to provide stable operation at 75mmole/s of chlorine flow rate and to achieve higher Cl_2 utilization. The chlorine flow was diluted with helium at several runs. At dilution chlorine with helium the partial oxygen pressure was supported equaled to ~25torr with aid of adjusting the slit valve. Experimental results of these tests are presented in the table.

	G_{He} mmole/s	G_c mmole/s	V(BHP), liter/s	P_1	T	η_w	U	Y
1	0	75	1.3	27	369	0.029	0.82	0.77
2	0	75	1.3	28	342	0.036	0.82	0.72
3	0	75	1.3	26	371	0.037	0.83	0.82
4	0	75	1.3	31	385	0.025	0.78	0.76
5	0	75	1.5	27	349	0.026	0.85	0.74
6	0	75	2	27	361	0.027	0.87	0.77
7	0	75	2	27	340	0.031	0.89	0.75
8	0	75	2	27	365	0.027	0.88	0.77
9	0	75	2	27	373	0.027	0.86	0.79
10	0	75	2	28	368	0.030	0.88	0.72
11	0	75	2	23	340	0.034	0.83	0.82
12	93	75	2	57	285	0.090	0.86	0.77
13	69	75	2	54	296	0.048	0.87	0.82
14	178	75	2	86	277	0.051	0.88	0.72
15	246	75	2	100	270	0.038	0.87	0.62
16	322	75	2	133	269	0.018	0.84	0.69
17	0	57	2	18	344	0.062	0.88	0.93
18	0	57	2	21	369	0.050	0.90	0.87

The raise of BHP volumetric flow rate V(BHP) up to 2 liter/s resulted in the raise of chlorine utilization on ~6%. The dilution of chlorine with helium led to decreasing of the gas temperature. The FGJSOG operated stable during all runs.

5. Investigation of the mixing efficiency of iodine at chlorine flow rates of (60÷80)mmole/s and nitrogen flow rates of (250÷500)mmole/s using the LIF method.

Development of the new ENB designs was directed on reaching of the low SOG pressure (20-25torr) at large oxygen flux through nozzle bank (up to 10mmole/cm²·s). Our previous investigations demonstrated the decrease of the SOG pressure at usage supersonic nozzles for driver nitrogen producing jets with large Mach number ~M=5 and low output static temperature ~(50÷60)K°. There are several methods for determination of the jets mixing efficiency but the laser induced fluorescence is the most descriptive method. This method was used for diagnostic of the flow mixing efficiency at testing of 3 new ejector nozzle banks developed and presented in Fig. 16 and in Fig. 30.

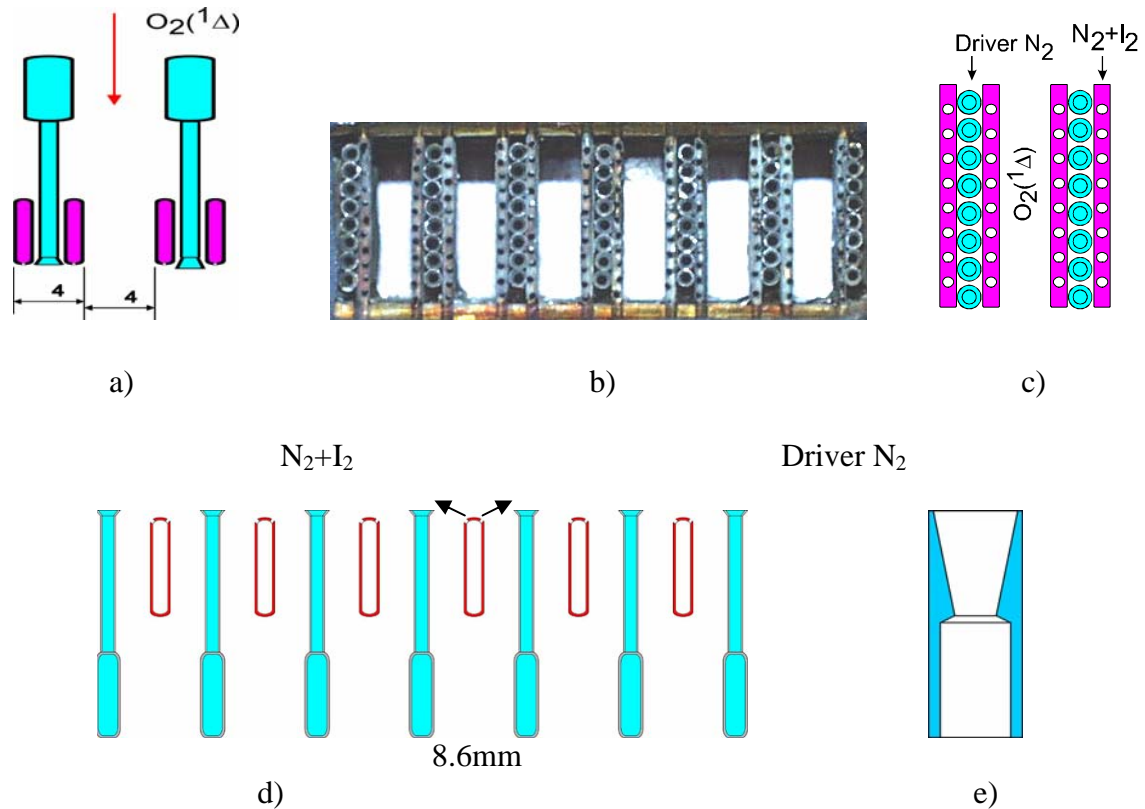


Fig.30.

ENB-2, upper (a) and front (c) views of an ENB-2 element; b) photograph of the front view; d) ENB-3, upper view; e) the real micro nozzle design for driver N_2 ; $d_{\text{throat}}=0.9\text{mm}$; $D_{\text{outlet}}=1.8\text{mm}$

5.1. LIF visualization of the flows produced by ENB-1

The Z-X plane beam from Ar-laser thickness of $\sim 1\text{mm}$ and width of 40mm was directed to the laser cavity (Fig.31). The laser induced fluorescence of molecular iodine was detected through filter OC-23 in Y direction by digital camera with time exposition $\sim 4\text{s}$. The distance between the nozzle bank and optical axis of the cavity can be changed by installing intermediate chambers (Fig.31). Emission of the LIF was detected for different positions of Ar-laser plane beam in Y direction. LIF visualizes the distribution of the primary flow (air) when molecular iodine was premixed only with the primary flow. Visualization of the secondary N_2 was provided by premixing I_2 with secondary

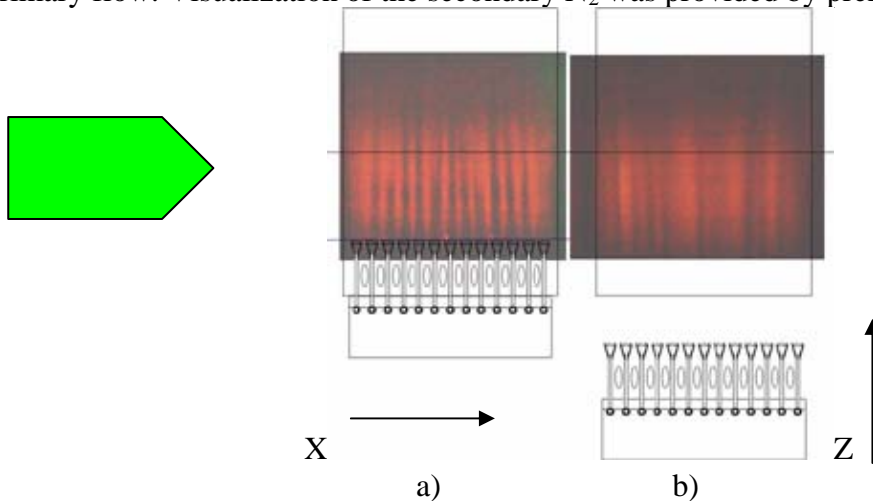


Fig. 31. LIF visualization of the primary flow from ENB-1. $G_1(\text{air})=75\text{ mmole/s}$, $G_2(N_2)=60\text{ mmole/s}$, $G_{DN}=500\text{ mmole/s}$

nitrogen only. The dark traces in the patterns depict the driver nitrogen jets. Distributions of the primary air at different distances from the central plane are presented in Fig. 32. Easily to see that $Y=3\text{mm}$, $Y=7\text{mm}$ (and evidently $Y=-1\text{mm}$) planes are located between rows of the supersonic nozzles in accordance with the nozzle period $\Delta Y=4\text{mm}$. Primary air occupied practically all cross section of the mixing chamber at $Z>50\text{mm}$ where the dark stripes practically vanish.

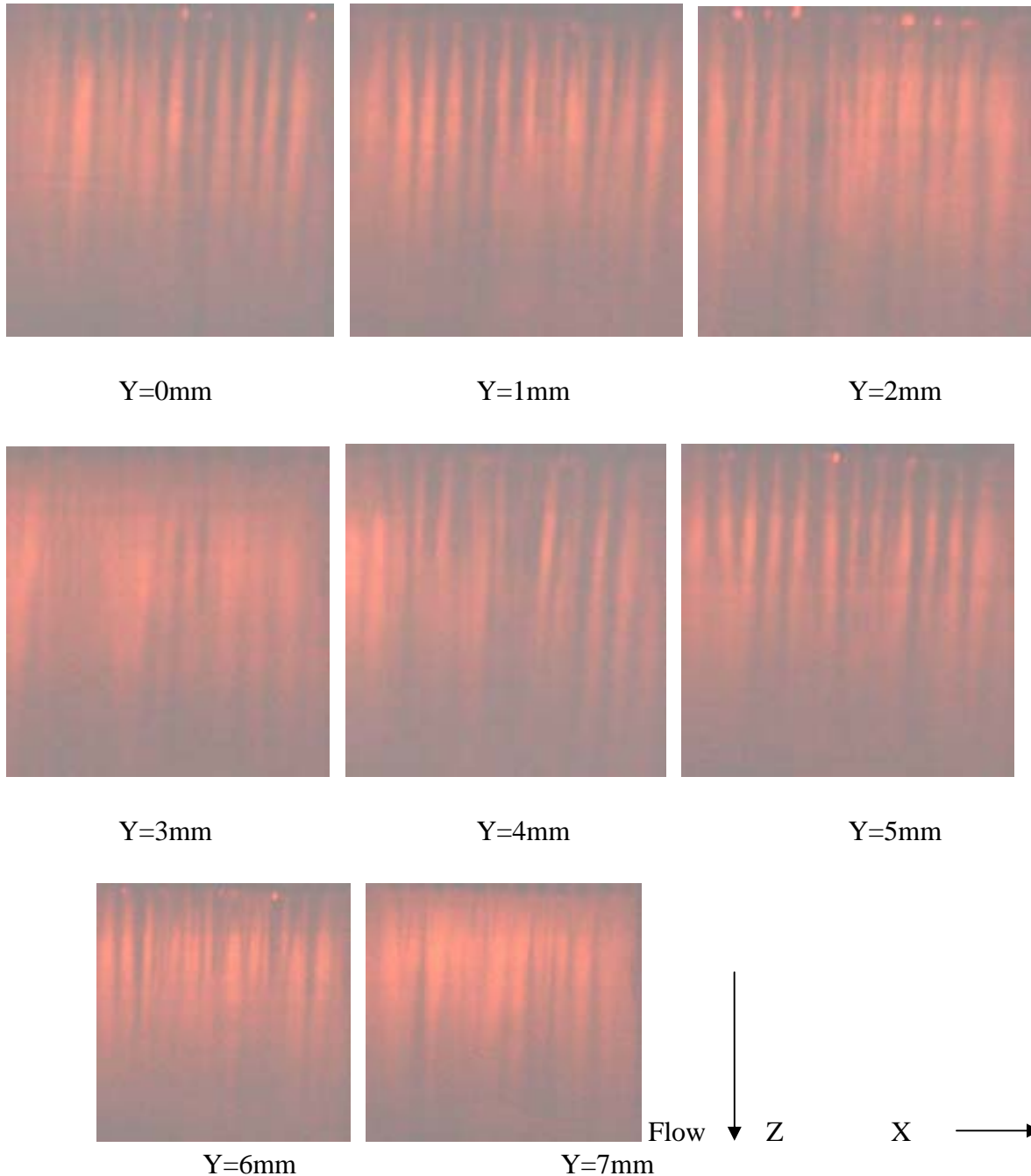


Fig.32. ENB-1. $\text{I}_2(\text{B-X})$ LIF. Upper edges of the LIF patterns are located at $Z=0\text{mm}$ from nozzle bank. I_2 vapor was premixed with primary air. Y is distance from the **center plane** of the mixing chamber. $G_{\text{DN}}=520\text{mmole/s}$; $G_1(\text{air})=75\text{mmole/s}$

Similar patterns at installation the intermediate chamber with length $\Delta z=28\text{mm}$ are presented in Fig. 33 and demonstrate the fast mixing air with the driver nitrogen.

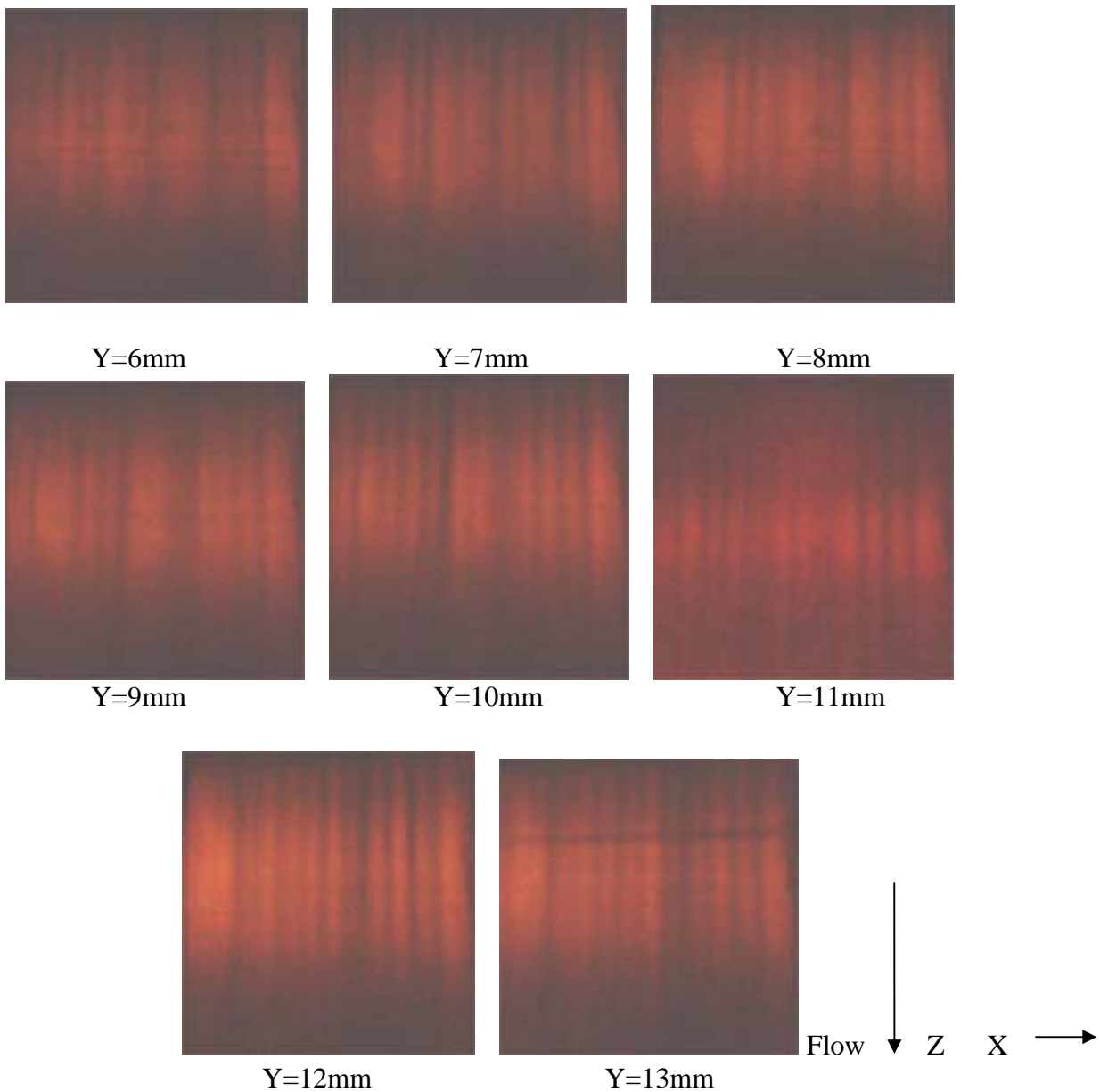
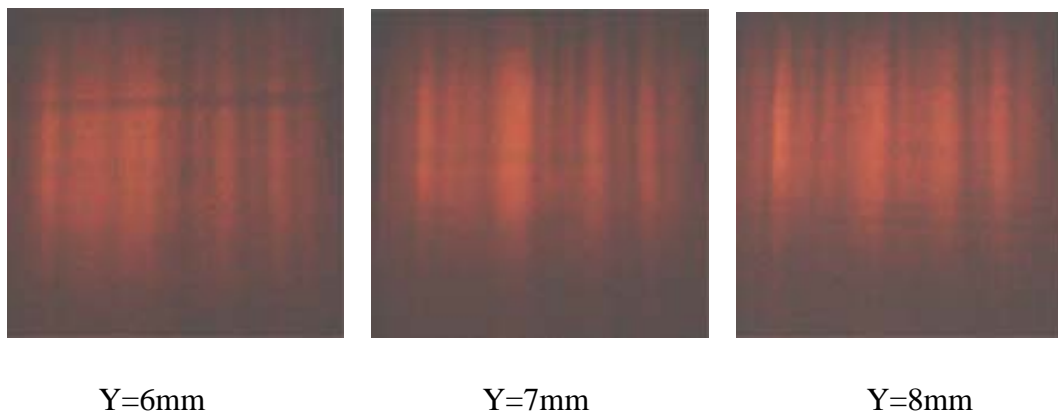


Fig.33. ENB-1. $I_2(B-X)$ LIF. Upper edges of the LIF patterns are located at $Z=28\text{mm}$ from nozzle bank. Iodine vapor was premixed with air. Y is distance from the **upper wall** of the mixing chamber. $G_{DN}=520\text{mmole/s}$; $G_1(\text{air})=75\text{mmole/s}$

Mixing efficiency of secondary N_2 with the driver N_2 is illustrated the patterns presented in Fig.34.



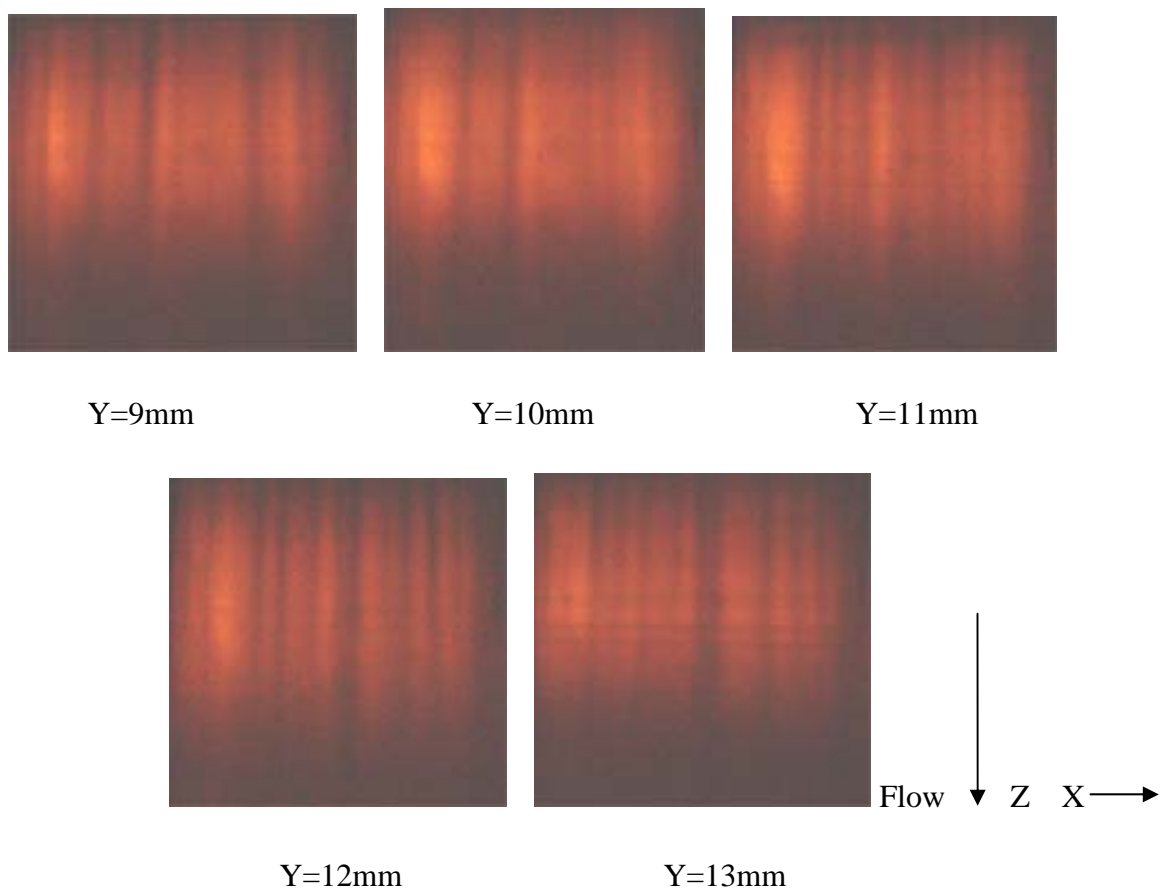
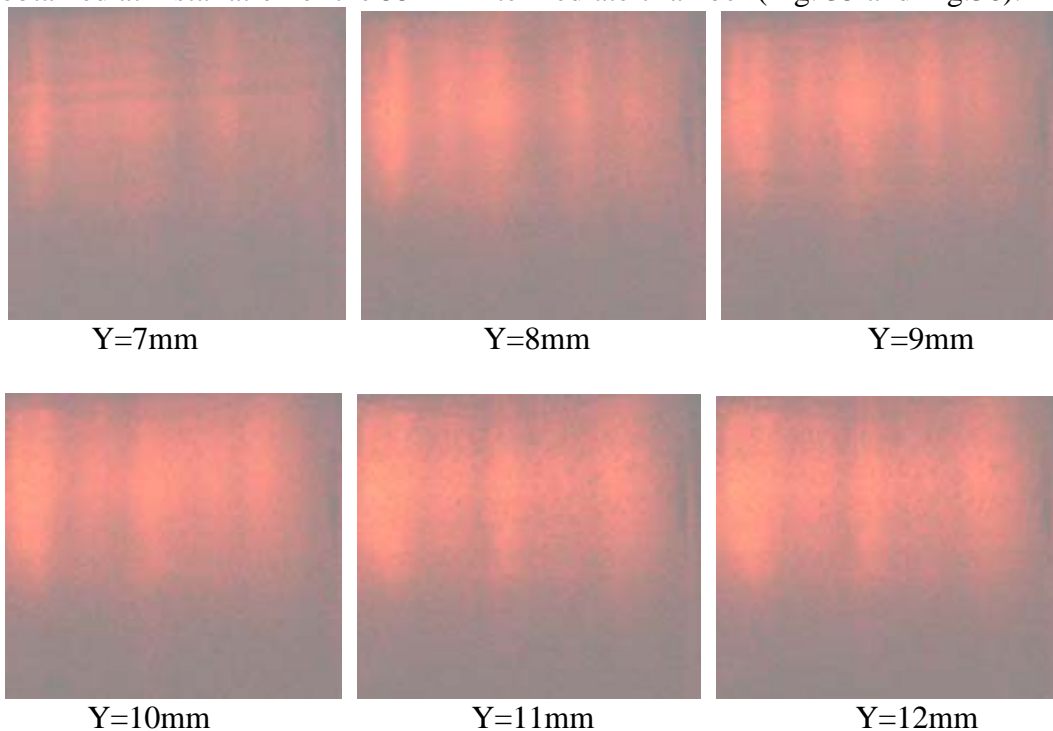


Fig. 34. ENB-1. $I_2(B-X)$ LIF. Upper edges of the LIF patterns locate at $Z=28\text{mm}$ from nozzle bank. Iodine vapor was premixed with secondary N_2 . Y is distance from the **upper wall** of the mixing chamber. $G_{DN}=520\text{mmole/s}$; $G_1(\text{air})=75\text{mmole/s}$.

Iodine with secondary N_2 are mixed enough at $Z>50\text{mm}$ for all positions (Y) of the Ar-laser knife. Good mixing secondary N_2 and primary air with driver nitrogen is more evident from LIF patterns obtained at installation of the 55mm intermediate chamber (Fig. 35 and Fig.36).



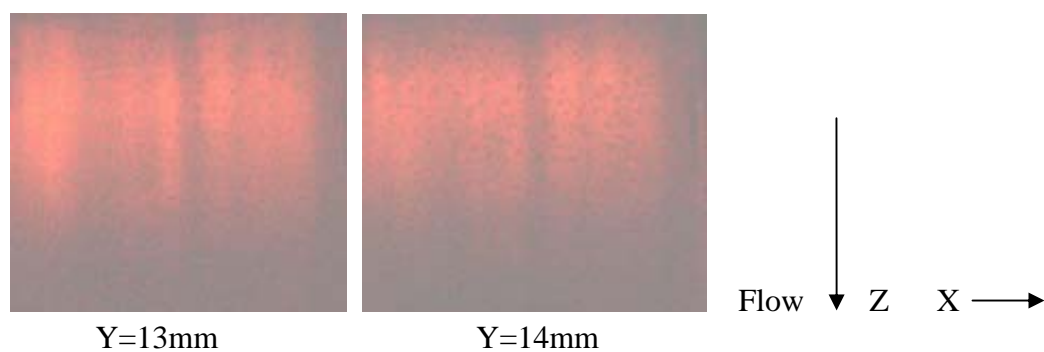


Fig.35. ENB-1. $I_2(B-X)$ LIF. Upper edges of the LIF patterns locate at $Z=55\text{mm}$ from nozzle bank. Iodine vapor was premixed with secondary N_2 . Y is distance from the **upper wall** of the mixing chamber. $G_{DN}=520\text{mmole/s}$; $G_1(\text{air})=75\text{mmole/s}$.

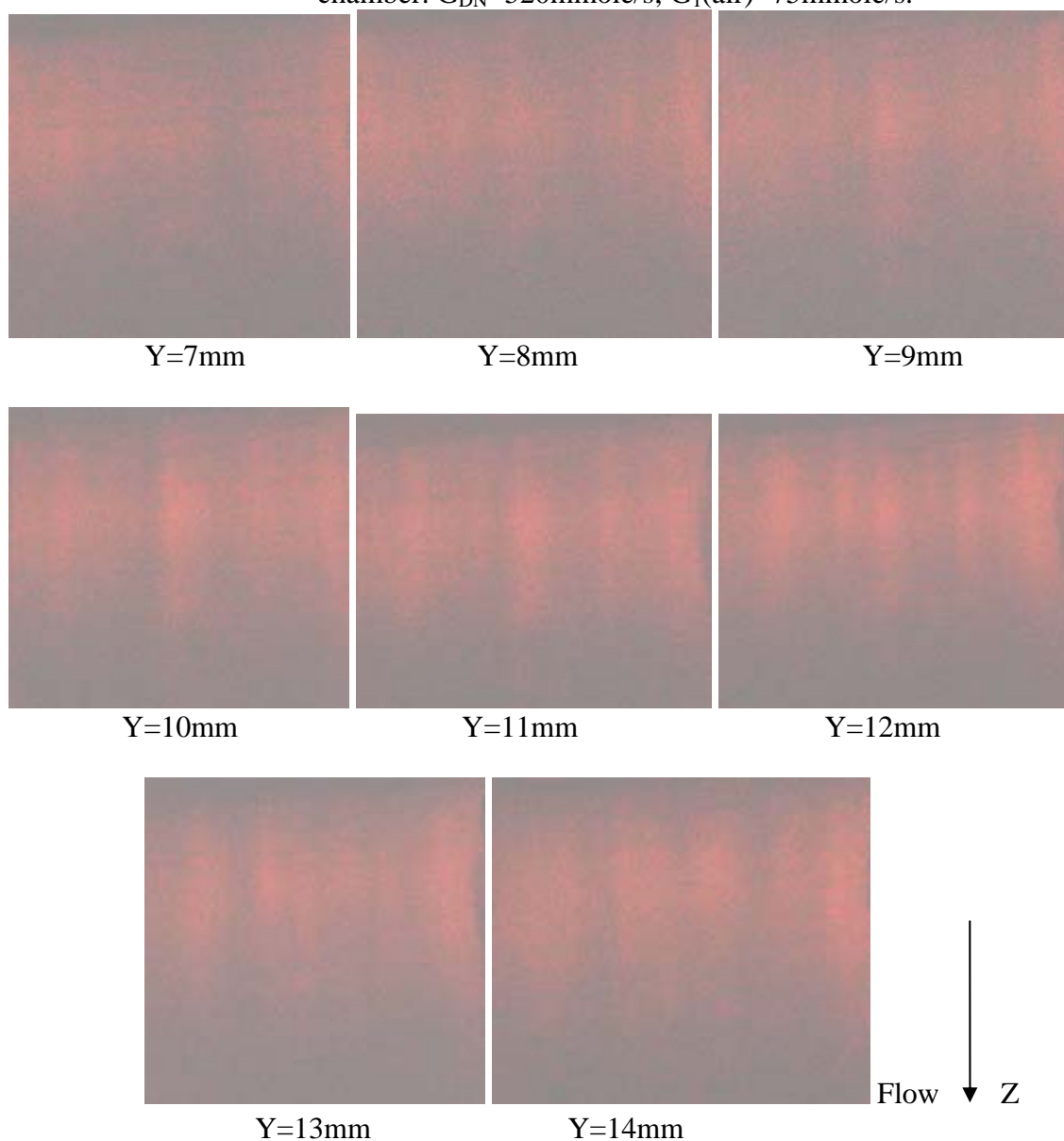


Fig. 36. ENB-1. $I_2(B-X)$ LIF. Upper edges of the LIF patterns locate at $Z=55\text{mm}$ from nozzle bank. Iodine vapor was premixed with air. Y is distance from the **upper wall** of the mixing chamber.

Small general changes of the LIF patterns (compare Fig.32 and Fig.37) were result of decreasing the driver N_2 flow rate from 520mmole/s to 270mmole/s. The weak oblique shock waves in the flow field were observed in the last case only.

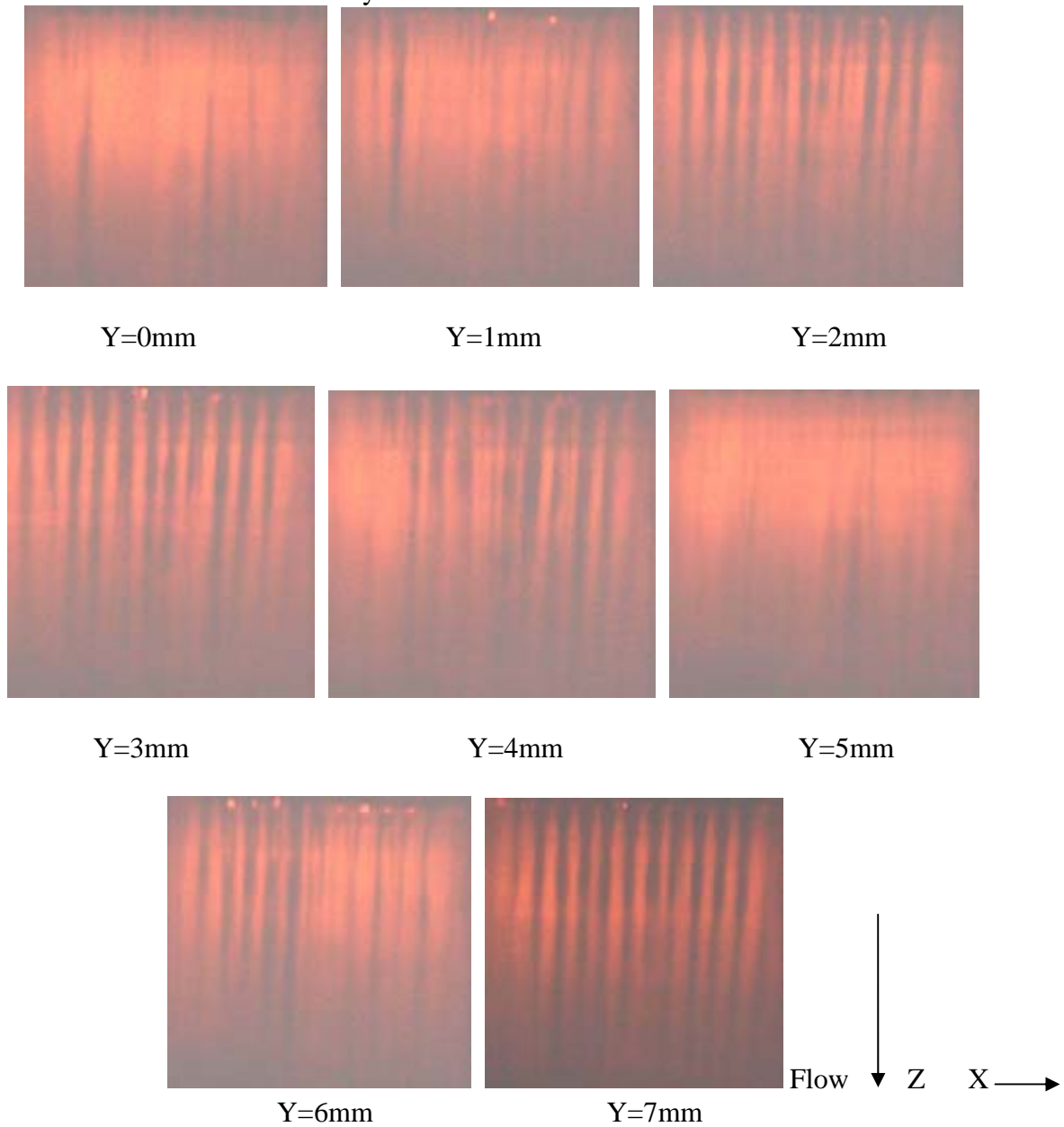


Fig.37. ENB-1. $I_2(B-X)$ LIF. Upper edges of the patterns locate at $Z=0$ mm from nozzle bank. Iodine vapor was premixed with air. Y is distance from the center plane of the mixing chamber.
 $G_{DN}=270$ mmole/s; $G_1(\text{air})=75$ mmole/s

5.2 LIF visualization of the flows produced by ENB-2 and ENB-3.

LIF patterns obtained with ENB-2 and ENB-3 at the intermediate chamber of 55mm length are presented in Fig.38 and Fig.39. The bad mixing efficiency of the driver N_2 with primary air and secondary N_2 was observed in these cases up to 90mm downstream nozzle banks. The flow had clearly layer structure.

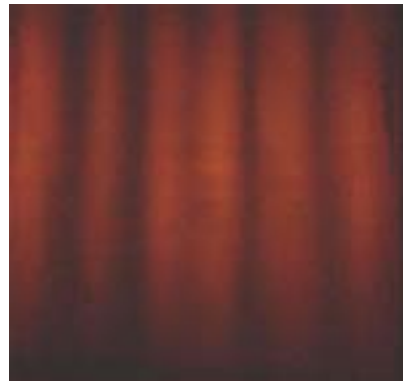


Fig.38. ENB-2. $I_2(B-X)$ LIF. Upper edges of the LIF patterns locate at $Z=55\text{mm}$ from nozzle bank. Iodine vapor was premixed with secondary N_2 . The laser knife of 5mm thickness is located in the center plane of the mixing chamber. $G_{DN}=520\text{mmole/s}$; $G_1(\text{air})=75\text{ mmole/s}$; $G_2(N_2)=60\text{ mmole/s}$

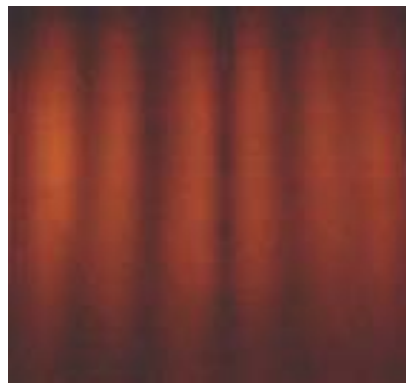


Fig. 39. ENB-3. $I_2(B-X)$ LIF. Upper edges of the LIF patterns locate at $Z=55\text{mm}$ from nozzle bank. Iodine vapor was premixed with secondary N_2 . The laser knife of 5mm thickness is located in the center plane of the mixing chamber. $G_{DN}=520\text{mmole/s}$; $G_1(\text{air})=75\text{ mmole/s}$; $G_2(N_2)=20\text{ mmole/s}$

LIF experiments have shown that ejector nozzle bank ENB-1 provides more fast mixing of all gas flows and this correlates with measurements of the Pitot pressure distributions at different distances from nozzle bank. It will be noted that contact high Mach number of the driver nitrogen flow ($M \approx 5$) with very low static temperature $T \approx (55 \div 60)\text{K}^\circ$ and oxygen flow containing of ~ 0.5 torr H_2O vapor creates very high possibility for water vapor condensation into very fine ice droplets (due to exclusively high oversaturation conditions). Then iodine vapor (and excited iodine atoms also) may be absorbed by this superfine ice aerosol. As result one may observe decreasing small signal gain downstream ENB-1. The last requires additional investigations with employing the diode laser spectroscopy or monitoring 1.315μ emission of excited iodine atoms.

Nozzle banks ENB-2 and ENB-3 can't provide fast mixing of all gas flows. The gas flow keeps clear layer structure up to $\sim 90\text{mm}$ from nozzle bank. However even partial mixing of the driver nitrogen with the oxygen-iodine mixture may result in enough effective lasing with such active medium.

6. Measurement small signal gain with aid of the Rigrod curves.

The lasing and small signal tests of 3 types of the ejector nozzle banks were continued. The Rigrod curves were used for determination small signal gain (SSG). Moreover monitoring emission of excited iodine atoms along gas flow $I^*(z)$ was employed for illustration of the dependencies of small signal gain $g(z)$. The sketch of COIL set-up is presented in Fig.40.

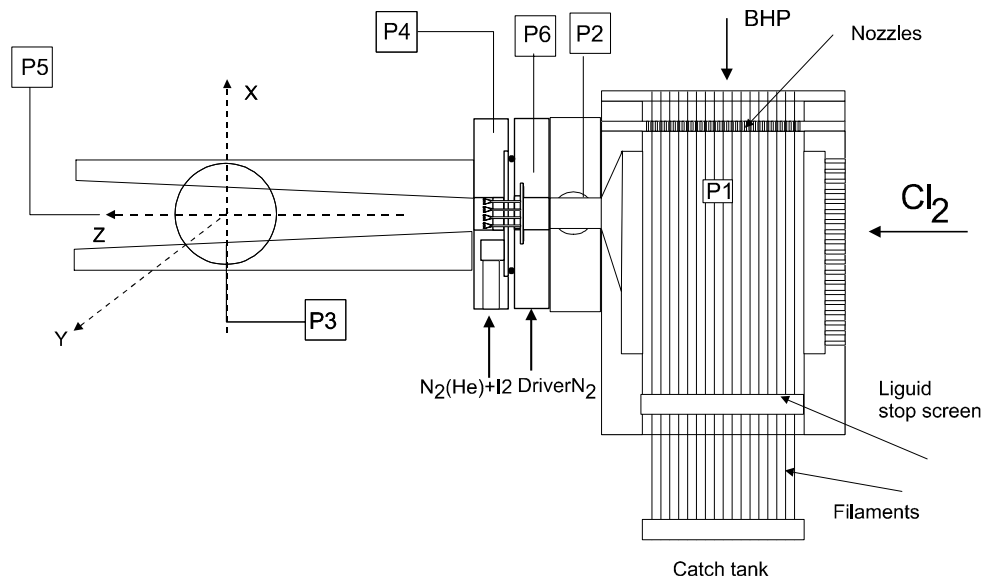


Fig.40. The sketch of COIL set-up with ENB.

The main parts of the COIL set-up are a cross-flow SOG with the filament-guided jets, the ejector nozzle bank (ENB) with the supersonic nozzles for the driver nitrogen and the optical cavity. The oxygen flow from FGJSOG was transported to the nozzle bank through a rectangular duct with the cross section of $60 \times 17 \text{ mm}^2$ and length of 40 mm. The gas flow generated by ENB with initial cross section of $17 \times 52 \text{ mm}^2$ issued to the laser cavity. The walls of the cavity were turned on 3° relative to the flow direction. The tunnels with mirrors were connected to this cavity so that the optical length of the resonator was 63 cm. The resonator was formed by spherical mirror of 5 m or 2 m in the curvature. The output laser power was measured from both mirrors by commercial laser power meters (Ophir and LPM-905 calibrated relatively Ophir). The gain length of the cavity along gas stream was 45mm. The gas from the laser cavity was exhausted into 15 m^3 tank preliminary pumped down to pressure less than 1 torr. At the gas-dynamic tests, LIF and $I^*(z)$ emission monitoring experiments the identical cavity was used without tunnels for mirrors. The transparent quartz windows were used as side walls of the cavity.

The lasing experiments were performed with using of mirror couples. The ratio of mirror transmission was determined from equation:

$$\frac{T_R}{T_L} = \frac{W_R}{W_L}$$

where T_R , T_L mirror transmission of “right” and “left” mirrors respectively, W_R and W_L the measured power of laser beams from corresponding mirrors respectively. **The absolute value of mirror transmissions were assumed as declared by manufactures.** This ratio was used to check the absolute value of mirror transmission. The small signal gain g was estimated as

$$g = (T_R + T_L)_{\max} / 2L_a$$

where $(T_R + T_L)_{\max}$ is the maximum value of the total mirror transmission at which a small but nonzero output power was detected. $L_a = 5.2 \text{ cm}$ is the lasing length.

6.1. SSG of the lasing medium produced by ENB-1.

Flow conditions and the estimated SSG.

BHP molarity	[KOH]=6.5M, [H ₂ O ₂]=7.5M
BHP temperature	-16C
BHP volumetric rate	1.2 L/s
Cl ₂ molar flow rate	57 mmole/s
Driver N₂ molar flow rate	480 mmole/s
Secondary N₂ molar flow rate	45 mmole/s
I ₂ molar flow rate	1 mmole/s
Distance between the nozzle outlet plane and the optical axis	48 mm
Pressure in FGJSOG-1	20 torr
Gas residence time in FGJSOG-1	6 ms
Cavity pressure	7.8 torr
Estimated SSG (Fig. 41)	>0.01cm⁻¹

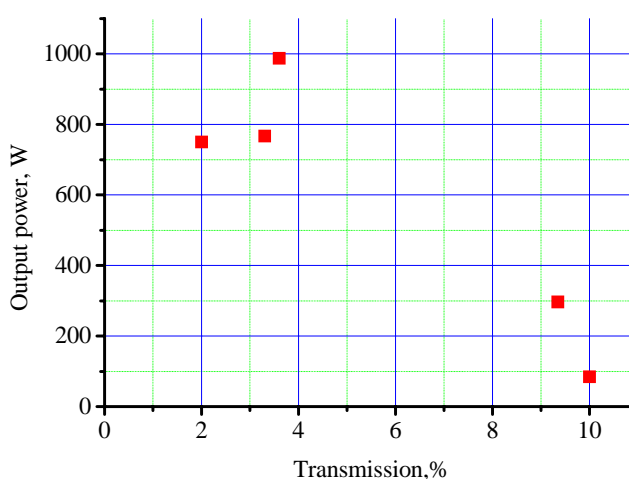


Fig. 41. Dependence of the total output power as a function of the total mirrors transmission.

BHP molarity	[KOH]=6.5M, [H ₂ O ₂]=7.5M
BHP temperature	-16C
BHP volumetric rate	1.2 L/s
Cl ₂ molar flow rate	57 mmole/s
Driver N₂ molar flow rate	500 mmole/s
Secondary He molar flow rate	45 mmole/s
I ₂ molar flow rate	1 mmole/s
Distance between the nozzle outlet plane and the optical axis	48 mm
Pressure in FGJSOG-1	20 torr
Gas residence time in FGJSOG-1	6 ms
Cavity pressure	8 torr
The output power 330W was detected for maximal total mirror transmission 10%.	
Estimated SSG	>0.01cm⁻¹

BHP molarity	[KOH]=6.5M, [H ₂ O ₂]=7.5M
BHP temperature	-16C
BHP volumetric rate	1.2 L/s
Cl ₂ molar flow rate	57 mmole/s
Driver N₂ molar flow rate	270 mmole/s
Secondary He molar flow rate	60 mmole/s
I ₂ molar flow rate	1 mmole/s
Distance between the nozzle outlet plane and the optical axis	48 mm
Pressure in FGJSOG-1	20 torr
Gas residence time in FGJSOG-1	6 ms
Cavity pressure	5 torr
The output power 439 W was detected for maximum total mirror transmission 10%. Estimated SSG	>0.01cm⁻¹

BHP molarity	[KOH]=6.5M, [H ₂ O ₂]=7.5M
BHP temperature	-16C
BHP volumetric rate	1.2 L/s
Cl ₂ molar flow rate	57 mmole/s
Driver N ₂ molar flow rate	270 mmole/s
Primary He molar flow rate	60 mmole/s
Secondary He molar flow rate	60 mmole/s
I ₂ molar flow rate	1 mmole/s
Distance between the nozzle outlet plane and the optical axis	48 mm
Pressure in FGJSOG-1	37.3 torr
Gas residence time in FGJSOG-1	5.5 ms
Cavity pressure	6.6 torr
The output power 312 W was detected for maximum total mirror transmission 11.9%. Estimated SSG	>0.012cm⁻¹

6.2. SSG of the lasing medium produced by ENB-2.

Flow conditions and the estimated SSG.

BHP molarity	[KOH]=6.5M, [H ₂ O ₂]=7.5M
BHP temperature	-16C
BHP volumetric rate	1.2 L/s
Cl ₂ molar flow rate	57 mmole/s
Driver N₂ molar flow rate	250 mmole/s
Secondary N₂ molar flow rate	60 mmole/s
I ₂ molar flow rate	1 mmole/s
Distance between the nozzle outlet plane and the optical axis	48 mm
Pressure in FGJSOG-1	20 torr
Gas residence time in FGJSOG-1	6 ms
Cavity pressure	8 torr
Estimated SSG (Fig. 42)	>0.01cm⁻¹

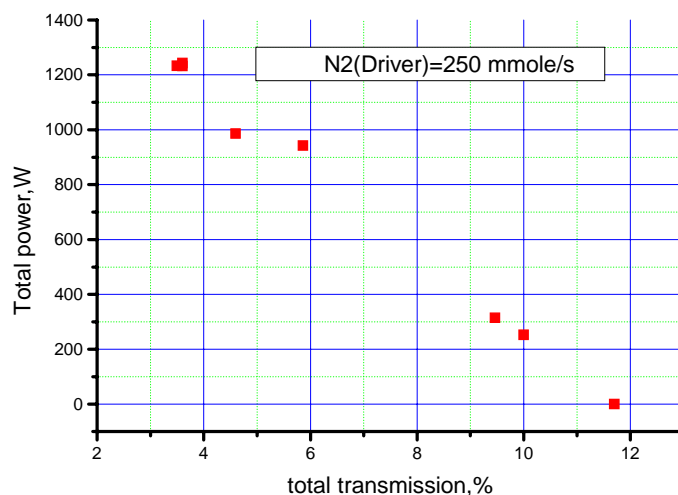


Fig. 42. Dependence of the total output power as a function of the total mirrors transmission.

BHP molarity	[KOH]=6.5M, [H ₂ O ₂]=7.5M
BHP temperature	-16C
BHP volumetric rate	1.2 L/s
Cl ₂ molar flow rate	57 mmole/s
Driver N₂ molar flow rate	500 mmole/s
Secondary N₂ molar flow rate	60 mmole/s
I ₂ molar flow rate	0.95 mmole/s
Distance between the nozzle outlet plane and the optical axis	48 mm
Pressure in FGJSOG-1	25 torr
Gas residence time in FGJSOG-1	7.5 ms
Cavity pressure	10 torr
Estimated SSG (Fig. 43)	>0.00 95cm⁻¹

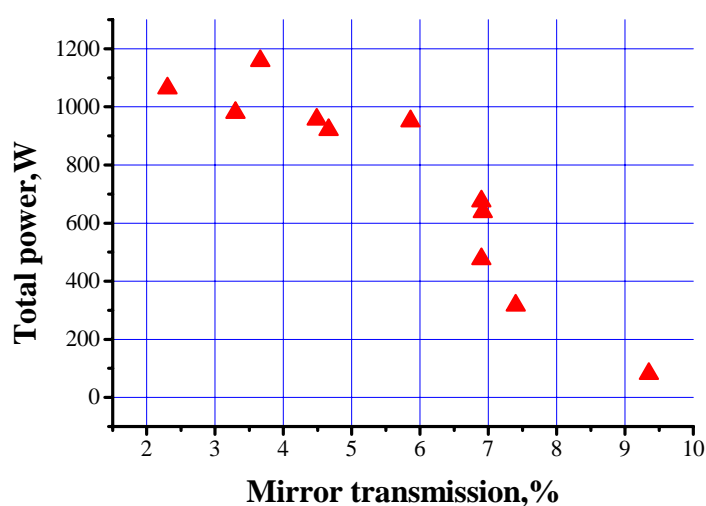


Fig.43. Dependence of the total output power as a function of the total mirrors transmission.

BHP molarity	[KOH]=6.5M, [H ₂ O ₂]=7.5M
BHP temperature	-7C
BHP volumetric rate	1.2 L/s
Cl ₂ molar flow rate	57 mmole/s
Driver N ₂ molar flow rate	500 mmole/s
Secondary N ₂ molar flow rate	60 mmole/s
I ₂ molar flow rate	0.95 mmole/s
Distance between the nozzle outlet plane and the optical axis	48 mm
Pressure in FGJSOG-1	25 torr
Gas residence time in FGJSOG-1	7.5 ms
Cavity pressure	10 torr
Estimated SSG (Fig.44)	>0.0 08cm ⁻¹

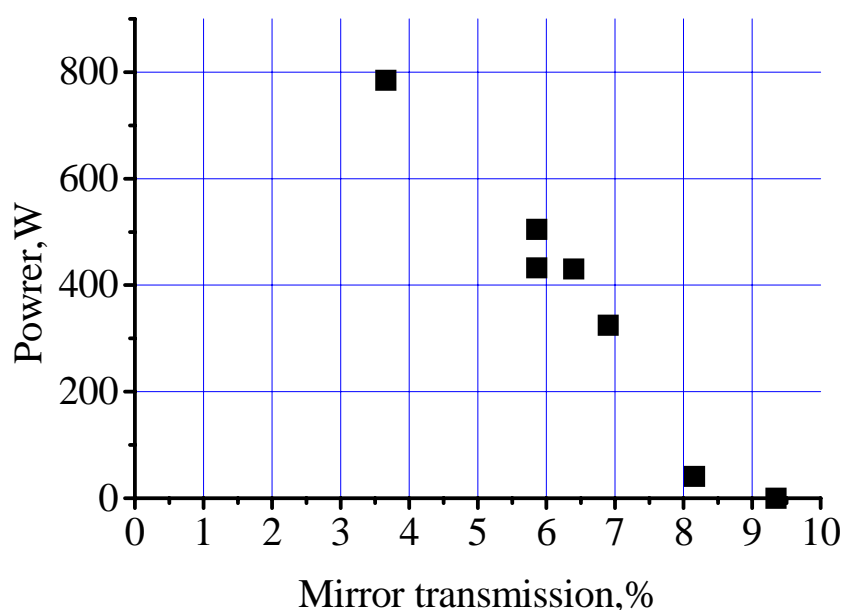


Fig.44. Dependence of the total output power as a function of the total mirrors transmission.

6.3. SSG of the lasing medium produced by ENB-3.

Flow conditions and the estimated SSG.

BHP molarity	[KOH]=6.5M, [H ₂ O ₂]=7.5M
BHP temperature	-16C
BHP volumetric rate	1.2 L/s
Cl₂ molar flow rate	72 mmole/s
Primary He molar flow rate	90 mmole/s
Driver N₂ molar flow rate	380 mmole/s
Secondary He molar flow rate	60 mmole/s
I ₂ molar flow rate	0.8 mmole/s
Distance between the nozzle outlet plane and the optical axis	48 mm
Pressure in FGJSOG-2	47 torr
Gas residence time in FGJSOG-2	8 ms
Cavity pressure	9.5 torr
Estimated SSG (Fig. 45)	>0.0 1cm⁻¹

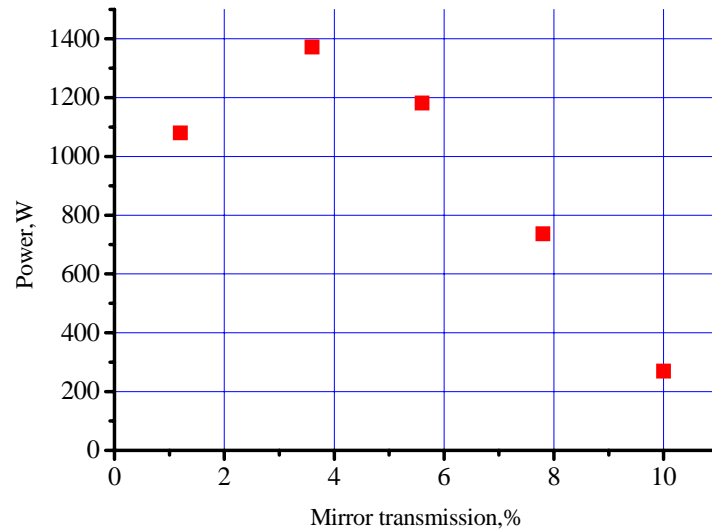


Fig.45. Dependence of the total output power as a function of the total mirrors transmission.

BHP molarity	[KOH]=6.5M, [H ₂ O ₂]=7.5M
BHP temperature	-16C
BHP volumetric rate	1.2 L/s
Cl ₂ molar flow rate	57 mmole/s
Primary He molar flow rate	90 mmole/s
Driver N₂ molar flow rate	400 mmole/s
Secondary He molar flow rate	120 mmole/s
I ₂ molar flow rate	1 mmole/s
Distance between the nozzle outlet plane and the optical axis	48 mm
Pressure in FGJSOG-2	37 torr
Gas residence time in FGJSOG-2	6.4 ms
Cavity pressure	9 torr
Nonzero power was detected for the total mirror transmission T _R +T _L =11.9%	
Estimated SSG	>0.0 12cm⁻¹

Though the gain medium had layer structure near region of the optical axis (~50mm downstream ENB) the small signal gain exceeded 1% cm⁻¹ for all nozzle banks. When ENB-2 was used SSG decreased from 0.095% cm⁻¹ up to 0.08% cm⁻¹ at increasing BHP temperature from -16 °C to -7 °C.

6.4 Distribution of the excited iodine atoms I* along the gas flow

The excited iodine atom I* concentration in the gain flow is

$$N_{I^*} = \frac{G_I}{A_g V_g} \frac{K_e Y}{(K_e - 1)Y + 1}$$

where G_I is the atomic iodine molar flow rate, A_g is the cross section area of the gain flow, V_g is the velocity of the gain flow, K_e = 0.75exp(401/T) is the equilibrium constant of the energy exchange O₂(¹Δ)+I ↔ O₂(³Σ)+I*, T is the gain flow temperature, Y is the O₂(¹Δ) yield. At temperatures lower than 200°K, when K_e >> 1, g ≈ N_{I*}σ. Therefore the I(²P_{1/2}) atom distribution along the flow direction approximately corresponds to the gain distribution. The distribution of I(²P_{1/2}) atoms along the z-direction was measured by detection of spontaneous emission at 1.315 μm.

The Ge-detector equipped with the filters was placed at distance of 160 mm (in y direction) from the glass window of the cavity. This detector could be moved in z-direction. A two small diaphragms were placed between the cavity and Ge-detector to measure 1.315 μm emission in y direction under small space angel Ω near $x=0$. Let assume that flow in cavity has two-dimensional structure (uniform in y-direction and not uniform in x-direction). It is good approximation of flow structure in the case of ENB-2 and ENB-3. The output signal of Ge-detector U_{Ge} at mixing plane jets is proportional to the average I^* concentration in y direction:

$$U_{\text{Ge}} \sim \int_0^{L_x} N_{I^*} dx \sim \frac{G_I}{V_g} \frac{K_e Y}{(K_e - 1)Y + 1} \sim 1/V_g$$

Where L_x is gain length along the optical axis.

The SSG of the flow is

$$g = \sigma \frac{G_I}{A_g V_g} \frac{(K_e + 0.5)Y - 0.5}{(K_e - 1)Y + 1}$$

where σ is the emission cross section. The gain along optical axis is

$$G = \int_0^{L_x} g dx \sim \sigma \frac{G_I}{H V_g} \frac{(K_e + 0.5)Y - 0.5}{(K_e - 1)Y + 1}$$

H is the average height (in y direction) of the gain flow.

At low gas temperature (when $K_e \gg (1-Y)/Y$) the gain is approximately proportional to the average iodine concentration or $G \sim U_{\text{Ge}}$

It is to be noted that the average height of the gain flow H increases along z direction.

Distribution of $I^*(z)$ emission for ENB-1 at $G_{\text{sec}}(N_2, \text{He})=60$ mmole/s, $G_{I_2}=1$ mmole/s is presented in Fig. 46. The increase of the driver nitrogen molar flow rate resulted in faster decrease of I^* emission along the flow. The analogous decrease of the small signal gain was found for the gain flow generated by our previous ejector nozzle banks [4]. We explain it by fast changing of the absolute gain flow velocity V_g at mixing with the higher Mach number and colder driver N_2 stream. The quenching of $O_2(^1\Delta)$, I^* and I recombination during flight time interval $\sim 2 \times 10^{-4}$ s through the cavity is too small to explain the fast drop of $I^*(z)$ emission along the flow. The decrease of the small signal gain $g(z)$ along the flow should be more intense for ENB-1 than increasing $H(z)$ due to two dimensional nature of the iodine jet expansion and mixing processes.

The distributions of $I^*(z)$ emission along the flow for ENB-2 are presented in fig. 47

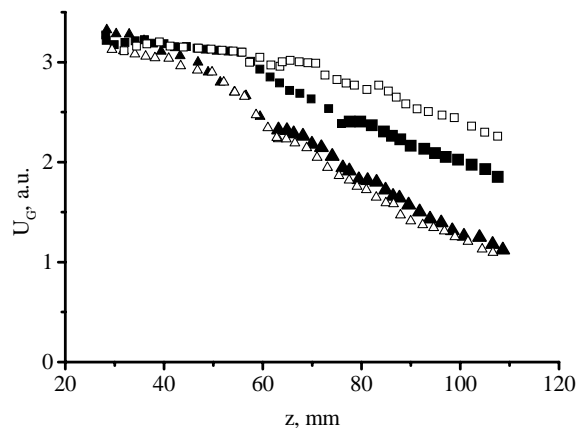


Fig.46. Output signal U_G as a function of the distance from the ENB-1. Molar flow rates: secondary gas (nitrogen-solid symbols, helium-open symbols) 60 mmole/s, molecular iodine 1 mmole/s.

Driver nitrogen molar flow rate: \blacktriangle , \triangle -500 mmole/s, \blacksquare , \square -250 mmole/s

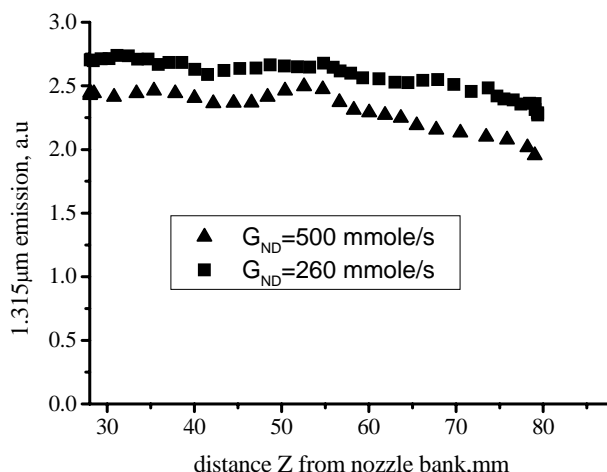


Fig.47. Distribution of the I^* emission along gas flow for ENB-2.

The initial signal U_G for ENB-2 is close to obtained for ENB-1. But the drop of I^* emission along gas flow for ENB-2 is less than for ENB-1. It can be explain by slower mixing rate of the gain flow with the driver nitrogen for ENB-2 than for ENB-1.

The studied nozzle banks with the supersonic nozzles for the driver nitrogen generate the supersonic gain flow with high Mach number and high potential recovered pressure. Simultaneously the small signal gain more than $10^{-2}/\text{cm}^{-1}$ has been estimated for all tested nozzle banks from the Rigrod curves. ENB-1 provides more fast mixing of all gas flows and this correlates with measurements of the Pitot pressure distributions at different distances from the nozzle bank. Monitoring 1.315μ emission of the excited iodine atoms demonstrated drops emission downstream ENB-1. Such drop may be explained by increasing of the gain flow velocity at mixing with the high-velocity driver N_2 . It is to be noted also that contact high Mach number of the driver nitrogen (up to $M \approx 5$) at very low static temperature (up to $T \approx 55 \div 60\text{K}^\circ$) with oxygen flow containing ~ 0.5 torr water vapor creates high possibility for water vapor condensation into super fine ice aerosol and formation of iodine clusters (due to high oversaturation conditions) [11]. Then iodine vapor (and iodine atoms also) may be absorbed by this fine ice aerosol and clusters. It is known that the rate constant for the iodine atom recombination reactions dramatically increase with decreasing the temperature [12, 13]. Recombination with formation of the simplest complex ($I\text{-H}_2\text{O}$) or I_3 can also take place. This may be second reason decreasing of $I^*(z)$ emission and small signal gain downstream ENB-1. But this requires additional investigations with using diode laser spectroscopy.

Dilution Cl_2 with He in ratio $\sim 1:1$ decreased dropping of the spontaneous emission excited iodine atoms at the driver nitrogen molar flow rate $G_{DN}=250\text{mmole/s}$ and it was not any changes at $G_{DN}=500\text{mmole/s}$ when driver flow had lower gas temperature.

In the case of ENB-2 the main mixing of the gain flow with the driver nitrogen flow occurs near aerodynamic throat and then the mixing slows down. In the case of ENB-1 the continuous mixing of the gain medium with the cold supersonic driver N_2 flow takes place. Therefore the gain decrease along the flow is substantially faster in the case of ENB-2. A SSG of gain flow generated by all three tested nozzle banks is higher than $1\%/ \text{cm}$ at the distance ~ 50 mm from ENB and BHP temperature -16°C . At increasing BHP temperature from -16°C to -7°C SSG produced by ENB-2 was reduced from $0.95\%/\text{cm}^{-1}$ to $0.8\%/\text{cm}^{-1}$.

The maximum chemical efficiency 24% and 23.5% have been obtained at 57 mmole/s of chlorine molar flow rate and at new mirrors with ENB-3 and ENB-1 respectively. The dilution of chlorine with helium in ratio close to 1:1 didn't increase substantially output power in the case of ENB-1. The employing of helium instead of nitrogen as a secondary buffer gas also doesn't result in substantial power enhancement.

7. COIL performance with ENB-1 and ENB-2 and dilution free of primary gas with He.

7.1. COIL performance with ENB-1.

Quality of the available mirrors was low enough. So both mirrors with transmittance more 1% were employed usually to decrease intra-cavity intensity and to prevent its' destruction. Series of the tests 7.1.1÷7.1.3 were performed at the highest driver N₂ molar flow rate G_{ND}=500mmole/s

7.1.1. COIL performance at using FGJSOG-1 as a source of O₂(¹Δ).

Gas flow and SOG parameters:

Chlorine molar flow rate, G ₁	57 mmole/s
Driver nitrogen molar flow rate, G _{DN}	500 mmole/s
Secondary Nitrogen molar flow rate, G ₂	varied
Optical axis - outlet nozzle plane distance, L _{oa}	48 mm
Type of SOG: BHP flow rate 1200 l/s, BHP temperature -16C	FGJSOG-1
Distance between Pitot tube and the outlet nozzle plane, L _p	75 mm

A typical temporal dependence of the output power is presented in Fig.48. Other results of these series are presented in Table.

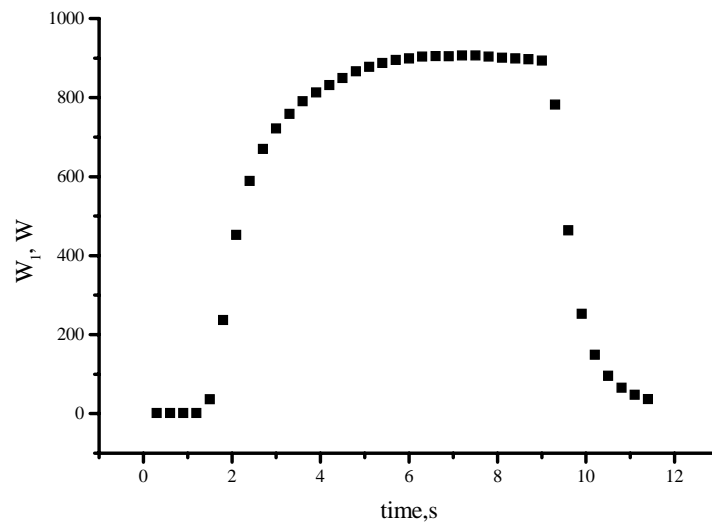


Fig. 48 Typical temporal dependence of the output power through the right mirror (test 4).

Test N	G ₂	G _{I2}	T	P1	P2	P3	P4	P5	W	η
1	30	0.72	3.6	21	21.3	8.0	129	77	876	17.0
2	60	0.76	3.6	22	21.3	8.4	235	80	924	17.9
3	45	0.75	3.6	21	19.6	8.3	187	78	953	18.4
4	45	0.84	3.6	21	19.2	8.5	187	81	1016	19.7
5	45	0.96	3.6	21	18.6	8.6	188	83	987	19.1
6	60	0.98	3.6	22	20.6	7.7	239	82	975	18.9
7	45	1	5.9	21	20.0	7.7	183	80	684	13.2
8	45	1	9.1	21	19.6	7.8	181	78	297	5.7
9	45	1	9.9	12	19.5	8.0	182	80	85	1.6
10	45	1	3.3	22	21.3	8.2	181	75	767	14.8
11	45	1	2.1	22	18.1	8.3	181	80	750	14.5

12	45	0.77	2	21	17.4	8.1	176	78	843	16.3
13	45	0.9	2	21	17.9	8.3	179	79	838	16.2
14	45	0.9	2	19	16.2	7.5	179	57	910	17.6

The secondary N₂ flow rate in the tests N.1-3 was varied. Then the iodine flow rate G_{I2} was varied at G₂=45 mmole/s. The optimization of the mirror transmission was performed at G₂=45 mmole/s and G_{I2}=1 mmole/s. The maximum chemical efficiency 19.7% have been achieved for G₂=45 mmole/s, G_{I2}=0.84 mmole/s, T=3.6%. Employing mirrors with low transmittance did not raise the chemical efficiency due to its' low optical quality. The estimated small signal gain exceeds 10⁻²cm⁻¹ because the nonzero power was detected at T=9.9% (Run 9).

7.1.2 COIL performance at using FGJSOG-2 as a source of O₂(¹Δ).

This generator has larger working reaction volume than FGJSOG-1. It provided higher chlorine utilization but had larger gas residence time.

Gas flow and SOG parameters.

Chlorine molar flow rate, G ₁	57 or 72 mmole/s
Driver nitrogen molar flow rate, G _{DN}	500 mmole/s
Secondary Nitrogen molar flow rate, G ₂	varied
Optical axis - outlet nozzle plane distance, L _{oa}	48 mm
Type of SOG: BHP flow rate 1300 l/s, BHP temperature -16°C	FGJSOG-2
Distance between Pitot tube and the outlet nozzle plane, L _p	75 mm

Result of these runs are presented in the Table

Test N	G _c	G ₂	G _{I2}	T%	P1	P2	P3	P4	P5	W ₁	W ₂	W	η
1	57	45	0.75	3.6	24.5	19.2	6.15	191		756	25.8	834.	16.2
2	57	60	0.85	3.6	22.6	19.4	6.6	233	85	707	25	781	15.1
3	72	60	0.91	3.6	30	25.5	7.6	237	91	988	38.4	1095	16.8
4	72	60	0.91	3.6	27.6	23.6	7.3	222	87	1001	38	1109	17.0
5	72	60	1	3.6	28.2	24.5	7.5	227	89	863	32	955	14.6

The use FGJSOG-2 as a source of O₂(¹Δ) with increased of gas residence time in the reaction zone did not improve COIL operation. Higher chlorine utilization could not compensate the negative effect on chemical efficiency of the raise of O₂(¹Δ) transport losses. The output power with this generator at G_c=57mmole/s became less. At G_c=72mmole/s it was practically the same as with FGJSOG-1 at G_c=57mmole/s.

7.1.3. COIL performance at using He as secondary buffer gas.

Gas flow and SOG conditions.

Chlorine molar flow rate, G ₁	72 mmole/s
Driver nitrogen molar flow rate, G _{DN}	500 mmole/s
Secondary He molar flow rate, G ₂	varied
Type of SOG: BHP flow rate 1300 l/s, BHP temperature -16°C	FGJSOG-2
Distance between Pitot tube and the outlet nozzle plane, L _p	75 mm

Results are presented in Table

Test N	L _{oa}	L _p	G ₂	G _{I2}	T%	P1	P2	P3	P4	P5	W	η
1	48	75	45	1.2	3.6	25.5	22.1	6.9	110	74	1061	16.3
2	48	75	45	1.1	3.6	26.7	23.7	6.7	100	72	1221	18.7
3	48	75	60	1.2	3.6	27.4	24.6	7.07	128	84	1184	18.2
4	48	75	60	1	3.6	27.1	24.7	6.76	120	77	1298	19.9
5	48	75	60	0.81	3.6	27.1	24.9	6.75	116	71	1269	19.5
6	48	75	60	0.55	3.6	27.2	24.9	6.6	109	72	852	13.1
7	48	75	85	1.15	3.6	28.5	26.1	7.06	154	83	1251	19.2

8	48	75	85	0.85	3.6	28.5	26	7.03	152	83	1162	17.8
9	48	75	85	1.4	3.6	29	26.4	7.2	155	83	1041	16.0
10	48	75	60	0.9	3.6	27.7	25.1	6.9	123	75	1089	16.7

Employing of helium instead of secondary nitrogen resulted in some increase of COIL power and efficiency. From this series we found that for these conditions the optimal iodine molar flow rate $G_{I_2} \approx 1 \text{ mmole/s}$ and optimal secondary helium molar flow rate is $45 \div 60 \text{ mmole/s}$. The next two experiments demonstrate that power substantially decreases at replacement of the optical axis downstream on 30mm.

N	L_{oa}	G_1	G_2	G_{I_2}	P1	P2	P3	P4	P5	W	η
1	48	57	60	1	3.6	21	19	8.1	125	887	17.1
2	78	57	60	1	3.6	26	26	6.6	133	417	8

This result is in accordance with previous experiments (Fig. 46) where was found that the concentration of excited iodine quickly decreases along the gain gas flow. Such output power drop can't be explained by fast quenching singlet oxygen and decreasing of the storage power. The reason of this phenomenon is very low gas temperature. The driver N_2 static temperature at the micro nozzle exit decreased at the raise molar flow rate from 250 to 500mmole/s and resulted in the more fast I^* drop along gas flow.

7.1.4. COIL performance at lower driver nitrogen flow rate $\sim 250 \text{ mmole/s}$.

Gas flow and SOG conditions:

Chlorine molar flow rate, G_1	57 mmole/s
Driver nitrogen molar flow rate, G_{ND}	270 mmole/s
Secondary Helium molar flow rate, G_2	60 mmole/s
Type of SOG: BHP flow rate 1200 l/s, BHP temperature-16°C	FGJSOG-1
Distance between the optical axis and the outlet nozzle plane, L_{oa}	48 mm

Results are presented in Table

Test N	G_2	G_{I_2}	T	P1	P2	P3	P4	W	η
1	60	1.06	3.6	19	16.4	6.3	119	1055	20.4
2	60	1	10	22	20	6.3	120	383	7.4
3	60	1.1	3.5	19	15.3	6.8	115	1017	19.7
4	60	1.1	1.47	19.1	15.3	6.1	112	905	17.5
5	60	1.13	1	19	15.2	6.6	115	1012	19.7
6	60	1.08	3.6	19	17	6.7	122	1015	19.7
7	60	0.93	1	19	17	6.4	117	921	17.8
8	60	1	10	19	15.5	5.5	126.6	346	6.7
9	60	1	6.4	18.7	15.4	5.8	114	823	16

It's to be noted that the estimated small signal gain is higher than $10^{-2}/\text{cm}$ (run 2). Chemical efficiency of 16% (run 9) for total mirror transmission 6.4% is only on 4.4% less than efficiency 20.4% for the total mirror transmission 3.6% (run 1)

The feature of this active medium consists in the very low static temperature which leads to such situation when practically all iodine atoms are in the excited state and inverted population practically doesn't depend on $O_2(^1\Delta)$ yield Y when the equilibrium constant $K_{eq} = 0.75 \exp(401/T) \gg 1$ and $Y \gg 1/K_{eq}$ at very low temperature

$$\Delta N = \left(Y - \frac{1}{(2K_{eq} + 1)} \right) \frac{(K_{eq} + 0.5)}{(K_{eq} - 1)Y + 1} N_I \approx N_I$$

For example $1/K_{eq}=0.0242$ at $T=100^\circ\text{K}$ and $1/K_{eq}=0.00167$ only at $T=60^\circ\text{K}$. Moreover with a decrease in temperature the small signal gain depends on Y weakly only and higher optical extraction is possible for a given gain/threshold ratio. Therefore the generation of a supersonic COIL gain medium at low temperature and with high small signal gain is preferable for high power operation. It's very important at employing of an unstable resonator inasmuch as this gives possibility to use resonator with higher magnification.

The next runs have been performed at the distance between exit plane of the nozzle bank and optical axis of 78 mm.

Test N	L_{oa}	G_2	G_{I2}	T	P1	P2	P3	P4	W	η
10	78	60	1	3.6	19.6	18	8.3	125	656	12.7
11	78	60	0.66	2.6	19.2	18.2	5.7	109	760	14.7

In run 10 the power was substantially less than in runs (N1, N5, N6). The decrease of iodine molar flow rate and mirror transmittance simultaneously (run 11) results in some increase power. This result also is in accordance with the registered fast drop of the excited iodine concentration along the gain gas flow (Fig. 46).

7.2. COIL performance with ENB-2.

7.2.1. COIL performance at the driver N_2 molar flow rate $G_{ND}=500\text{mmole/s}$.

Gas flow and SOG conditions.

Chlorine molar flow rate G_1	57 mmole/s
Driver nitrogen molar flow rate, G_{DN}	500 mmole/s
Secondary Nitrogen molar flow rate, G_2	varied
Type of SOG: BHP flow rate 1200l/s, BHP temperature -16°C	FGJSOG-1

The results are presented in Table and Fig. 49.

Test N	$G_2(N_2)$	G_{I2}	T	P ₁	P ₂	P ₃	P ₄	W	η	$P_1\tau_R$
1	20	0.80	3.6	24	22	9.8	76	1059	20.5	0.231
2	32	0.80	3.6	25	22	9.5	113	1104	21.4	0.169
3	45	0.88	3.6	24	22	9.8	153	1153	22.3	0.156
4	60	0.95	3.6	25	23	10.2	192	1158	22.4	0.160
5	60	0.93	5.8	25	23	10.1	193	950	18.4	0.161
6	60	0.96	2.3	25	23	10.1	191	1063	20.6	0.159
7	60	0.94	3.3	24	23	10.1	191	980	19.0	0.159
8	60	0.89	4.66	25	23	10.0	191	921	17.8	0.162
9	60	0.97	6.92	24	23	10.0	191	639	12.4	0.159
10	60	0.93	4.49	25	23	10.2	192	957	18.5	0.159
11	60	0.95	6.9	25	23	10.2	191	675	13.1	0.163
12	60	0.94	6.9	26	23	10.2	190	476	9.2	0.181
13	60	0.97	9.35	24	23	10.0	190	81	1.6	0.159
14	60	0.94	7.4	24	23	10.1	189	317	6.1	0.157

It was found from these data that the optimal secondary nitrogen molar flow rate is equal to $G_2=60\text{mmole/s}$, optimal iodine molar flow rate $\sim 1\text{ mmole/s}$.

For these conditions the dependence of laser power on mirror transmittance is presented in Fig.49.

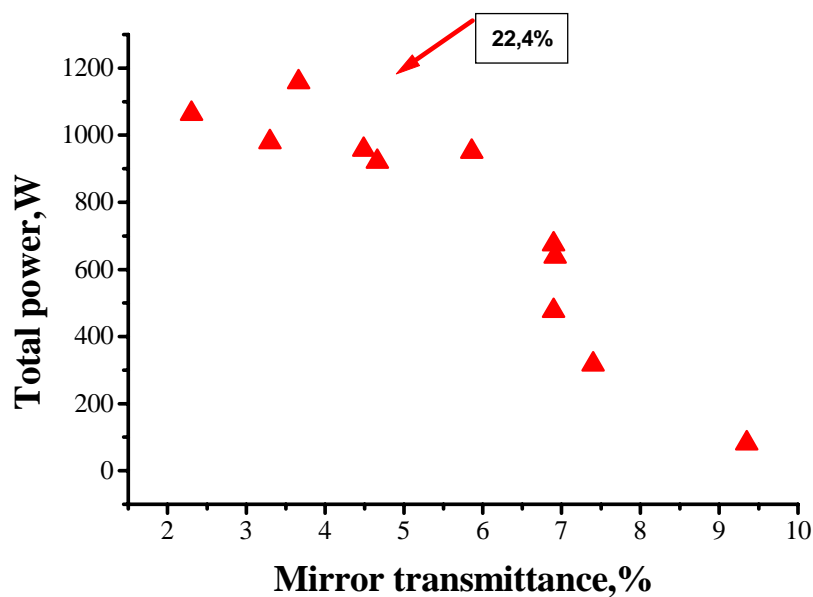


Fig.49. Dependence of the output power on the total mirror transmittance.

The highest power of 1158W and efficiency of 22.4% have been obtained in Run 4. Dependence of the COIL power on the BHP temperature is very important for COIL thermal management. At conditions (series 7.2.1., run 4) dependence of the output power on the BHP temperature is presented in Fig.50. Output power drops on ~26% at the raise BHP temperature from -25°C to -6°C.

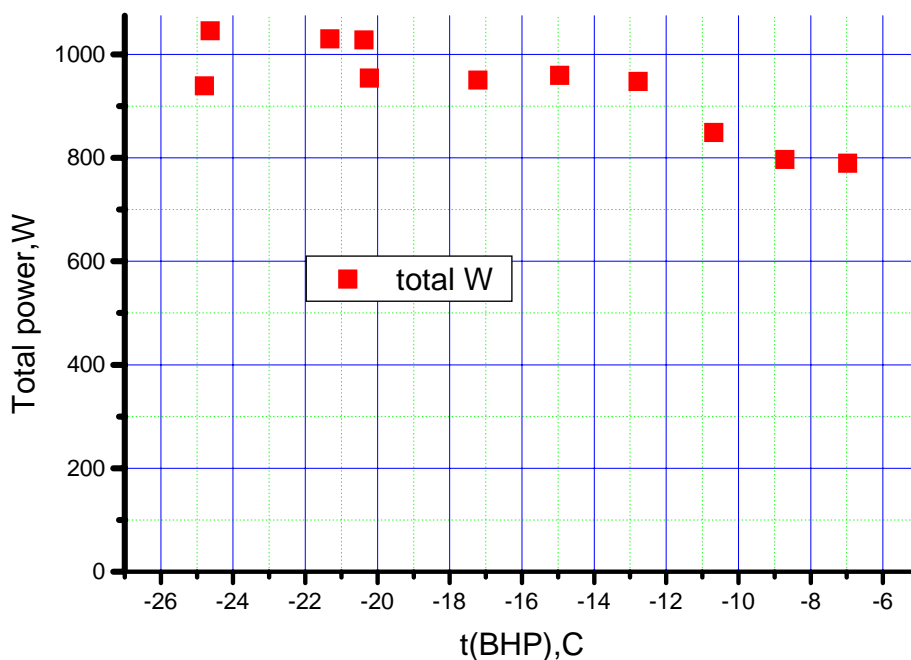


Fig.50. Dependence of the output power on the BHP temperature

Then COIL tests were made at higher chlorine flow rate (72mmole/s) with FGJSOG-2. These experiments demonstrated lower chemical efficiency than at employing FGJSOG-1.

Gas flow and SOG conditions.

Chlorine molar flow rate G_1	72 mmole/s
Driver nitrogen molar flow rate, G_{DN}	varied
Secondary Nitrogen molar flow rate, G_2	varied
Type of SOG: BHP flow rate 1300 l/s, BHP temperature -16C	FGJSOG-2

N	G_{DN}	$G_2(N_2)$	P_{I2}	T%	P1	P2	P3	P4	W	η
1	310	60	0.85	3.6	25.5	24.9	8	223	1056	16.2
2	310	60	0.85	3.6	26	25.5	7.6	223	999	15.3
3	310	60	0.72	3.6	25.9	25.6	7.5	218	977	15
4	310	60	0.85	3.6	26.3	25.6	7.5	224	1038	15.9
5	310	60	0.85	3,5	26.6	27.2	7.5	223	1209	18.5
6	500	60	0.85	3,5	27.6	27.6	10.3	218	1075	16.5
7	500	100	1.2	3,5	28.8	29.2	10.7	245	1112	17

7.2.2. The COIL performance at lower driver N_2 molar flow rate $G_{DN}=250$ mmole/s.

Gas flow and SOG conditions:

Chlorine molar flow rate G_1	57 mmole/s
Driver nitrogen molar flow rate, G_{DN}	250 mmole/s
Secondary Nitrogen molar flow rate, G_2	varied
Type of SOG: BHP flow rate 1200 l/s, BHP temperature -16C	FGJSOG-1

The results are presented in Table .

Test N	$G_2(N_2)$	G_{I2}	T%	P1	P3	P4	P5	W	η
1	30	0.72	3.6	19	8.2	127	70	1049	20.3
2	60	0.77	3.6	19	8.1	243	63	1137	22.0
3	60	0.68	3.6	19	7.7	234	67	979	18.9
4	60	0.67	3.6	20	7.8	236	64	1048	20.3
5	60	0.90	3.6	22	8.2	240	61	1039	20.1
6	60	0.75	3.6	19	7.9	247	61	1233	23.9
7	60	0.76	3.6	19	7.9	242	62	1243	24.1
8	60	0.77	3.5	21	8.0	244	63	1233	23.9
9	60	0.76	5.86	19	8.2	243	61	943	18.3
10	60	0.77	9.46	20	8.7	243	60	315	6.1
11	60	0.77	10	19	8.5	245	60	252	4.9
12	60	0.77	4.6	19	8.5	248	61	986	19.1
13	60	0.76	11.7	19	8.6	244	60	1	0.0

The optimal flow rates $G_2=60$ mmole/s and $G_{I2}=0.8$ mmole/s have been found. Dependence of the output power on mirror transmission at these conditions is presented in Fig.51.

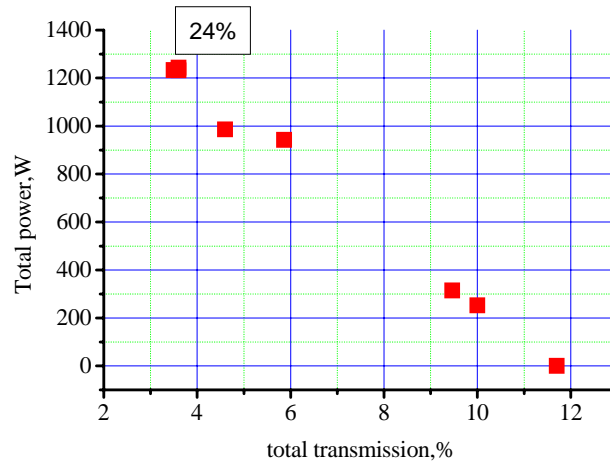


Fig. 51. Dependence of the output power on the mirror transmission.

The best results obtained at dilution free of primary chlorine are summarized in the Table.

Series	Test N	Nozzle bank	Type of SOG	L_{oa}	G_{ND}	G_1	G_2	G_{I2}	T	P1	P3	W	η , %
7.1.1	5	ENB-1	FGJSOG-1	48	500	57	45(N ₂)	0.84	3.6	19.2	8.5	1013	19.7
7.1.2	4	ENB-1	FGJSOG-2	48	500	72	60(N ₂)	0.91	3.6	27.6	7.3	1109	17
7.1.3	4	ENB-1	FGJSOG-2	48	500	72	60(He)	1	3.6	27.1	6.8	1298	19.9
7.1.4	1	ENB-1	FGJSOG-1	48	270	57	60(He)	1.06	3.6	19	6.3	1055	20.4
7.2.1	4	ENB-2	FGJSOG-1	48	500	57	60(N ₂)	0.95	3.6	25	10.2	1158	22.4
7.2.2	5	ENB-2	FGJSOG-2	48	500	72	60(N ₂)	0.85	3.5	26.6	7.5	1209	18.5
7.7.2	8	ENB-2	FGJSOG-1	48	250	57	60(N ₂)	0.76	3.6	19	7.9	1243	24.1

Employing of the supersonic micro nozzles for driver N₂ gives possibility to reduce the SOG pressure and to raise O₂(¹Δ) yield. Maximal reached COIL chemical efficiency was 20.4% for ENB-1 and 24.1% for ENB-2. Change of secondary nitrogen on helium resulted in some increase of the chemical efficiency due to the raise of the iodine injector conductivity and reducing of the maximal local iodine concentration at the same I₂ flow rate. The output power decreases on ~25% with increase of the BHP temperature from -25°C to -6°C.

The ENB-1 with micro nozzles produces high Mach number very cold jets of the driver N₂ and provides more fast mixing its with gain flow than ENB-2. The output power drops fast at replacement of the optical axis downstream ENB-1 on 30mm. This can't be explained by fast quenching singlet oxygen and decreasing of the storage power. The reason of given phenomenon connected with lowering of the iodine atom concentration. It may be iodine recombination $I^* + I_2 \rightarrow I_3$, attachment iodine atoms to surface of the ice or salt aerosols or iodine condensation at very low gas temperature. Decreasing of the driver N₂ static temperature at the micro nozzle exit at the raise driver N₂ molar flow rate from 250 to 500mmole/s lead to the more fast I* drop along gas flow. The indicated circumstances didn't allow attaining high COIL chemical efficiency with ENB-1 without preheating driver gas. The same reasons (namely bad mixing efficiency (Fig. 38), the stratified structure of the gas flow with higher temperature of the gain layers, slow I* emission drop (Fig. 47)) may be responsible for higher chemical efficiency of the COIL attained with ENB-2 and at lower the driver N₂ flow rate. It was supposed that premixing helium with the primary gas may increase the static gas temperature of the completely mixed flow and weaken gain degradation along gas flow.

8. COIL performance at chlorine dilution with helium with ratio $\text{Cl}_2:\text{He}\approx 1:1$

8.1. COIL performance with ENB-1.

Dilution of chlorine with helium allows to decrease the partial chlorine pressure in SOG and $\text{O}_2(^1\Delta)$ loss and to raise the gas static temperature in the cavity. In most of tests the secondary helium was used to increase gas conductivity of the iodine injector orifices, to reduce the initial local iodine concentration and $\text{O}_2(^1\Delta)$ loss in the region of intense iodine dissociation.

8.1.1. COIL performance at $G_{\text{ND}}=260$ mmole/s, $G_1=57$ mmole/s and FGJSOG-1.

From COIL tests with chlorine dilution free the optimal secondary helium molar flow rate of 60mmole/s and iodine molar flow rate of 1 mmole/s have been found. The same flow rates were used in tests at dilution of chlorine with helium. The perforated plate was installed at the gas outlet from the SOG. This plate formed the choke allowed to control the SOG pressure and generator operation stability.

Gas flow and SOG parameters

Chlorine molar flow rate G_1	57 mmole/s
Driver nitrogen molar flow rate, G_{DN}	260 mmole/s
Primary helium molar flow rate, G_{He1}	60 mmole/s
Secondary helium molar flow rate, G_2	60 mmole/s
Molecular iodine molar flow rate, G_{I2}	1 mmole/s
Total pressure in SOG	38 torr
Plenum pressure	18.5 torr
Cavity wall pressure	6.8 torr
Distance between the optical axis and the nozzle outlet, L_{oa}	48 mm
FGJSOG: BHP flow rate 1200 l/s, BHP temperature -16C	FGJSOG-1

The initial partial chlorine pressure in SOG was equal to ~ 19.5 torr. A several sets of mirrors were used in COIL tests. The output power depended not only on value of the total mirror transmission but on its' quality too. Dependence of the output power on the mirror transmission is presented in Fig. 52. Maximal power of 1114W with chemical efficiency of 21.6% was attained at the mirror transmission of 3.6%. SSG exceeded $1.2\% \text{ cm}^{-1}$.

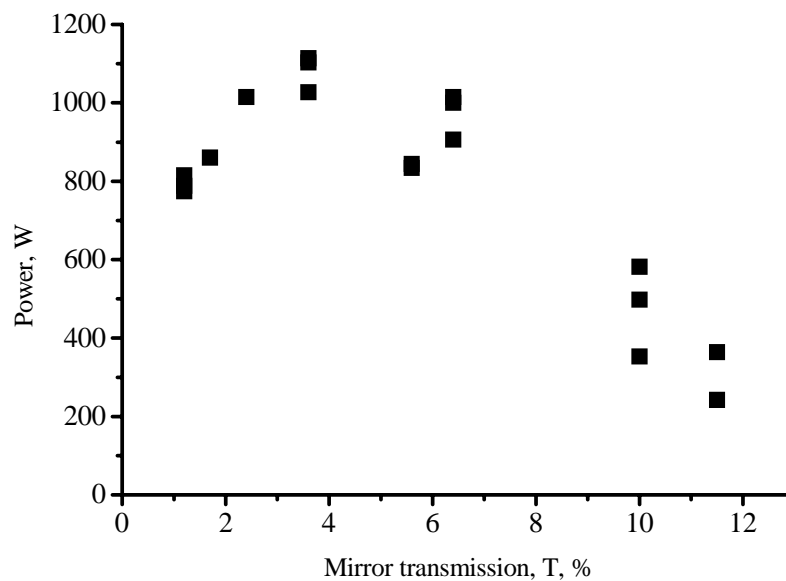


Fig.52. Dependence of the output power on the total mirror transmittance.

When the optical axis was placed at 88 mm downstream of exit plate of ENB-1 the output power substantially decreased. For example, at total mirror transmission 3.6% the output power was equal to 870W only (chemical efficiency of 16.8%).

8.1.2. COIL performance at $G_{ND}= 260$ mmole/s, $G_1=57$ mmole/s and FGJSOG-2.

The next tests were performed with FGJSOG-2 and lower pressure in SOG at the same gas flow conditions as in previous tests. The initial partial chlorine pressure in SOG was equal to ~12.5 torr.

Gas flow and SOG parameters

Chlorine molar flow rate G_1	57 mmole/s
Driver nitrogen molar flow rate, G_{DN}	260 mmole/s
Primary helium molar flow rate, G_{He1}	66 mmole/s
Secondary helium molar flow rate, G_2	62 mmole/s
Molecular iodine molar flow rate, G_{I2}	1 mmole/s
Total pressure in SOG	25 torr
Plenum pressure	20 torr
Cavity wall pressure	8.0 torr
Distance between the optical axis and the nozzle outlet, L_{oa}	48 mm
FGJSOG: BHP flow rate 1300 l/s, BHP temperature -16C	FGJSOG-2

Some tests were performed with the new of mirrors having transmittance 1.5%. Dependence of the output power on the mirror transmission is presented in Fig.53. Maximal power of 1215W with chemical efficiency of 23.5% was attained at two new mirrors with transmission 1.5%. SSG exceeded $1.2\% \text{ cm}^{-1}$. It was the first test when COIL with FGJSOG-2 operated better then with FGJSOG-1.

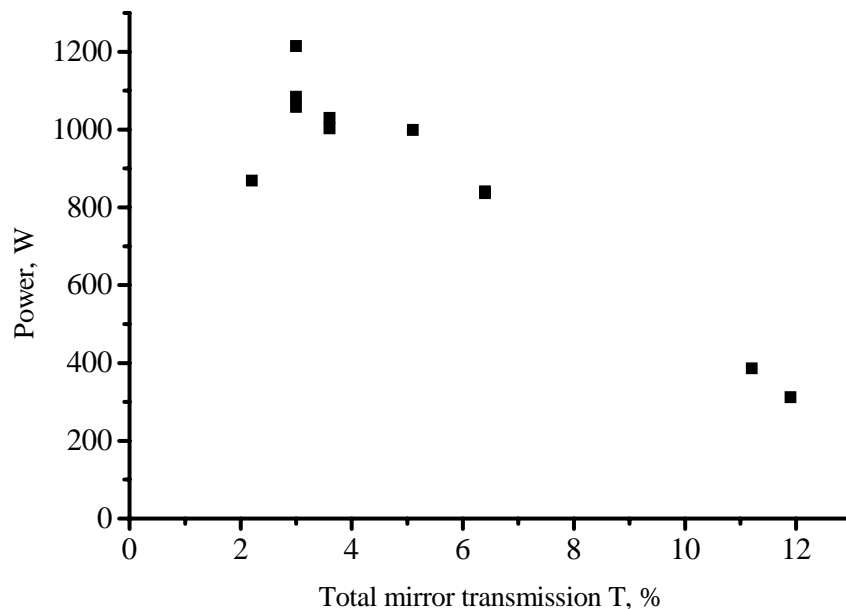


Fig. 53. Dependence of the output power on the total mirror transmittance.

8.1.3. COIL performance at $G_{DN}= 500$ mmole/s, $G_1=57$ mmole/s and FGJSOG-1.

Chlorine molar flow rate G_1	57 mmole/s
Driver nitrogen molar flow rate, G_{DN}	500 mmole/s
Primary helium molar flow rate, G_{He1}	60 mmole/s
Secondary helium molar flow rate, G_2	60 mmole/s
Molecular iodine molar flow rate, G_{I2}	1 mmole/s
Total pressure in SOG	40 torr
Plenum pressure	20 torr
Cavity wall pressure	7.1 torr
Distance between the optical axis and the nozzle outlet, L_{oa}	48 mm
FGJSOG: BHP flow rate 1200 l/s, BHP temperature -16C	FGJSOG-1

Maximal output power of 842W at employing of FGJSOG-1, $G_{DN}=500$ mmole/s and $T=3.6\%$ (713W at $T=6.4\%$) was substantially less than 1114W for $G_{DN}=260$ mmole/s or 1215W for $G_{DN}=260$ mmole/s and FGJSOG-2. Possible hydrogen peroxide used in these tests had bad quality.

8.1.4. COIL performance at $G_{ND}=500$ mmole/s, $G_1=72$ mmole/s and FGJSOG-2.

Chlorine molar flow rate G_1	72 mmole/s
Driver nitrogen molar flow rate, G_{DN}	500 mmole/s
Primary helium molar flow rate, G_{He1}	60 mmole/s
Secondary helium molar flow rate, G_2	60 mmole/s
Molecular iodine molar flow rate, G_{I2}	1 mmole/s
Total pressure in SOG	33 torr
Plenum pressure	27.6 torr
Cavity wall pressure	7.3 torr
Distance between the optical axis and the nozzle outlet, L_{oa}	48 mm
FGJSOG: BHP flow rate 1300 l/s, BHP temperature -16C	FGJSOG-2

The initial partial chlorine pressure in the SOG was equal to 18 torr. For these operational conditions maximal output power of 1264W (chemical efficiency of 19.4%) has been obtained at total mirror transmission 3.6% (1006W at $T=6.4\%$).

8.2. COIL performance with ENB-2 at $G_{DN}=500$ mmole/s, $G_1=72$ mmole/s.

Chlorine molar flow rate G_1	72 mmole/s
Driver nitrogen molar flow rate, G_{DN}	500 mmole/s
Secondary nitrogen molar flow rate, G_2	75 mmole/s
Primary helium molar flow rate, G_{He1}	60 mmole/s
Molecular iodine molar flow rate, G_{I2}	1 mmole/s
Total pressure in SOG	40 torr
Plenum pressure	33 torr
Cavity wall pressure	10 torr
Distance between the optical axis and the nozzle outlet, L_{oa}	48 mm
FGJSOG: BHP flow rate 1300 l/s, BHP temperature -16C	FGJSOG-2

Maximum output power of 1082W has been obtained at 3.6% mirror transmission and was less than in the case of COIL operation with ENB-1 at the same conditions.

8.3. COIL performance with ENB-3 at $G_{ND}=380$ mmole/s, $G_1=72$ mmole/s.

Chlorine molar flow rate G_1	72 mmole/s
Driver nitrogen molar flow rate, G_{DN}	380 mmole/s
Secondary nitrogen molar flow rate, G_2	varied
Primary helium molar flow rate, G_{He1}	60 mmole/s
Molecular iodine molar flow rate, G_{I2}	0.8 mmole/s
Distance between the optical axis and the nozzle outlet, L_{oa}	48 mm
FGJSOG: BHP flow rate 1300 l/s, BHP temperature -16C	FGJSOG-2

Optimization of the output power on the secondary nitrogen molar flow rate was made at total mirror transmission $T=5.6\%$. Results of this optimization are presented in Fig.54.

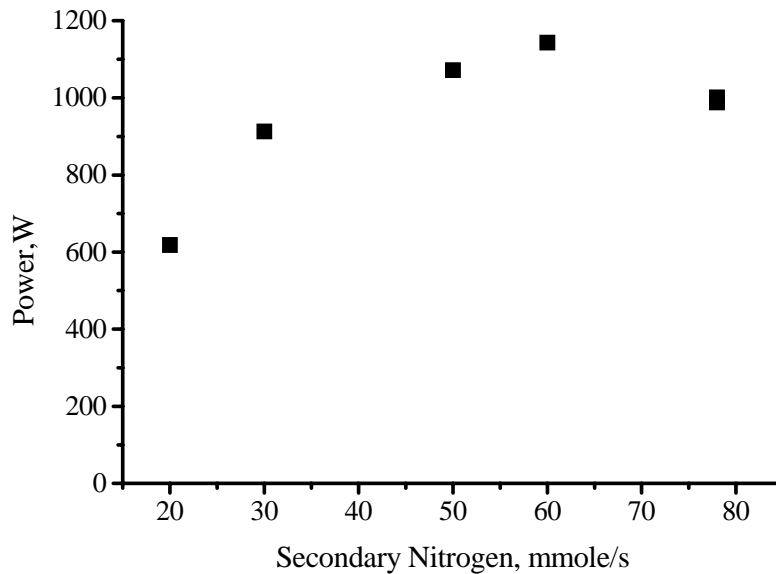


Fig.54. Dependence of the output power on secondary nitrogen molar flow rate.

Optimal secondary N_2 molar flow rate of 60mmole/s was determined. Then the primary helium was increased to 90mmole/s at the secondary nitrogen molar flow rate 60mmole/s. This led to the raise of the SOG pressure on 1.5torr. Dependence of the output power on the total mirror transmission is presented in Fig.55.

Chlorine molar flow rate G_1	72 mmole/s
Driver nitrogen molar flow rate, G_{DN}	380 mmole/s
Secondary nitrogen molar flow rate, G_2	60 mmole/s
Primary helium molar flow rate, G_{He1}	90 mmole/s
Total pressure in SOG	47 torr
Plenum pressure	42 torr
Cavity wall pressure	9.5 torr
Molecular iodine molar flow rate, G_{I2}	0.8 mmole/s
Optical axis- exit plane of the nozzle bank distance, L_{oa}	48 mm
FGJSOG: BHP flow rate 1300 l/s, BHP temperature -16C	FGJSOG-2

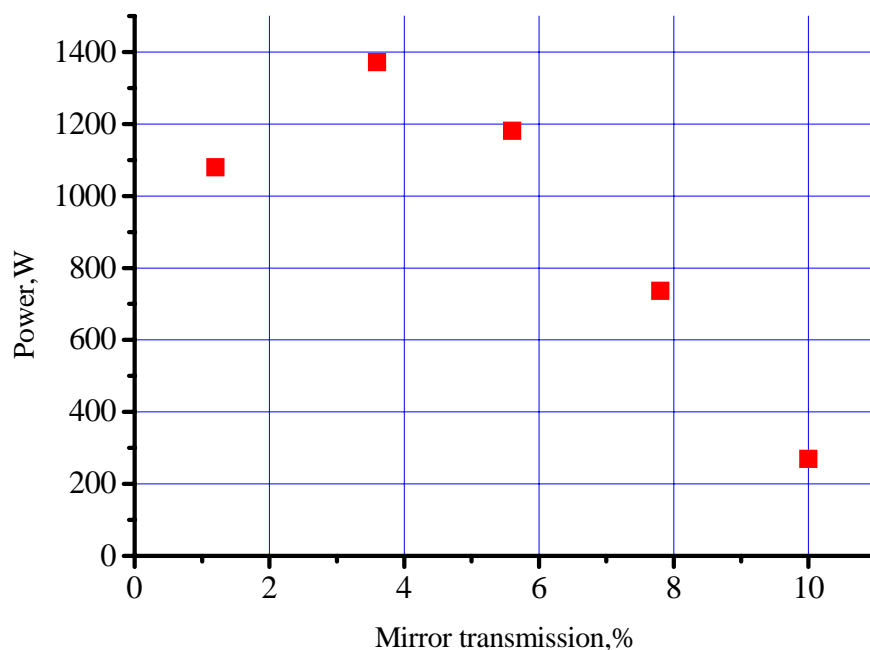


Fig.55. Dependence of the output power on the mirror transmission.

In spite of the fact that ENB-3 could not provide good mixing of the flows the maximal output power of 1372 W and chemical efficiency 21% attained at the total mirror transmission of 3.6% were not bad.

Pre-dilution chlorine with helium has twice influence on the mixing flows. From the one hand pre-dilution chlorine increases of the primary gas heat capacity and sonic velocity what promotes the rise of the gain medium temperature at the mixing with cold driver N_2 . From the other hand the additional raise of the static temperature at the chlorine pre-dilution is provided by more intense braking of the driver nitrogen and the partial pressure and temperature recovery in the mixing chamber. Pre-dilution of the chlorine with helium changes also the adiabatic exponent and effective molecular weight of the primary gas mixture and as result leads to the rise of the duct conductivity, decreasing SOG oxygen partial pressure, increasing singlet oxygen yield and chemical efficiency.

Lasing experiments with all nozzles bank demonstrated some raise of the chemical efficiency at pre-dilution chlorine with helium $Cl_2:He \approx 1:1$. After discussion with Partner it was reached a decision to continue the given investigations at more higher pre-dilution of the chlorine with helium up to $Cl_2:He = 1:2; 1:3; 1:4$. Moreover Partner established the additional requirement. Plenum pressure of the primary flow has to be equal to ~ 60 torr at chlorine flow rate of 60mmole/s and the highest dilution $Cl_2:He \approx 1:4$.

9. COIL performance with ENB-1 at higher chlorine dilution with helium $Cl_2:He \approx 1:(2\div 4)$.

9.1 Results of LIF and "cold" gasdynamic tests.

Pre-dilution of chlorine with helium changes the adiabatic constant and the effective molecular weight of the gas mixture. This leads to the rise of the duct conductivity, decreasing the partial oxygen pressure in SOG and increasing singlet oxygen yield. The rise of SOG pressure to required level may be provided by simple installation of the choke slit shutter between generator and nozzle bank. But the plenum pressure may be increased only by the change of the nozzle design or development new nozzle bank. Preliminary estimations made for ENB-1 showed necessity to increase resistance for the primary flow to attain of the required plenum pressure of ~ 60 torr. It was

possible to realize at small change the nozzle design. The plates of 1mm thickness were attached to all nozzle bank walls. For example, this allowed to raise the plenum pressure of such blocked ENB-1 at $\text{Cl}_2:\text{He}=1:2$ from $\sim 20\text{torr}$ to $\sim 32\text{torr}$. Results of the “cold” aerodynamic tests of the blocked ENB-1 at different pre-dilution chlorine with helium are presented in Table.

	$G_{\text{Primary air}}$ mmole/s	$G_{\text{Primary He}}$ mmole/s	$G_{\text{Driver N}_2}$ mmole/s	$G_{\text{Secondary He}}$ mmole/s	P_{Plenum} torr	$P_{\text{cavity,48mm}}$ torr	$P_{\text{cavity,105mm}}$ torr
1	60	60	500	60	32,4	5.6	7.6
2	60	130	520	60	40.7	6.3	10.3
3	60	150	520	60	42.7	6.7	10.9
4	60	240	520	66	48.2	7.6	13
5	83	240	520	66	52.7	8.1	
6	83	320*)	520	66	61.4	9.9	
7	100	320*)	520	66	65.1	10.1	

*) Orifice of the ball valve in the supplying duct of the primary helium restricted maximal value of gas molar flow rate.

Easily to see that the plenum pressure at dilution $\text{Cl}_2:\text{He}=1:4$ is closed to 60torr when the primary gas (air) molar flow rate equal to $\sim 80\text{mmole/s}$. So the cross section area of the nozzle bank equal to 7.6cm^2 this air molar flow rate provides the average flux $\sim 10\text{mmole/cm}^2\cdot\text{s}$. If one removes the plates attached to ENB-1 walls then oxygen flux through nozzle bank exceeds $12\text{mmole/cm}^2\cdot\text{s}$ at dilution $\text{Cl}_2:\text{He}=1:4$ and the plenum pressure $\sim 60\text{torr}$. In this case it is necessary to use SOG with practically twice higher throughput.

Laser induced fluorescence of molecular iodine was used for estimation of the mixing efficiency. ENB-1 has periodical structure with $\Delta x=\Delta y=4\text{mm}$. LIF patterns visualize the regions located of $28\div 78\text{mm}$ downstream the nozzle bank for different position of the plane Ar-laser beam with step in vertical direction $\Delta y=1\text{mm}$ or $\Delta y=2\text{mm}$ (Fig.56÷59). Easily to see the sharp dark stripes. These stripes point out the incompleteness of the mixing process.

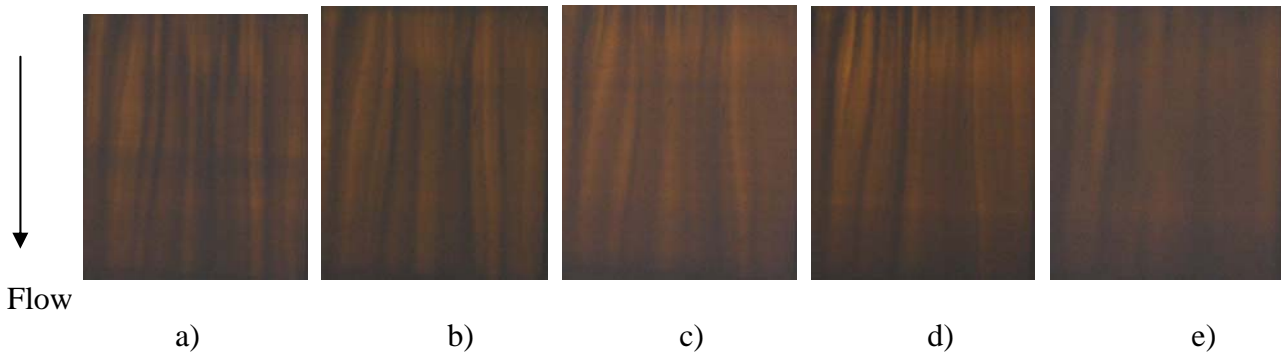


Fig.56 LIF patterns. $G_{\text{Primary air}}=60\text{mmole/s}$, $G_{\text{Primary He}}=60\text{mmole/s}$, $G_{\text{Driver N}_2}=520\text{mmole/s}$, $G_{\text{Secondary He}}=60\text{mmole/s}$. Ar-laser beam position relatively the central plane of the cavity:
a) $y=-2\text{mm}$, b) $y=-1\text{mm}$, c) $y=0\text{mm}$, d) $y=1\text{mm}$, e) $y=2\text{mm}$

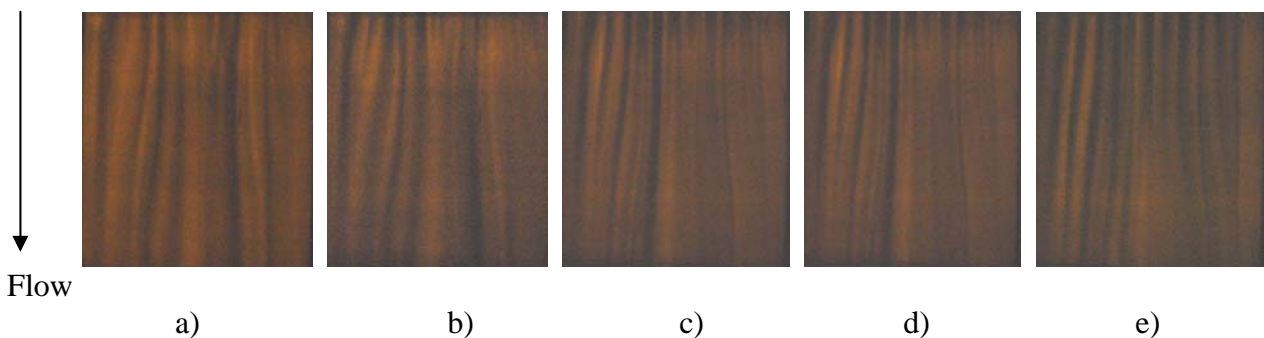


Fig.57 LIF patterns. $G_{\text{Primary air}}=60\text{mmole/s}$, $G_{\text{Primary He}}=130\text{mmole/s}$, $G_{\text{Driver N}_2}=520\text{mmole/s}$, $G_{\text{Secondary He}}=60\text{mmole/s}$. Ar-laser beam position relatively the central plane of the cavity:
a) $y=-2\text{mm}$, b) $y=-1\text{mm}$, c) $y=0\text{mm}$, d) $y=1\text{mm}$, e) $y=2\text{mm}$

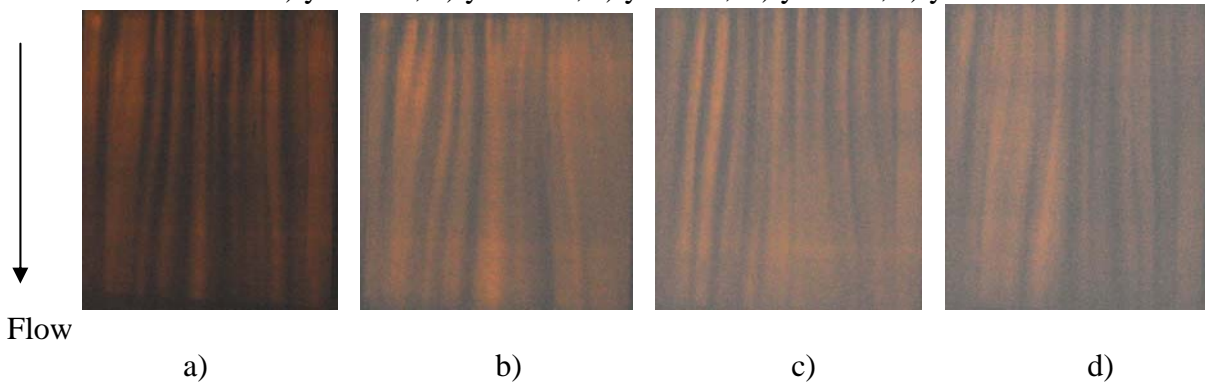


Fig. 58. LIF patterns. $G_{\text{Primary air}}=60\text{mmole/s}$, $G_{\text{Primary He}}=150\text{mmole/s}$, $G_{\text{Driver N}_2}=520\text{mmole/s}$, $G_{\text{Secondary He}}=60\text{mmole/s}$. Ar-laser beam position relatively the central plane of the cavity:
a) $y=-2\text{mm}$, b) $y=0\text{mm}$, c) $y=2\text{mm}$, d) $y=4\text{mm}$

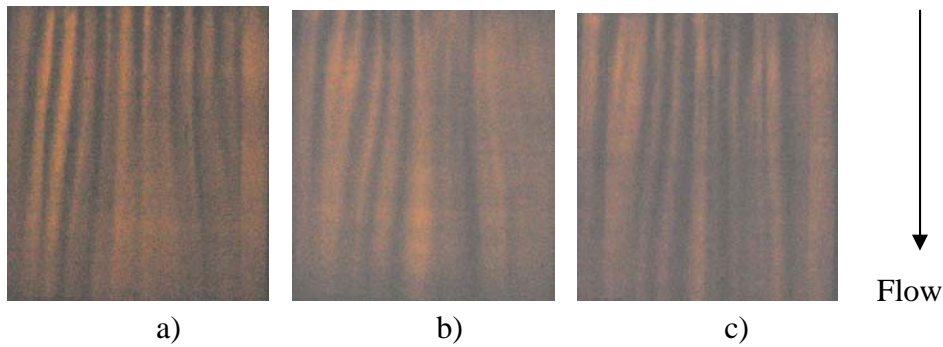


Fig. 59. LIF patterns. $G_{\text{Primary air}}=60\text{mmole/s}$, $G_{\text{Primary He}}=240\text{mmole/s}$, $G_{\text{Driver N}_2}=520\text{mmole/s}$, $G_{\text{Secondary He}}=60\text{mmole/s}$. Ar-laser beam position relatively the central plane of the cavity:
a) $y=-2\text{mm}$, b) $y=0\text{mm}$, c) $y=2\text{mm}$.

Installation of the intermediate chamber shifted the visualized region $80\div 130\text{mm}$ downstream (fig.60÷63). According these LIF patterns the mixing process in the flow is closer to completeness at these distances.

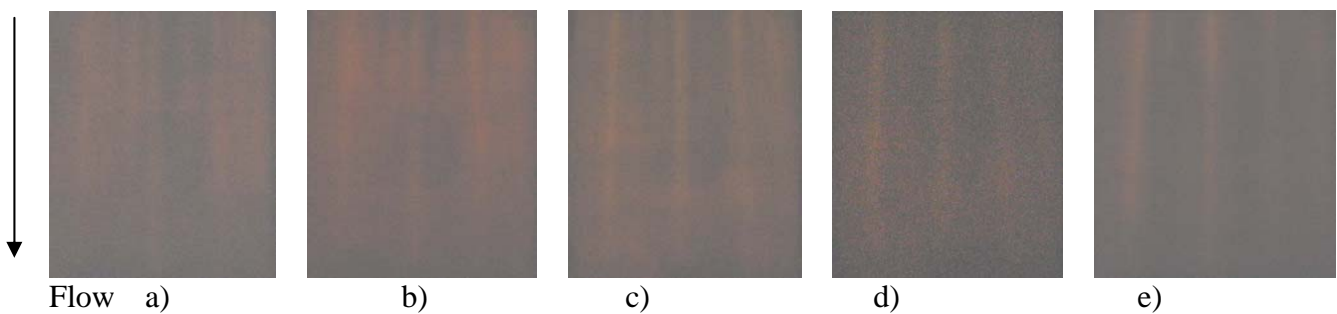


Fig.60. LIF patterns. $G_{\text{Primary air}}=60\text{mmole/s}$, $G_{\text{Primary He}}=60\text{mmole/s}$, $G_{\text{Driver N}_2}=520\text{mmole/s}$, $G_{\text{Secondary He}}=60\text{mmole/s}$. Ar-laser beam position relatively the central plane of the cavity:
a) $y=-2\text{mm}$, b) $y=-1\text{mm}$, c) $y=0\text{mm}$, d) $y=1\text{mm}$, e) $y=2\text{mm}$

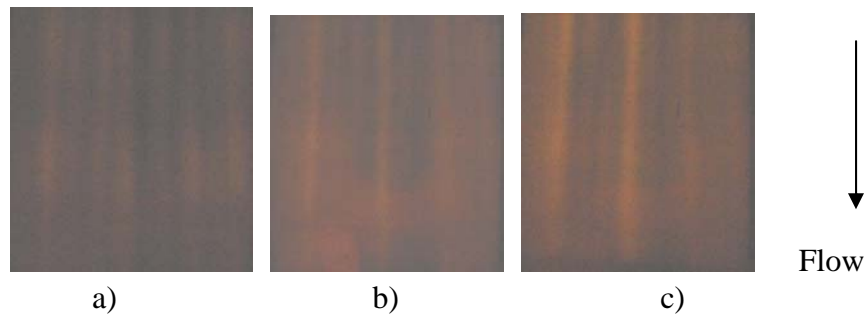


Fig.61. LIF patterns. $G_{\text{Primary air}}=60\text{mmole/s}$, $G_{\text{Primary He}}=130\text{mmole/s}$, $G_{\text{Driver N}_2}=520\text{mmole/s}$, $G_{\text{Secondary He}}=60\text{mmole/s}$. Ar-laser beam position relatively the central plane of the cavity: a) $y=-2\text{mm}$, b) $y=0\text{mm}$, c) $y=2\text{mm}$

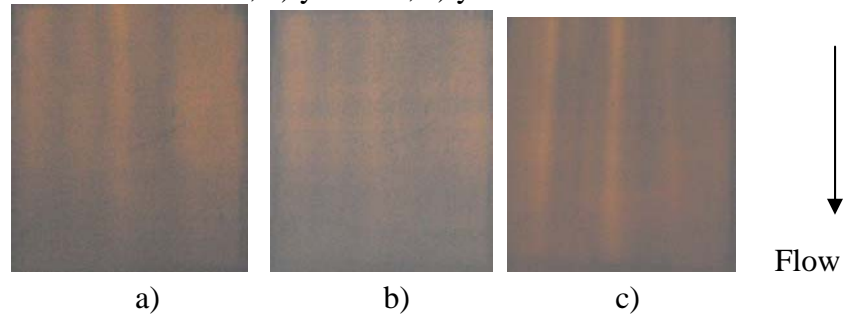


Fig.62. LIF patterns. $G_{\text{Primary air}}=60\text{mmole/s}$, $G_{\text{Primary He}}=150\text{mmole/s}$, $G_{\text{Driver N}_2}=520\text{mmole/s}$, $G_{\text{Secondary He}}=60\text{mmole/s}$. Ar-laser beam position relatively the central plane of the cavity: a) $y=-2\text{mm}$, b) $y=0\text{mm}$, c) $y=2\text{mm}$

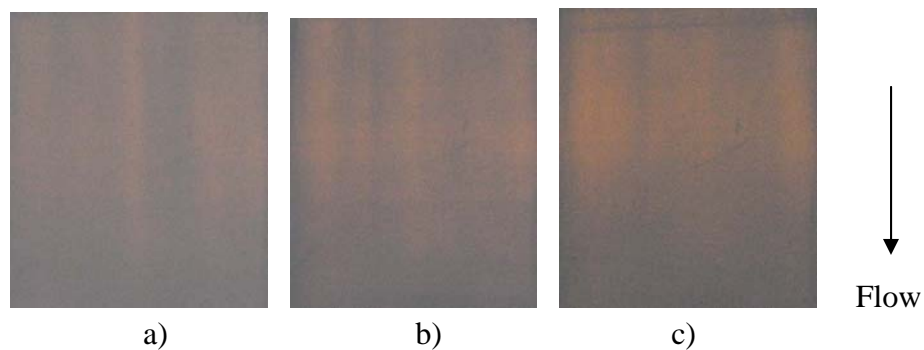
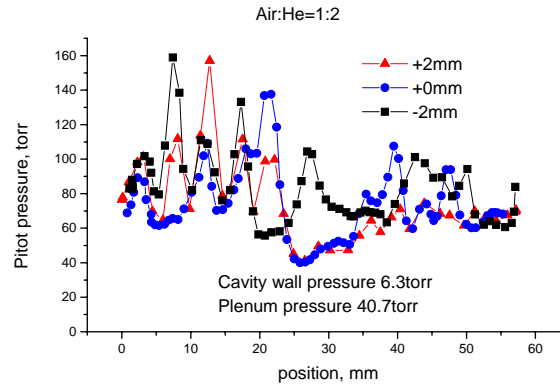
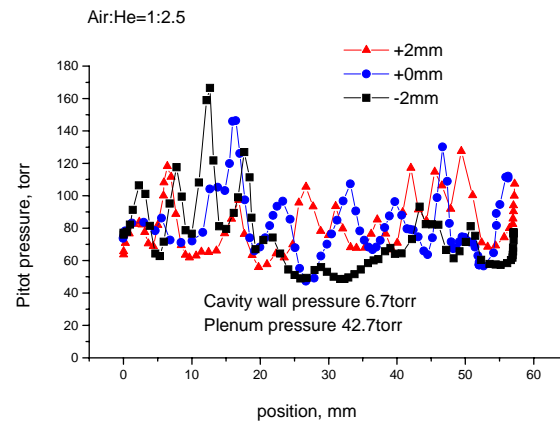


Fig.63. LIF patterns. $G_{\text{Primary air}}=60\text{mmole/s}$, $G_{\text{Primary He}}=240\text{mmole/s}$, $G_{\text{Driver N}_2}=520\text{mmole/s}$, $G_{\text{Secondary He}}=60\text{mmole/s}$. Ar-laser beam position relatively the central plane of the cavity: a) $y=-2\text{mm}$, b) $y=0\text{mm}$, c) $y=2\text{mm}$

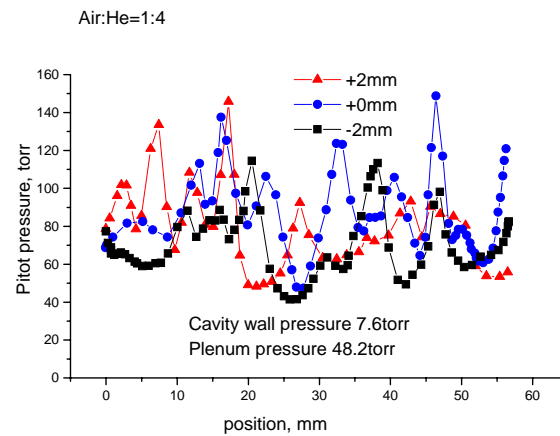
Damping of the Pitot pressure pulsation gives additional information about the mixing efficiency in the flow also. The special device which allowed to replace the Pitot tube with outer diameter 1.5mm on all duct wideness ($\Delta x \sim 50\text{mm}$) for $\sim (5 \div 7)\text{sec}$ test with the coordinate monitoring has been used for such measurements. This device gave possibility to change the scanning line location of the Pitot pressure gauge in vertical direction (along Y axis). Pitot pressure distributions $P_{\text{Pitot}}(x)$ at all dilutions have small scale inhomogeneous up to distances $\Delta z \sim 78\text{mm}$ (Fig. 64). These distributions indicate on the bad flow mixing.



a)



b)

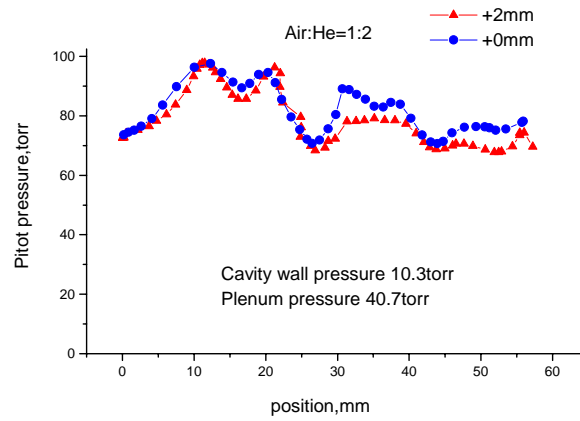


c)

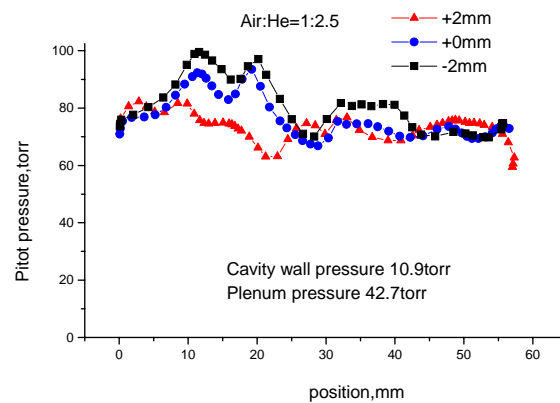
Fig. 64. Pitot pressure distributions at $G_{\text{Primary air}}=60\text{mmole/s}$, $G_{\text{Driver N}_2}=520\text{mmole/s}$, $G_{\text{Secondary He}}=60\text{mmole/s}$, $z=78\text{mm}$.

a) $G_{\text{Primary He}}=120\text{mmole/s}$; b) $G_{\text{Primary He}}=150\text{mmole/s}$; c) $G_{\text{Primary He}}=240\text{mmole/s}$

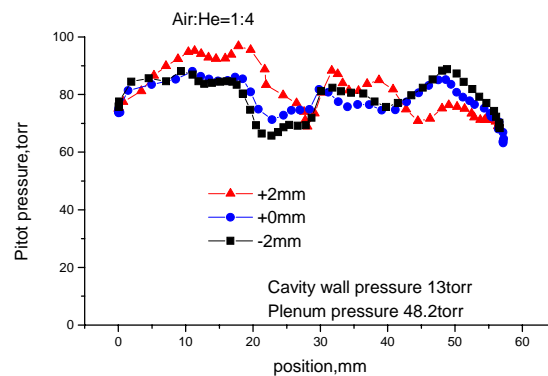
But the distributions $P_{\text{Pitot}}(x)$ obtained at $\sim 130\text{mm}$ from the nozzle bank (fig. 65) practically have not the small scale pulsations.



a)



b)



c)

Fig.65. Pitot pressure distributions at $G_{\text{Primary air}}=60\text{mmole/s}$, $G_{\text{Driver N}_2}=520\text{mmole/s}$, $G_{\text{Secondary He}}=60\text{mmole/s}$, $z=130\text{mm}$.

b) $G_{\text{Primary He}}=120\text{mmole/s}$; b) $G_{\text{Primary He}}=150\text{mmole/s}$; c) $G_{\text{Primary He}}=240\text{mmole/s}$

The average Pitot pressure depends weakly on He dilution and was equal to $\sim 80\text{torr}$. There are the large scale disturbances only on the Pitot pressure distributions which were generated on the duct side walls due to the growing thickness of the boundary layers. These conclusions correlate with results of the LIF observations analysis. Braking of the driver N_2 and the partial pressure and temperature recovery during mixing the flows leads to the increasing of the static pressure at the raise the primary helium molar flow rate and along gas flow (see table with results of the “cold” gasdynamic tests of the blocked ENB-1).

9.2 Development of the centrifugal bubble singlet oxygen generator (CBSOG).

The using filament guided jet singlet oxygen generators provided the stable COIL operation. But it had insufficiently good chlorine utilization and high BHP volumetric flow rate. A bubble type SOG was the first chemical source of oxygen with the $O_2(^1\Delta)$ yield sufficient for successful COIL performance [14]. The gas-liquid reaction interface in this SOG is a surface of the floating bubbles generated when chlorine gas is bubbled through a column of BHP. The flows with the partial oxygen pressure higher than 10 torr are required for efficient high power COIL [15]. Experiments have shown that it is quite difficult to produce droplet free high pressure oxygen flow with high a $O_2(^1\Delta)$ yield and a low level of residual chlorine at earth gravity conditions of bubble SOG operation [16-18]. However the productivity of a bubbler mass-transfer apparatus is repeatedly higher when the bubbling liquid column is under high centrifugal acceleration. Indeed, as acceleration increases, the size of generated bubbles decreases, its floating velocity increases, mass transfer processes are intensified repeatedly, and the droplet carry-over reduces [19]. Hence, a high chlorine utilization and $O_2(^1\Delta)$ yield can be attained at higher oxygen pressures in bubble SOG with BHP column under centrifugal acceleration. The acceleration can be created by rotating of the BHP layer with high angular velocity [20] or by moving of the BHP layer at a high velocity along a concave wall [21].

The 1-st version of the developed centrifugal bubble SOG was used for previous COIL lasing test with no blocked NB at chlorine flow rate $G_{Cl_2}=60\text{mmole/s}$, driver N_2 flow rate $G_{DN_2}=250\text{mmole/s}$ and $Cl_2:He=1:1.5$. This SOG provides high chlorine utilization (up to 95%), the singlet oxygen yield more 60% at low BHP volumetric flow rate (~ 240 ml/s) and excellent aerosol separation. The cavity optical axis during lasing experiments was located on the distance of 63 mm downstream ENB. The goal of these tests consists in the determination of the optimal height of the BHP layer on the SOG perforated cylindrical surface for chlorine inlet. Results of these tests are presented in the Table.

N	P_{BHP} , torr	G_{HePrim} , mmol/s	G_{HeSec} , mmol/s	P_{I_2} , torr	$T_{total}\%$	P_{Plenum} , torr	P_{cavity} , torr	P_{I_2cell} , torr	H_{BHP} , mm	η , %
1	510	90	65	2	3	29	9.5	123	5,5	21.8
2	540	90	65	2	3	30	9.5	124	6	22
3	570	90	65	2	3	28.	8.9	124	6,4	24.6
4	600	90	65	2	3	30	8.7	125	8	25
5	600	90	90	2	3	25	8.8	150	8	24.8

Here P_{BHP} is pressure in the supplying BHP tank which determines BHP volumetric flow rate ($210\div 240\text{ml/s}$) and the layer thickness H_{BHP} .

Chlorine utilization and chemical efficiency increased with the raise of the BHP layer thickness. Maximal chemical efficiency of 25% was attained at the BHP layer thickness of ($7\div 8$)mm and was higher than at the usage of the filament guided JSOG with BHP volumetric flow rate ~ 1200 ml/s. These results became the basis for the further usage of the developed CBSOG in further LIF and COIL lasing tests.

General view of the ejector COIL set-up with CBSOG is presented in fig. 66. One portion of the primary helium (up to 120mmole/s) was premixed with chlorine and the other portion of the primary helium ($60\div 120\text{mmole/s}$) was premixed with the effluent SOG flow in the intermediate chamber between SOG and ENB due to feature of the centrifugal bubble SOG operation.

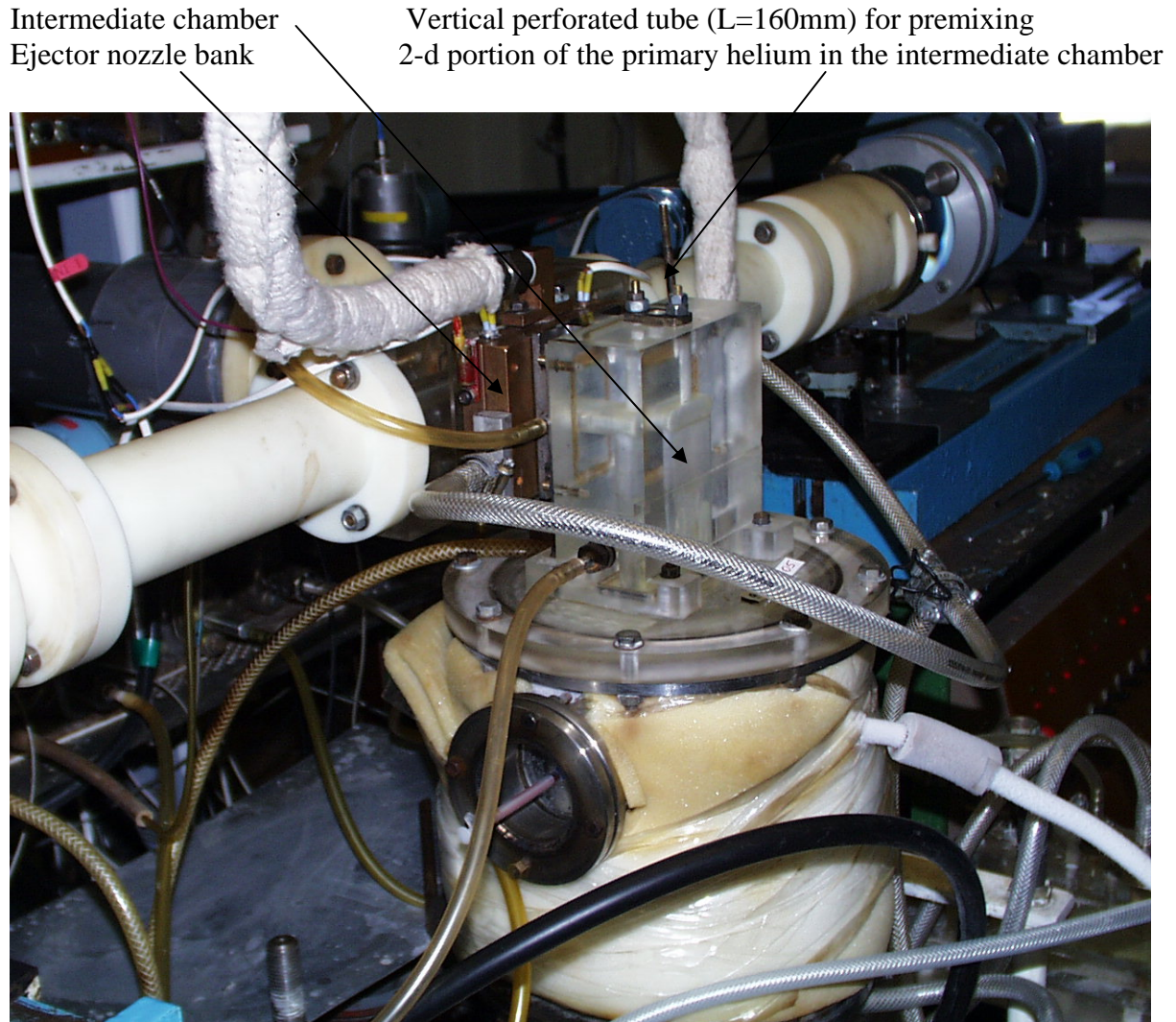


Fig. 66. General view of the COIL with new centrifugal bubble SOG and the blocked ENB-1.

9.3. Distribution of the excited iodine atoms I^* emission along the gas flow in the experiments with the blocked ENB-1 at higher dilution primary gas with helium.

The narrow band interference filter was installed additionally in given experiments to suppress possible residual yellow emission from zone of the intense iodine dissociation. The I^* emission distributions along gas flow at co- and counter flow scanning for $G_{I_2}=0.9\text{mmole/s}$, $G_{\text{He,sec}}=60\text{mmole/s}$ are presented in Fig. 67. It turned out unexpectedly, that emission of the excited iodine atoms drops on the distance of 120mm from ENB approximately 2 times practically at all dilutions primary gas with helium. Increasing of dilution primary gas with helium didn't lead to the noticeable distinctions in distributions of the $I^*(z)$ emission. There is no any explanation of such behavior $I^*(z)$ now.

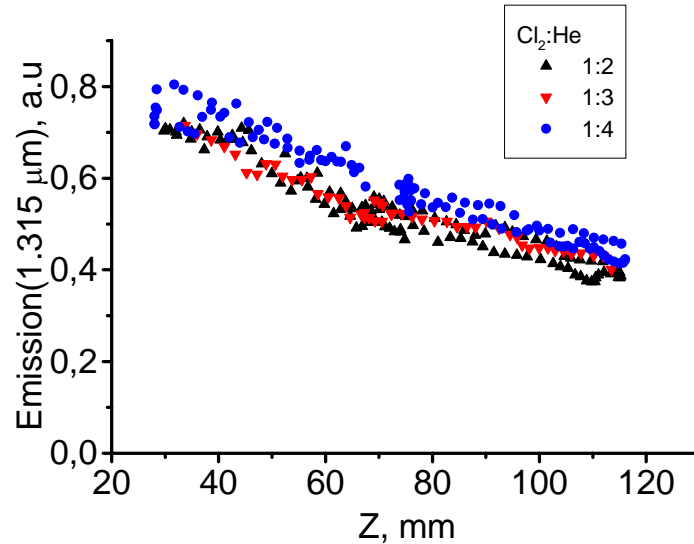


Fig.67. Distribution of emission of the excited iodine atoms I* along gas flow for the blocked ENB-1. $G_{DN}=500\text{mmole/s}$.

9.4. Results of the lasing experiments with the blocked ENB-1 at higher dilution primary gas with helium.

All new mirrors with transmittance of $T=1,5\%$ (6 copies) were destroyed after previous experiments with laser power (1200÷1350)W. It was found in one week after lasing tests that the dielectric covers of these mirrors disconnected from the substrates. The highest power was attained namely with these mirrors. So mirrors of other manufacturer with transmittance $T=1,0\%$ were used in further experiments. Results of the tests with blocked ENB-1 at chlorine flow rate $G_{Cl_2}=60\text{mmole/s}$, $Cl_2:He=1:2$ and optical axis location of 63 mm downstream ENB are presented in Table.

N	G_{DN2} mmol/s	G_{HePr} , mmol/s	G_{HeSec} , mmol/s	P_{I_2} , torr	$P_{\text{iodine cell}}$, torr	T%	Chem Eff
1	500	120	90	2	172	2	22.5
2	500	120	90	2	174	2	22
3	500	120	90	2	169	2	20,6
4	500	120	90	2	175	2	20.4
5	500	120	90	2	179	2	19.8
6	500	120	60	2	130	2	22.6
7	500	120	120	2	198	2	22,1
8	500	120	30	2,6	74	2	16
9	500	120	90	2,5	182	2	19.3
10	500	120	90	1,6	171	2	19.9
11	500	120	90	1,3	170	2	19.8
12	500	120	90	2	182	2,3	16.5
13	500	120	90	2	185	2,6	17.1
14	500	120	90	2	179	3,6	18.4
15	500	120	90	2	180	11,2	2

Five first tests illustrate inadequate mirrors' quality due to continue dropping of the laser power and chemical efficiency with each next test from the maximal value of 22.5% (1225W, 1-st run) to

19.8% (1075W, 5-th run). It's to be noted that mirrors restored the initial state in a few days. Chemical efficiency depended weekly on the iodine molar flow rate in the range $G_{I_2}=(0.7\div 1.25)$ mmole/s ($P_{I_2}=(1.3\div 2.5)$ torr) and on secondary helium in the range $G_{HeSec}=(60\div 120)$ mmole/s. Small signal gain was estimated from dependence of the total output power on the total laser transmission (runs 11÷15) and equal to $\sim 1.1\%$ cm^{-1} . A plenum pressure in given test was close to 40torr. Pitot pressure depends on location of the Pitot tube in the duct and was not measured.

Higher dilution the primary gas with He was provided by injection primary helium (secondary portion) through the perforated tube in the intermediate chamber between SOG and ENB. Results of the lasing tests at chlorine flow rate $G_{Cl_2}=60$ mmole/s, dilution $Cl_2:He=1:3$ and $1:4$ are presented in Table.

N	G_{DN} mmole/s	G_{HePr1} mmole/s	G_{HePr2} mmole/s	G_{HeSec} mmole/s	P_{I_2} torr	$P_{iodine\ cell}$ torr	T%	Chem. Eff.
1	500	120	0	90	2	174	2	22
2	500	120	0	90	2	169	2	20,6
3	500	120	60	90	2	174	2	21,7
4	500	120	60	120	2	204	2	23,7
5	500	120	60	60	2	127	2	21
7	500	120	60	30	2,5	81	2	19,6
8	500	120	60	90	2,6	180	2	20,5
9	500	120	60	90	1,5	162	2	19,6
10	500	120	60	150	2	242.	2	21,0
11	500	120	60	90	2	162	11,2	1
12	500	120	120	90	2	163	11,2	0,2
13	500	120	120	90	2	175	2	20
14	500	120	120	90	2,5	182	2	19,7
15	500	120	120	90	1,5	169	2	12,8
16	500	120	120	90	1,6	172	2	15,1

Ejector COIL operation at chlorine dilution with helium from 1:1 to 1:4 demonstrated the weak dependence of the chemical efficiency on the dilution degree. Attained maximal chemical efficiencies were $\sim 21\div 24\%$ and SSG exceeded 1% cm^{-1} at all dilutions. Small differences of the chemical efficiencies attained at different dilution degrees and the inadequate quality of the used mirrors do not allow separating unambiguously effect of dilution the primary gas with helium and the mirrors' degradation.

10. Conclusion

1. Theoretical analysis of ENB parameters and initial flows' parameters which determined SOG pressure, $O_2(^1\Delta)$ losses and COIL efficiency was made. Requirements to the nozzle bank design were formulated on the base of this analysis.

It was shown that the usage of the high Mach number supersonic nozzles for the driver nitrogen instead of sonic cylindrical nozzles provides possibility of minimizing the blocking of the primary oxygen flow. Elimination of the gasdynamic choking effect permits to increase oxygen flux through the ENB at the same pressure. As it should be from calculations the oxygen-iodine flow with higher pressure recovery, lower temperature, and a higher small signal gain could be produced.

2. Three versions of the ENB with supersonic nozzles for the driver nitrogen have been developed, manufactured and tested. During "cold" gasdynamic tests with the usage of Pitot tube scanning across flow and LIF of iodine it was found that the acceptable mixing efficiency of the flows at the distance ~ 100 mm downstream nozzle bank provides only one

- ENB-1 with turbulizing tabs and of 4mm periodical structure. This nozzle bank provided of 100torr the potential recovery pressure at the driver nitrogen molar flow rate of 500mmole/s.
3. Two version of the filament guided jet singlet oxygen generator were developed to decrease aerosol carry-over from SOG and to provide high ejector COIL operation stability at chlorine flow rate of 80mmole/s. Indeed, its' tests conformed the solution of the problems put by. However reaching of the high chlorine utilization was difficult due to bad renewal of the jet contact surface. Even ~90% chlorine utilization was reached at considerable volumetric BHP flow rate of 1.3litter/s. Later the centrifugal bubble SOG was developed to provide ejector COIL operation at the considerable dilution primary gas with helium. High chlorine utilization up to 95%, singlet oxygen yield ~60% and good aerosol separation were reached at low volumetric BHP flow rate $\sim 240\text{cm}^3/\text{c}$ in this generator.
 4. The Rigrod dependencies of the output power on the total mirrors' transmittance were used for investigation the gain properties of the active medium formed by the developed nozzle banks. These dependencies demonstrated high enough small signal gain ($\geq 1\%\text{cm}^{-1}$) with all ENB.
 5. It is found that intensity of the spontaneous emission of the excited iodine atoms drops fast along the flow produced by ENB-1. The drop appears more intense at the higher driver nitrogen molar flow rate $G_{\text{DN}}=500\text{mmole/s}$ and does not depend on dilution primary gas with helium. At $G_{\text{DN}}=250\text{mmole/s}$ degradation of the spontaneous emission becomes weaker and decreases even at dilution chlorine with helium 1:1. This bank provides fast enough mixing of the flow and reaching low temperatures of the oxygen-iodine layers at which SSG and intensity of the spontaneous emission of the excited iodine atoms become proportional each other. Therefore the drop of the spontaneous emission means the small signal gain drop. The known quenching reactions in the oxygen-iodine medium can't cause substantial losses of $\text{O}_2(^1\Delta)$ during the dwell time of the flow through the cavity chamber, approximately equal to 10^{-4} seconds. Clusters formation and heterogeneous condensation iodine on the superfine aerosol surface may be reasons of the observed SSG drop. Active medium produced by ENB-2 mixes slower and the observed drop of the spontaneous emission of the excited iodine atoms is considerably weaker.
 6. COILs with all developed nozzle banks demonstrate similar maximal chemical efficiencies $\sim 23\div 25\%$ in spite of the fact that its mixing efficiencies of the active medium differ strongly. In the case ENB-1 replacement of the optical axis on 30mm downstream leads to considerable decreasing of the output power. This correlates with results of monitoring along gas flow intensity of the spontaneous emission of the excited iodine atoms.
 7. Dilution chlorine with helium in ratio $\text{Cl}_2:\text{He}=1:1$ in COIL with ENB-1 at drive nitrogen molar flow rate of $G_{\text{DN}}=250\text{mmole/s}$ led to some decrease of the spontaneous emission drop, increasing of the output power and chemical efficiency. It was not observed any essential influence of the dilution primary gas with helium on COIL operation with ENB-1 at $G_{\text{DN}}=500\text{mmole/s}$. It was supposed that higher dilution primary gas with helium up to $\text{Cl}_2:\text{He}=1:4$ may increase the output power and chemical efficiency. However conducted investigations did not justify hopes. Monitoring of intensity of the spontaneous emission of the excited iodine atoms $I^*(z)$ and lasing experiments at $G_{\text{DN}}=500\text{mmole/s}$ and dilutions $\text{Cl}_2:\text{He}=1:(1\div 4)$ did not find any noticeable changes.
 8. Developed ejector nozzle bank ENB-1 with additional nozzles for the iodine vapor injection provided engendering conditions for considerably fast flows mixing (on distances $\sim 100\text{mm}$). Small signal gain exceeded $1\%\text{cm}^{-1}$ on the distances $\sim 50\text{mm}$ where flow has stratified structure. However SSG considerably decreases on the distance where the flow mixing is completed due to the formation of the different clusters. The maximal chemical efficiencies $\sim 23\div 25\%$ were attained also at the optical axis located on distance of $\sim 50\text{mm}$ downstream ENB. Pre-mixing helium with the primary flow even at $\text{Cl}_2:\text{He}=1:4$ could not to improve situation. It's possible that iodine is bound with water clusters and the increase of the gas static temperature at pre-mixing helium does not destroy its.

9. The thin wire mesh was installed on the some distance downstream nozzle bank in the ejector COIL with injection iodine vapor by the high pressure driver nitrogen for increasing the static gas temperature of the cold mixed flow [22]. Flow around wires formed set of the oblique shock waves in the flow after damping of which partial pressure and temperature recovery takes place. The raise of temperature on several tens led to destruction of $(N_2)_n$ -I clusters binding atomic iodine in this laser. It's possible that this method may be more efficient than dilution the primary flow with helium.

11. References

1. V.N.Azyazov, M.V.Zagidullin, V.D.Nikolaev, V.S.Safonov, *Quantum Electronics*, **27**, 477 (1997)
2. T.T. Yang, A. Browmik, D. Burde, R. Clark, S. Carroll, R.A. Dickerson, J. Eblen, T. Gylys, Y.C. Hsia, R. Humphreys-JR, L.F. Moon, S.C. Hurlock, A Tomassian. *Proc. SPIE*, **4760**, 537 (2002)
3. V.D. Nikolaev, M.V. Zagidullin, G.D. Hager, T.J. Madden. *AIAA Paper 2427 – 2000*
4. V.D. Nikolaev, M.V. Zagidullin, M.I. Svistun, B.T. Anderson, R.F. Tate, and G.D. Hager. *IEEE J.Quantum Electronics*, **38**, 421 (2002)
5. G.D. Hager, N.A. Khvatov, M.I. Svistun, V.D. Nikolaev, M.V. Zagidullin. *Appl. Phys. A77*, 325 (2003)
6. Cherkez A. Ya., “About one-dimensional theory for non-calculated supersonic gas jet”, *Izvestiya of Soviet Union Academy of Sciences, Mechanics & Mechanical engineering*, #5, pp. 13-25, (1962)
7. G.N. Abramovich, “Applied Gasdynamics”, Moscow, Nauka, (1976)
8. T.T. Yang, R.A. Dickerson, L.F. Moon, Y.C. Hsia, *AIAA Paper 2000-2425*, 31st AIAA Plasmadynamics & Lasers Conference, 19-22 June, 2000, Denver, CO
9. G. Koppenwallner, C. Dankert, “Homogeneous condensation in N_2 , Ar, and H_2O free jets”, *J. Phys. Chem.*, **91**, 2482-2486, (1987)
10. J. Vetrovec, “Singlet Oxygen Generator with Filament-Guided Jets”, *Proc. SPIE*, Vol. 3574, 546-549 (1998)
11. P.D. Whitfield, D.E. Hagen, M.B. Trueblood, W.M. Barnett, C. Helms, “Experimental investigation of homogeneous and heterogeneous nucleation condensation processes and products in COIL” *Proc. SPIE*, Vol. 1871, 277 (1993)
12. J.A. Blake, G. Burns, *J. Chem. Phys.*, **54**, 1480, (1971)
13. L.K.K. Ip, G Burns, *J. Chem. Phys.*, **56**, 3155, (1972)
14. W.E. McDermott, N.R. Pchelkin, D.J. Benard, and R.R. Bousek, *Appl. Phys.Lett.*, **32**, 496, (1978)
15. K.A. Truesdell, C.A. Helms, G.D. Hager. *Proc. SPIE*, **2502**, 217 (1994)
16. O. Spalek, J. Kodymova, and A. Hirsl, *J. Appl. Phys.*, **62**, 2208 (1987)
17. V.N. Azyazov, N.P. Vagin, N.L. Kuprianov, and N.N. Yuryshhev, *Journal of Soviet Laser Research*, **14**, 114, (1993)
18. P.V. Avizonis and K.A. Truesdell. *Proc.SPIE*, **2502**, 180 (1994)
19. A.I. Safonov, and V.S. Krylov. *Theoretical Foundation of Chemical Engineering (in Russian)*, **6**, 51 (1972)

20. M.V. Zagidullin Proceedings of 2nd International Workshop «Iodine laser and Application», Czechoslovakia, 163 (1989)
21. G. Emanuel, Proc. SPIE, **5448**, 233 (2004)
22. J. Marshall, K. Healey, B. Croker, K. Kendrick, T. T. Yang, Y. C. Hsia, R. A. Dickerson, L. Forman, “COIL Power Extraction Enhanced by Reducing/Eliminating Iodine Clusters in a High Mach Number Nitrogen Mixing Nozzle”, COIL R&D Workshop 2005, Stuttgart, Germany, 5-6 September 2005

12. List of the published papers and reports with abstracts.

1. G.D. Hager, V.D. Nikolaev, M.I. Svistun, M.V. Zagidullin, «Lasing performance of a chemical oxygen iodine laser (COIL) with advanced ejector-nozzle banks», Applied Physics A, (Material Sciences & Processing), A77, 325-329, (2003).
Khvatov N.A., Nikolaev V.D., Svistun M.I., Zagidullin M.V., G.D. Hager, «Lasing performance of a chemical oxygen iodine laser (COIL) with advanced ejector nozzle banks», Proc. SPIE Vol. 4760, 550-559, 2003

The experimental results have demonstrated that ejector nozzle concepts can simultaneously achieve high chemical efficiency and high pressure recovery. The estimated small signal gain of the gain medium generated by these nozzle banks was from 0.5% - 0.8%/cm. In laser experiments with all nozzle banks (NB-1 - NB-5), Pitot pressures the order of 80 torr and Mach numbers of ~2 in the cavity mixing chamber have been achieved. The geometry of a given ejector nozzle bank and gas flow conditions effect the power extraction and chemical efficiency. The main factors for high efficiency and high power are small mixing scale, high area for the oxygen flow, dilution of chlorine by helium and the arrangement of nozzles. A chemical efficiency of 25% at a power level of ~900W was obtained for NB-1 having the smallest mixing scale, parallel injection of all flows and dilution of oxygen by helium. The highest power ~1.2kW with a chemical efficiency of 19.5% and 160W/cm² of specific output power was achieved with NB-5 having the largest area for the oxygen flow and dilution of oxygen by helium.

2. M.V.Zagidullin, V.D. Nikolaev, M.I. Svistun, N.A. Khvatov, G.D. Hager “High gain, high pressure, highly efficient COIL”, Proceedings of SPIE, v.5448, 1139-1146, 2004

The nozzle banks with supersonic nozzles for the driver nitrogen have been developed for generation of the gain medium of chemical oxygen-iodine laser. The nozzle bank is supplied by oxygen flow from the cross-flow SOG. Results of aerodynamic tests, visualization of flows by laser induced fluorescence, monitoring of the excited iodine atoms emission and laser power extraction are presented. The total power exceeding 1 kW with chemical efficiency more than 24% was obtained in 5 cm gain length COIL at chlorine dilution free. The lasing was observed even for the total mirror transmission more than 10%.

3. V.D. Nikolaev, M.I. Svistun, M.V. Zagidullin, “Ejector COIL”, Proceedings of SPIE, vol. 5479, 10-18, 2004

The historical ejector-like chemical oxygen iodine laser (COIL) contribution at the Lebedev Physical Institute, Samara Branch is briefly presented. Two possible schemes of such COIL which provide the high exhaust pressure are considered. The high-pressure hot driver nitrogen is carrier of iodine vapor in the first scheme. In the second version the additional nozzles with the low-pressure secondary nitrogen are employed for injection iodine vapor but the pure high-pressure driver nitrogen has the room temperature. The last COIL version was investigated in Lebedev Physical Institute in more detail and results of these investigations are presented. This ejector nozzle bank

generates gain medium with high Mach number, low temperature and high gain. A high chemical efficiency up to 25% and the potential pressure recovery up 90 torr have been achieved simultaneously.

4. M.V. Zagidullin, V.D. Nikolaev, M.I. Svistun, N.A. Khvatov, G.D. Hager, "Efficient chemical oxygen-iodine laser driven by centrifugal bubble singlet oxygen generator", *Applied Physics Letters*, v.86, p.25-26 (2005)

Efficient production of singlet oxygen in a bubble singlet oxygen generator (BSOG) under the influence of centrifugal acceleration, 136g, has been obtained. An output power of 770W with chemical efficiency of 25.6% has been achieved in a small-scale, supersonic chemical oxygen-iodine laser supplied by the centrifugal BSOG. The ratio of the output power to the basic hydrogen peroxide volumetric flow rate was 4.3 KJ/liter. Efficient COIL operation with the centrifugal BSOG demonstrates the potential for mobile lasers.

5. M.V. Zagidullin, V.D. Nikolaev, M.I. Svistun, N.A. Khvatov, G.D. Hager, "Characteristics of gain medium for an ejector COIL with supersonic nozzles for driver buffer gas", *Appl. Phys. A* 81, 311-315 (2005)

The use of supersonic nozzles for the driver nitrogen in an ejector nozzle bank, (ENB), for chemical-oxygen iodine laser, (COIL), resulted in the elimination of the choking effect for the primary oxygen flow and formation of a low temperature gain medium. The ENB generates a supersonic gain medium with a Mach number greater than 2.2, and a temperature less than 200°K. The potential recovered pressure was 90 torr with a small signal gain greater than 10^{-2} cm^{-1} . With a 5 cm gain length for this nozzle the output power was 1.2 kW with a chemical efficiency of 23.4%. A strong decay of $I(^2P_{1/2})$ spontaneous emission, ($I(^2P_{1/2})$ concentration), along the gain medium flow was observed.

6. M.V. Zagidullin, V.D. Nikolaev, M.I. Svistun, N.A. Khvatov, "Oxygen-iodine ejector laser with a centrifugal bubbling singlet oxygen generator", *Quantum Electronics*, **35** (10), 907-908, (2005)

It is shown that if an ejector supersonic COIL is fed by singlet oxygen from a centrifugal bubble generator operating at acceleration of ~400g the laser output power achieves a value 1264 W at chemical efficiency 24,6% at volumetric BHP flow rate of $208 \text{ cm}^3 \text{ s}^{-1}$ and specific chlorine flux of $1,34 \text{ mmole s}^{-1}$ per square centimeter of the bubbler surface.

12. List of presentations at conferences and meetings with abstracts

1. Presentation V.D. Nikolaev, M.V. Zagidullin, M.I. Svistun, "Ejector COIL" has been made on the International Conference "Laser Optics 2003", June 30-July 4, St. Petersburg, Russia.

The historical ejector-like chemical oxygen iodine laser (COIL) contribution at the Lebedev Physical Institute, Samara Branch is briefly presented. Two possible schemes of such COIL which provide the high exhaust pressure are considered. The high-pressure hot driver nitrogen is carrier of iodine vapor in the first scheme. In the second version the additional nozzles with the low-pressure secondary nitrogen are employed for injection iodine vapor but the pure high-pressure driver nitrogen has the room temperature. The last COIL version was investigated in Lebedev Physical Institute in more detail and results of these investigations are presented. This ejector nozzle bank generates gain medium with high Mach number, low temperature and high gain. A high chemical efficiency up to 25% and the potential pressure recovery up 90 torr has been achieved simultaneously.

2. Presentation Nikolaev V.D., Svistun M.I., Zagidullin M.V., Hager G.D., "Ejector COIL with supersonic nozzles for driver N₂" has been made on International GCL-HPL-2004 Conference, 30 August-3 September 2004, Prague, Czech Republic.

Employing of the conical high Mach number supersonic nozzles and extremely high-pressure driver nitrogen gives possibility to minimize cross section area occupied by driver N₂ and to decrease the plenum oxygen pressure at high O₂ flux through the ejector nozzle bank (ENB), to reach high gain and chemical efficiency. Developed ENB has dimensions of 52 x 16 mm². Conical micro nozzles for driver nitrogen has exit to throat area ratio more 22 and operate at 5 atm stagnation pressure. Previous "cold" gasdynamic tests of this ENB at using of 80 mmole/s air instead of oxygen, 60 mmole/s secondary N₂ (I₂ vapor carrier) and of 530 mmole/s driver nitrogen demonstrated low pressures in the generator ~23.3 torr. Static and Pitot pressures at the distance ~85 mm down stream nozzle bank were equal to 7 torr and 82 torr correspondently. The cross section area of the mixing chamber F increased along gas flow and was 1.4 times more than ENB outlet area. Pitot pressure should be higher at using parallel channel therefore $P_{\text{Pitot}} \sim 1/F$. Estimated Mach number was ~3.

3. Presentation M. V. Zagidullin, V. D. Nikolaev, M.I. Svistun, N. A. Khvatov, "Efficient COIL driven by SOG with filaments-guided jets" has been made on International GCL-HPL-2004 Conference, 30 August-3 September 2004, Prague, Czech Republic.

The dependence of chlorine utilization on its molar flow rate and small dependence on gas residence in reaction zone indicate that strong depletion of on the jet surface in FGJSOG takes place. More smooth filament-guided jets provide lower utilization but they are more stable and consequently they generate lower amount of BHP droplets. The estimated specific surface gas-BHP contact area ~14 cm⁻¹ is higher than specific surface ~5 cm⁻¹ in JSOG with free jets. But for achievement of high chlorine utilization the required BHP volumetric rate is comparable and even higher than in SOG with free jets. These facts indicate that in the case of free jets the convective mass transfer of in BHP much stronger than in the case of filament guided jets. The supersonic COIL with ejector nozzle bank was supplied by oxygen flow from FGJSOG. In laser experiments the clogging of nozzles by dry deposit was not observed. The chemical efficiency more than 24% has been obtained.